JAERI-M
83-091

EVALUATION REPORT ON CCTF CORE-I REFLOOD TESTS C1-5 (RUN 14), C1-10(RUN 19) AND C1-12 (RUN 21)
—EFFECT OF CONTAINMENT PRESSURE—

June 1983

Hajime AKIMOTO and Yoshio MURAO

日本原子力研究所
Japan Atomic Energy Research Institute

JAERI-M レポートは，日本原子力研究所が不定期に公刊している研究報告書です。
入手の問合わせは，日本原子力研究所技術情報部情報資料課（〒319—11 茨城県那珂郡東海村）あて，お申しこしください。なお，このほかに財団法人原子力弘済会資料センター（〒319—11 茨城県那珂郡東海村日本原子力研究所内）で複写による実費頒布をおこなっております。

JAERI-M reports are issued irregularly.
Inquiries about availability of the reports should be addressed to Information Section, Division of Technical Information, Japan Atomic Energy Research Institute, Tokai-mura, Naka-gun, Ibaraki-ken 319—11, Japan.

編集兼発行　日本原子力研究所
印　　刷　日立高速印刷株式会社

Evaluation Report on CCTF Core-I Reflood Tests C1-5 (Run 14), C1-10 (Run 19) and C1-12 (Run 21)
—— Effect of Containment Pressure ——

Hajime AKIMOTO and Yoshio MURAO
Department of Nuclear Safety Research
Tokai Research Establishment, JAERI
(Received May 28, 1983)

Three tests C1-5 (Run 14), C1-10 (Run 19) and C1-12 (Run 21) were performed using the Cylindrical Core Test Facility to study the effect of the containment pressure on the core cooling and the system behaviors during the reflood phase of a PWR-LOCA. The containment pressures of these tests were 0.15, 0.20 and 0.30 MPa for the tests C1-10, C1-5 and C1-12, respectively. Through the comparison of the test results from these three tests, the following results were obtained.

(1) The higher containment pressure gave the higher heat transfer coefficient in the core. This resulted in the lower turnaround temperature, the shorter turnaround time and the shorter quench time at the higher containment pressure.

(2) In the higher containment pressure test, the higher core water head, the higher upper plenum water head, the higher downcomer water head in the early period and the lower downcomer water head in the later period were observed than those in the lower containment pressure test. This resulted in the higher pressure drop through the intact loop in the early period of the tests and the lower pressure drop in the later period of the test with the containment pressure.

(3) The pressure drop through the broken cold leg pressurized the primary system. The pressure drop through the broken cold leg was decreased with the containment pressure.

(4) The core inlet mass flow rate was increased with the containment pressure as observed in the FLECHT-SET phase B1 test. In quantity, however, the effect of the containment pressure on the increase of

the core inlet mass flow rate was less in the CCTF than that in the FLECHT-SET. The less sensitivity in the CCTF was attributed mainly to the great pressure drop through the broken cold leg, which was not observed in the FLECHT-SET with big broken cold leg.

(5) The system effect of the containment pressure was explained quantitatively.

Keywords: Reactor Safety, Loss-of-coolant, PWR Reflood, Pressure Effect, System Behavior, Core Inlet Mass Flow Rate, Containment Pressure

---

The work was performed under contract with the Atomic Energy Bureau of Science and Technology of Japan.

大型再冠水円筒第一次炉心試験Ｃ１－５（Run14），Ｃ１－10（Run19）及びＣ１－12.(Run21)評価報告書

― コンテインメント圧力の影響 ―

日本原子力研究所東海研究所安全工学部
秋本　肇・村尾　良夫

（１９８３年５月28日受理）

加圧水型原子炉の冷却材喪失事故再冠水期における炉心冷却挙動とシステム挙動に及ぼすコンテインメント圧力の影響を調べるために，円筒炉心試験装置を用いて３回の試験を行なった。試験Ｃ１－10，Ｃ１－５，Ｃ１－12のコンテインメント圧力は，それぞれ0.15, 0.20，0.30MPa であった。試験結果の比較検討から以下のことが明らかとなった。

(1) コンテインメント圧力が高くなる程，炉心内での熱伝達が良くなった。その結果ターンアラウンド温度は低くなり、ターンアラウンド時刻は短かくなり，クエンチ時刻も短かくなった。

(2) コンテインメント圧力の高い試験では，コンテインメント圧力の低い試験よりも，高い炉心水頭と上部プレナム水頭が観察され，ダウンカマ水頭に関しては，初期高く実験後期では低くなることがわかった。この結果健全ループ差圧は，初期はコンテインメント圧力が高い試験程高く後期で低くなった。

(3) 破断コールドレグで大きな圧力損失が観察され，一次系圧力が高められた。破断コールドレグ圧力損失は、コンテインメント圧力が高くなる程低くなった。

(4) コンテインメント圧力が高い時程炉心入口流量が高くなった。この傾向はＦＬＥＣＨＴ－ＳＥＴ 試験と同様であったが，圧力上昇に伴なう入口流量の増加割合はＦＬＥＣＨＴ－ＳＥＴ 試験に比べて小さかった。これは主に円筒炉心試験では大きな破断コールドレグ圧力損失が存在したことに起因していると考えられる。

(5) コンテインメント圧力によるシステム効果を定量的に説明することができた。

本報告書は，電源開発促進対策特別会計施行令に基づき，科学技術庁からの委託により行なった研究の成果である。

Contents

目　　次

List of tables and figures

1. INTRODUCTION

The containment pressure is one of the most important parameters for the thermal-hydraulic behaviors during the reflood phase of a loss-of-coolant-accident (LOCA) of a pressurized water reactor (PWR).

Many studies have been performed to study the effect of the pressure on the core cooling characteristics during the reflood phase.[1]~[3] One of the typical tests is the so-called forced feed tests. In the forced feed test, the core cooling characteristics have been examined by feeding the ECC water into the core since it is very easy to establish the desired coolant conditions at the core inelt. Many researches were performed with the forced feed system. They found that rewetting rate was increased clearly with pressure.[1],[2]

However, the coolant conditions at the core inlet is determined by the system effect in the actual PWR. Hence, the so-called system experiment have been performed to study the system effect during the reflood phase. The FLECHT-SET Phase B1 test represents a typical test of the system experiments.[3] They observed that the higher containment pressure resulted in the increase of the core inlet mass flow rate. The FLECHT-SET has 10×10 heater rods. The core flow area is scaled down by factor of 1/370. It has one intact loop with triple flow area and one broken loop for the simulation of a four-loop PWR. However, the FLECHT-SET results still include the problem in the similarity with actual PWRs. In the FLECHT-SET tests, the ECC water was injected into the bottom of the downcomer instead of the cold leg injection, because the stable operation of the facility was disturbed by the condensation in the containment tank. The FLECHT-SET tests were performed, keeping the downcomer water head constant by adjusting the ECC water injection rate into the bottom of the downcomer. It is still necessary to investigate the system effect under the similar ECC water injection conditions with the PWR system.

The Cylindrical Core Test Facility (CCTF) was designed to provide information on the thermal-hydraulic behavior and the core cooling behavior during the refill and the reflood phases of a hypothetical loss-of-coolant-accident of a PWR.[4] The vertical dimensions and the length of the system components were kept as close to the reference PWR as possible. Each flow area of the system component is scaled down in proportion to the scaling factor of the core flow area, that is, 1/21.4. The CCTF has four primary loops with the component simulators of a PWR. The ECC injection

system of CCTF consists of the accumulator system and the low pressure coolant injection system. Both can inject the ECC water into the lower plenum and the cold legs similar with actual PWR.

Three tests were performed in the CCTF to study the effect of the containment pressure on the thermal-hydraulic behavior during the reflood phase of a PWR-LOCA under the similar ECC water injection conditions with the actual PWR. The containment pressures of the three tests were 0.15 MPa (test C1-10), 0.20 MPa (test C1-5) and 0.30 MPa (test C1-12). The purpose of this report is to describe the containment pressure effect in the CCTF tests referring to the FLECHT-SET results.

The main test results from the three CCTF tests are shown in Appendixes B through D. The explanation of the Tag. IDs is indicated in Appendix A.

2. EXPERIMENT

2.1 Test facility

The CCTF was designed to reasonably simulate the flow conditions in the primary system of a 4-loop PWR during the refill and reflood phase of a loss-of-coolant accident (LOCA). The reference reactors are the Trojan reactor in the United States and, in certain aspects, the Ohi reactor in Japan. The vertical dimensions and the flow pathes of the system components in the CCTF are kept as close to the reference reactor as possible. The flow area of each system component is scaled down in proportion to the scaling factor of the core flow area, that is, 1/21.4. The break location was assumed to be near the surface of the biological shield of the pressure vessel, that is, just the downstream of the injection port of the emergency core cooling (ECC) water.

Figure 1 shows the schematic of the CCTF. The facility is equipped with four primary loops which are composed of three intact loops and one broken loop. Each loop has a hot-leg-piping section, an active steam generator, a loop-seal-piping section, a pump simulator, an ECC water injection port, and a cold-leg-piping section.

The steam generator is of U-tube and shell type. The tube length is about 15 m and it is shorter by about 5 m than that of the reference reactor. However, it is long enough to simulate the heat transfer characteristics between the primary and the secondary sides of the steam generator. The secondary side is filled with the saturated water at high pressure ($\sim$5.2 MPa).

Each pump simulator is equipped with an orifice plate to simulate the flow resistance and with vanes to simulate the counter current flow limit characteristics of the pump in the reference PWR.

The emergency core cooling system (ECCS) of the CCTF consists of the accumulator (Acc) and the low pressure coolant injection (LPCI) systems. Each system is connected to the ECC ports attached at the cold legs and the lower plenum of the pressure vessel.

The containment vessel is simulated with two tanks, that is, the containment tanks 1 and 2 in Fig. 1. The containment tank 1 is equipped with a steam-water separator to collect the water flowing through the broken cold leg from the pressure vessel. The total volume of the two tanks is smaller than the volume of the containment vessel in the reference reactor system. Then, the pressure in the containment tank 2 is kept

constant by mean of a pressure control system. The steam in the containment tank 2 is exhausted to the atmosphere through the pressure regulation valve.

Figure 2 shows the schematic of the pressure vessel of the CCTF.

The core consists of 32 bundles arranged in a cylindrical configuration. Each bundle contains 57 heater rods and 7 non-heated rods. The heater rods consists of 12 high, 17 medium and 28 low power rods. The power ratios of the high, medium and low power rods to the bundle-average power are 1.1, 1.0 and 0.95, respectively. The heated length of the heater rods is 3.66 m and the axial peaking factor of each rod is 1.49. The power supply to the bundles is subdivided into three radial regions as shown in Fig. 2. The power supply to each region can be controlled independently, then the radial power distribution can be controlled in the CCTF. The power can be changed with time to simulate the reactor decay heat.

The design of the upper plenum internals is based on that for the Westinghouse 17×17 array fuel assemblies. The radial dimension of each internal is scaled down by factor of 8/15 from that of the reference reactor. The quantities of internals in the CCTF is in proportion with those in the reference reactor. The CCTF has 12 control rod guide tubes, 4 support columns, 8 stub mixer, 2 orifice plates and 6 open holes.

The downcomer is an annulus with 61.5 mm gap in the CCTF. In the scaling of the CCTF downcomer, the volume of the baffle region of the reference reactor was added to the volume of the downcomer. The CCTF has a wider downcomer. However, the wider downcomer provides more conservatisms in the downcomer water accumulation rate.

The outside wall of the downcomer is constructed of carbon steel cladded with 5 mm stainless steel. The thickness of the carbon steel is 85 mm. The wall is preheated to a certain temperature before the test to simulate the heat release from the vessel wall in the reference reactor.

The main dimensions of the CCTF are summarized in Table 1.

2.2 Instrumentation

Many differential-pressure transducers and thermocouples are installed in the CCTF to measure the transients of the differential pressure, the fluid temperature and the wall temperature.

The transients of temperature are measured using the almel-chromel sheathed thermocouples with the outer diameter of 0.5 mm. The expected error is 0.5 % in the temperature measurement. About 900 sheathed thermocouples are burried on the outside clad surface of the heater rods in the

core. About 100 sheathed thermocouples are installed to measure the wall and fluid temperature inside the pressure vessel. And about 150 thermocouples are installed to measure the wall and fluid temperatures along the four primary loops and in the secondary side of the steam generators.

The transients of pressure are measured using the differential pressure cells in the containment tanks, the pressure vessel and the inlet plenums of the steam generator. Along the primary loops, the transients of the differential pressure are measured section by section. In the downcomer, the transients of the differential pressure are measured at 5 vertical sections every 90 degree along the pressure vessel wall. In the core, the transients of the differential pressure are measured at every 0.61 m vertical section. The expected error of the differential-pressure cells is ±0.3%.

ECC water injection rates are measured with the electromagnetic flowmeters at 6 locations.

Including other detecters, more than 1600 channels are recorded every 0.2 s or 0.5 s.

2.3 Test procedure and conditions

The test procedures were as follows: After establishing the initial conditions of the test, the lower plenum was filled with saturated water to a specified level of 0.9 m. Electric power was supplied to the heater rods of the core. When the maximum temperature reached the specified temperature, the water in the accumulator tanks was injected into the lower plenum (the Acc/LP mode). When the water was estimated to reach the bottom of the core, the decay of the heating power was initiated. After the assumed time delay, the injection location was changed from the lower plenum to the ECC ports of the three intact cold legs. The ECC water was still supplied from the accumulator and this period is defined as the accumulator mode (Acc mode). After a specified time delay, the injection mode was transferred from the accumulator mode to the low pressure coolant injection (LPCI) mode. The water injection rate was reduced about one-nineth of the Acc mode in the LPCI mode.

The test conditions of the tests C1-10, C1-5 and C1-12 are listed in Table 2. The containment pressure of the tests C1-10, C1-5 and C1-12 were set at 0.15, 0.20 and 0.30 MPa, respectively. The initial downcomer wall temperature was set to make the superheat of the downcomer wall identical among the three tests.

3. RESULTS AND DISCUSSION

3.1 Core cooling behavior

Figure 3 shows the comparison of the clad surface temperatures at the midplane of a high power rod in the high power region. The linear power and clad surface temperature were 2.66 kW/m and 880 K at 0 s, respectively. The maximum temperature in each temperature history is called the turnaround temperature and the time to the maximum temperature recording is called the turnaround time. The rapid temperature drop is shown between 200 and 400 s in each temperature history. This phenomenon is the so-called quench and the time to the quench is called the quench time. Figure 3 shows that the higher containment pressure leads to the shorter turnaround time and the lower turnaround temperature at the midplane of the peak power rod.

Figure 4 shows the effect of the containment pressure on the turnaround time and temperature at various elevation along the averaged power rod. The turnaround time and temperature shown in Fig. 4, indicate the arithmetic averages of those from 14 average power rods. The maximum of the turnaround temperatures is shown at the elevation of 2.44 m in both tests. The maximum temperature in the 0.30 MPa test is lower by 96 K than that in the 0.15 MPa test along the average power rod. For the peak power rod, the maximum temperature in the 0.30 MPa test was lower by 67 K than that in the 0.15 MPa test. Figure 5 shows the containment pressure effect on the quench time along the average power rods. The higher containment pressure results in the faster quench at evergy elevation, especially above 1.83 m. The quench times above 1.83 m in the 0.30 MPa test are about 60% of those at the corresponding elevations in the 0.15 MPa test.

The higher containment pressure resulted in the shorter turnaround time, the lower turnaround temperature and the shorter quench time in the CCTF. Figure 6 shows the comparisons between the CCTF and a series of FLECHT results of the temperature rise and the quench time at the midplane of the peak power rod. Temperature rise is defined as the difference of the turnaround temperature from the initial clad temperature. The test conditions of each test are summarized in Table 3. The FLECHT LOW FLOODING TEST was performed with the forced feed water injection under the higher peak power than the other tests.[2] The FLECHT-SET Phase B1 tests were performed with the gravity feed injection, however, the water was injected into the bottom of the downcomer and the water injection rate was adjusted

to keep the downcomer water head constant. The overflow of the water in the downcomer was avoided to prevent from the condensation in the containment tank. The injection of the ECC water into the bottom of the downcomer resulted in the high subcooling of the fluid at the core inlet. The CCTF pressure effect tests, that is, the tests C1-5, C1-10 and C1-12, were performed with the ECC water injection into the cold legs similar with the actual PWR ECC injection system. The ECC water was heated because of the energy transfer with the steam flowing from the steam generator and the heat release from the superheated downcomer wall and resulted in the lower core inlet subcooling than those in the other tests. The CCTF FLECHT-coupling tests were performed under the similar test conditions with the FLECHT-SET Phase B1 tests. The ECC water was injected into the lower plenum, however, the ECC injection rate was kept constant instead of keeping the downcomer water head constant. Even though the test conditions of each test is different each other, the higher containment pressure results in the lower temperature rise and the faster quench in Fig. 6.

Even through the CCTF FLECHT-coupling tests were performed under the similar conditions with the FLECHT-SET Phase B1 tests, the sensitivity of the temperature rise and the quench time is less than that in the FLECHT-SET tests.

Figures 7(a) and (b) show the evaluated heat transfer coefficients from the temperature histories shown in Fig. 3 by solving the differential equation of the heat conduction of the heater rod. Figure 7(a) shows that the heat transfer coefficient in the 0.30 MPa test is higher than that in the 0.15 MPa test. This result is consistent with the privious researches. Because the quench front propagated faster in the 0.30 MPa test than in the 0.15 MPa test, the comparison of the heat transfer coefficient at the same time from the reflood start includes both effects induced by the different system pressure and the different distance from the quench front. Figure 7(b) shows the comparison of the heat transfer coefficients plotted versus the distance from the quench front using the data shown in Fig. 7(a). Figure 7(b) shows that the heat transfer coefficient increases as the quench front approaches and that the heat transfer coefficient in the 0.30 MPa test is higher than that in the 0.15 MPa test. This is attributed to the increase of the steam density with the system pressure.

3.2 System behavior

Figure 8 shows the comparison of the core and downcomer water heads between the 0.15 MPa (test C1-10) and 0.30 MPa (test C1-12) tests. The core water head in the 0.30 MPa test is about 9% higher than that in the 0.15 MPa test in the CCTF. While in the FLECHT-SET tests, about 70% higher core water head was observed in the 0.41 MPa test (Run 3105B) than that in the 0.15 MPa test Run 2714B).

In the FLECHT-SET Phase B1 tests, the ECC water was injected into the bottom of the downcomer and the fluid temperature at inlet was nearly the same as the ECC water temperature (340 K) in both tests. The subcooling of the fluid at the core inlet was 44 K and 76 K in the 0.15 MPa and the 0.41 MPa tests of the FLECHT-SET, respectively. The higher core inlet subcooling increases the core water head due to the incipience of the boiling at the higher elevation.[2][3]

On the other hand, the ECC water was injected into the cold legs in the CCTF tests similar to the actual PWR. The ECC water with the subcooling of 85 K was mixed with the steam from the steam generator and heated due to the energy transferred from the condensed steam. And it was also heated due to the heat release from the superheated downcomer wall which was not simulated in the FLECHT-SET tests. The core inlet subcooling was about 20∿5 K in both of the 0.30 and 0.15 MPa tests in the CCTF because the subcooled ECC water was heated due to the condensation of steam in the cold leg and the heat release from the downcomer wall.

It can be considered that the different sensitivity of the core water head on the containment pressure between the CCTF test and the FLECHT-SET is attributed to the difference of the ECC water injection method between both facilities.

Figure 8 shows that the higher containment pressure results in the higher downcomer water head before 60 s and the lower downcomer water head after 80 s. Just after the switching of the ECC injection mode from the Acc mode to the LPCI mode, the discrepancy between the tests becomes maximum and it decays by 60 s. This results suggests that the descrepancy between the tests is caused by the difference of the flow behavior in the Acc injection period and the transition period following the switching of the ECC injection mode from the Acc mode to the LPCI mode. At 20 s, the downcomer water head in the 0.30 MPa was higher by 4.6 kPa than that in the 0.15 MPa. The descrepancy is equivalent to the water mass of 72 kg in the CCTF downcomer because the cross-sectional flow area of the CCTF downcomer

is 0.197 m^2. As described later, the mass flowed from the downcomer to the core was 92 kg higher in the 0.30 MPa test than that in the 0.15 MPa test by 20 s because of the higher core inlet mass flow rate in the 0.30 MPa test. The overflowed mass flow rate through the broken cold leg was nearly equal to zero by 20 s in both tests. The water mass flow rate from the cold legs was slightly higher in the 0.30 MPa test than that in the 0.15 MPa test because of the slightly higher accumulator injection rate. It is supposed that the higher downcomer water head in the 0.30 MPa test than that in the 0.15 MPa test is caused by the slightly higher accumulator injection rate in the 0.30 MPa test than that in the 0.15 MPa test.

After the switching of the ECC injection mode, the increasing rate of the downcomer water head in the 0.30 MPa is smaller than that in the 0.15 MPa test. This resulted from the higher core inlet mass flow rate in the 0.30 MPa test than that in the 0.15 MPa test.

The saturated behavior of the downcomer water head starts at about 110 and 130 s in the 0.30 MPa and 0.15 MPa tests, respectively. After the time, it can be considered that the downcomer fluid is spilled over through the broken cold leg. The equivalent level of the bottom of the broken cold leg nozzle is lower in the 0.30 MPa than that in the 0.15 MPa because of the lower water density in the 0.30 MPa.

Figure 9 shows the comparison of the water head in the upper plenum between the 0.15 MPa (C1-10), 0.20 MPa (C1-5) and 0.30 MPa (C1-12) tests. The higher containment pressure resulted in the more water accumulation in the upper plenum as observed in the FLECHT-SET Phase B1 tests. It can be considered that the higher steam density at higher pressure resulted in the greater separation of the water in the upper plenum due to the lower steam velocity, as reported in the evaluation report of the FLECHT SET Phase B1 tests.[3]

Figure 10 shows the comparison of the pressure drop through the intact loop 2. Good synmetry of the differential pressure was observed among the three intact loops in the CCTF. The higher containment pressure results in the higher loop pressure drop before 60 s and the lower loop pressure drop after 80 s. The pressure drop through the intact loop ΔP_I is related to the downcomer water head ΔP_D, the core water head ΔP_C and the upper plenum water head ΔP_U by

$$\Delta P_I = \Delta P_D - \Delta P_C - \Delta P_U \qquad (1)$$

The higher pressure drop before 60 s is attributed to the higher downcomer water head. And the lower pressure drop after 80 s is caused by the lower downcomer water head, the higher core and upper-plenum water-heads at higher containment pressure.

After 130 s, the pressure chop through the intact loop is nearly constant with time in each test. The ΔP_I is about 24 kPa and 20.5 kPa in the 0.15 MPa and 0.30 MPa tests, respectively. ΔP_I in the 0.30 MPa is about 20% lower than that in the 0.15 MPa test.

Figure 11 shows the comparison of the pressure drop through the broken loop. The pressure drop through the broken loop ΔP_B is related to the pressure drop through the intact loop ΔP_I and the pressure drop through the broken cold leg ΔP_{BCL} by

$$\Delta P_B = \Delta P_I + \Delta P_{BCL} \tag{2}$$

In the FLECHT-SET Phase B1 tests, ΔP_{BCL} was small because of the ECC injection method. Then, ΔP_B was nearly equal to ΔP_I in the FLECHT-SET Phase B1 tests. In the CCTF tests, some water from the cold legs was overflowed through the broken cold leg and the great pressure drop through the broken cold leg was observed. Then, ΔP_B was a few times of ΔP_I in the CCTF test. The mass flow rate through the broken loop $\dot{m}_B$ is related to the steam density in the broken loop ρ_B, the flow area of the broken loop A_L and ΔP_B by

$$\dot{m}_B = A_L \cdot \sqrt{\frac{2\rho_B \Delta P_B}{K_B}} \quad . \tag{3}$$

The increase of ΔP_B results in the increase of the mass flow rate through the broken loop. ΔP_{BCL} also contributes to pressurize the loop pressure and results in the higher steam density. In the 0.15 MPa test, ΔP_B is about 2.9 time of ΔP_I and the steam density in the hot leg was about 25% higher than that estimated assuming that $\Delta P_{BCL} = 0$. It can be considered that $\dot{m}_B$ is increased about 90% by the effect of the pressure drop through the broken cold leg. In the 0.30 MPa test, the increase of $\dot{m}_B$ attributed to ΔP_{BCL} is estimated to be 52%. These results show that the increase of $\dot{m}_B$ due to ΔP_{BCL} is decreased with the containment pressure.

Figure 12 shows the comparisons of the core inlet mass flow rate and the core inlet mass flow between the 0.15 and 0.30 MPa tests. The core

inlet mass flow rate was calculated from the mass balance relation in the pressure vessel. The error of the evaluated core inlet mass flow rate was estimated to be 15% at most. The core inlet mass flow in Fig. 12 shows the integral of the evaluated core inlet mass flow rate.

Table 4 shows the comparison of the time-averaged core inlet mass flow rate among the 0.15 MPa (C1-10), 0.20 MPa (C1-5) and 0.30 MPa (C1-12) tests. The average core inlet mass flow rates between 0 and 20, 20 and 80, 80 and 300 s in the 0.30 MPa test are higher by 26%, 23% and 18% than those in the 0.15 MPa test, respectively. The differences between both tests are higher than the error in the estimation of the core inlet mass flow rate. Then, it can be concluded that the core inlet mass flow rate increases with the containment pressure in the CCTF. The same dependence of the core inlet mass flow rate on the containment pressure was observed in the FLECHT-SET results. They reported in the evaluation report of the FLECHT-SET Phase B1 tests that the core inlet mass flow rate in the 0.41 MPa test (Run 3105B) was 48% higher than that in the 0.15 MPa test (Run 2714B) after the high injection period, that is, in the LPCI injection period. It seems that the dependence of the core inlet mass flow rate on the containment pressure is less in the CCTF test than that in the FLECHT-SET Phase B1 tests.

The core inlet mass flow rate $\dot{m}_F$ is related to the water accumulation rate in the core $\dot{m}_C$, the water accumulation rate in the upper plenum $\dot{m}_U$ and the mass flow rate through the four primary loops $\dot{m}_L$ by the following equation:

$$\dot{m}_F = \dot{m}_C + \dot{m}_U + \dot{m}_L \quad , \tag{4}$$

where

$$\dot{m}_L = A_L \cdot \{ 3 + \sqrt{(1 + \frac{\Delta P_{BCL}}{\Delta P_I})} \} \sqrt{\frac{2\rho_{gI}\Delta P_I}{K_I}} \quad , \tag{5}$$

ρ_{gI}, K_I and A_L indicate the steam density in the intact loop, the flow resistance coefficient through the intact loop and the loop flow area. In the derivation of Eq. (5), it was assumed that the flow resistance coefficient through the broken loop is identical with those through the intact loops because the configulation of the broken loop is almost the same as that of the intact loops.

In the LPCI injection period, $\dot{m}_C$ and $\dot{m}_U$ were relatively small to $\dot{m}_L$. Hence, the increase of the core inlet mass flow rate with the containment

pressure is attributed mainly to the increase of $\dot{m}_L$.

In the FLECHT-SET tests, ΔP_{BCL} was nearly equal to zero. Then, the increase of $\dot{m}_L$ can be attributed to ρ_{gI} and ΔP_I. The steam density in the upper plenum is estimated to be 0.946 and 2.303 kg/m^3 in the 0.15 MPa and 0.41 MPa test, assuming that the steam in the upper plenum is in the saturated condition. The ratio of the steam density in the 0.41 MPa test to that in the 0.15 MPa test is 2.43. This ratio leads to 56% increase of the core inlet mass flow rate based on Eq. (5). ΔP_I in the FLECHT-SET tests was decreased with the containment pressure because the core water head was increased due to the higher core inlet subcooling at higher pressure test. This acts to reduce the core inlet mass flow rate with containment pressure based on Eq. (5) in the FLECHT SET.

In the CCTF tests, great ΔP_{BCL} was observed and it decreased with the containment pressure. And ΔP_{BCL} also caused the pressure vessel to be pressurized. The steam densities in the upper plenum were estimated to be 1.280 and 1.894 kg/m^3 in the 0.15 and 0.30 MPa tests, respectively. The estimated steam densities, assuming that $\Delta P_{BCL} = 0$, were 1.020 and 1.753 kg/m^3 in the 0.15 and 0.30 MPa tests, respectively. The ratio of steam densities are 1.480 and 1.719 in two cases. With the steam density ratio of 1.719, about 31% increase of $\dot{m}_L$ is expected through the contribution of ρ_{gI} in Eq. (5). On one hand, 22% increase of $\dot{m}_L$ is expected through the contribution of ρ_{gI} with the steam density ratio of 1.480. The containment pressure effect through the contribution of ρ_{gI} is weakened by the effect of ΔP_{BCL} in the CCTF test.

The ΔP_{BCL} affects the core inlet mass flow rate through the term of $\{3+\sqrt{1+(\Delta P_{BCL}/\Delta P_I)}\}$ in Eq. (5). This term indicates the effect of the ΔP_{BCL} through the pressure drop across the broken loop. As described by Eqs. (2) and (3), the increase of the ΔP_{BCL} results in the higher pressure drop through the broken loop and the mass flow rate through the broken loop. The values of $\{3+\sqrt{1+(\Delta P_{BCL}/\Delta P_I)}\}$ were about 4.74 and 4.53 in the LPCI injection period of the 0.15 and 0.30 MPa test. The higher value of the 0.15 MPa test is attributed mainly to the higher ΔP_{BCL} in the test. The higher value of $\{3+\sqrt{1+(\Delta P_{BCL}/\Delta P_I)}\}$ shows that the containment pressure effect on the core inlet mass flow rate, that is, the increase of the core inlet mass flow rate with the containment pressure is weakened by the

existence of ΔP_{BCL} in the CCTF, because ΔP_{BCL} was decreased with the containment pressure in the CCTF tests.

The effect of the containment pressure on the increase of the core inlet mass flow rate was less in the CCTF than that in the FLECHT-SET. The less sensitivity in the CCTF was attributed mainly to the great pressure drop through the broken cold leg, which was not observed in the FLECHT-SET with big broken cold leg.

4. CONCLUSION

Three tests C1-5 (Run 14), C1-10 (Run 19) and C1-12 (Run 21) were performed using the Cylindrical Core Test Facility to study the effect of the containment pressure on the core cooling and the system behaviors during the reflood phase of a PWR-LOCA. The containment pressures of these tests were 0.15, 0.20 and 0.30 MPa for the tests C1-10, C1-5 and C1-12, respectively. Through the comparison of the test results from these three tests, the following results were obtained.

(1) The higher containment pressure gave the higher heat transfer coefficient in the core. This resulted in the lower turnaround temperature, the shorter turnaround time and the shorter quench time at the higher containment pressure.

(2) In the higher containment pressure test, the higher core water head, the higher upper plenum water head, the higher downcomer water head in the early period and the lower downcomer water head in the later period were observed than those in the lower containment pressure test. This resulted in the higher pressure drop through the intact loop in the early period of the tests and the lower pressure drop in the later period of the test with the containment pressure.

(3) The pressure drop through the broken cold leg pressurized the primary system. The pressure drop through the broken cold leg was decreased with the containment pressure.

(4) The core inlet mass flow rate was increased with the containment pressure as observed in the FLECHT-SET phase B1 test. In quantity, however, the effect of the containment pressure on the increase of the core inlet mass flow rate was less in the CCTF than that in the FLECHT-SET. The less sensitivity in the CCTF was attributed mainly to the great pressure drop through the broken cold leg, which was not observed in the FLECHT-SET with big broken cold leg.

(5) The system effect of the containment pressure was explained quantitatively with Eqs. (4) and (5).

Acknowledgement

The authors are much indebted to Messrs. T. Sudoh, T. Iguchi, J. Sugimoto and T. Okubo for their technical support and valuable discussions. We would like to express our thanks to Dr. M. Nozawa, Deputy director general of Tokai Research Establishment, Dr. S. Katuragi, Director of Nuclear Research Center, Dr. Hirata, Director of Reactor Safety Department, and Dr. K. Hirano, Deputy Director of Reactor Safety Department, for their guidance and encouragement for this program.

References

(1) Sawan, M.E. and Carbon, M.W. : Nucl. Eng. Des. 32, pp.191-207, (1975).
(2) Lilly, G.P. et al. : WCAP-8838, (1977).
(3) Waring, J.P. and Hochreiter, L.E. : WCAP-8583, (1975).
(4) Murao, Y. et al. : J. Nucl. Sci. and Technol. 19[9], pp.705-719, (1982).

Acknowledgement

The authors are much indebted to Messrs. T. Sudoh, T. Iguchi, J. Sugimoto and T. Okubo for their technical support and valuable discussions. We would like to express our thanks to Dr. M. Nozawa, Deputy director general of Tokai Research Establishment, Dr. S. Katuragi, Director of Nuclear Research Center, Dr. Hirata, Director of Reactor Safety Department, and Dr. K. Hirano, Deputy Director of Reactor Safety Department, for their guidance and encouragement for this program.

References

(1) Sawan, M.E. and Carbon, M.W. : Nucl. Eng. Des. 32, pp.191-207, (1975).
(2) Lilly, G.P. et al. : WCAP-8838, (1977).
(3) Waring, J.P. and Hochreiter, L.E. : WCAP-8583, (1975).
(4) Murao, Y. et al. : J. Nucl. Sci. and Technol. 19[9], pp.705-719, (1982).

Table 1 Main dimensions of the Cylindrical Core Test Facility.

COMPONENT		PWR	JAERI	RATIO
PRESSURE VESSEL				
VESSEL INSIDE DIAMETER	(mm)	4394 (173")	1084	
VESSEL THICKNESS	(mm)	216 (8 1/2")	90	
CORE BARREL OUTSIDE DIAMETER	(mm)	3974	961	
CORE BARREL INSIDE DIAMETER	(mm)	3760	929	
THERMAL SHIELD OUTSIDE DIAMETER	(mm)	4170		
THERMAL SHIELD INSIDE DIAMETER	(mm)	4030		
DOWNCOMER LENGTH	(mm)	4849	4849	1/1
DOWNCOMER GAP	(mm)	114.3	61.5	
DOWNCOMER FLOW AREA	(m^2)	4.23	0.197	1/21.44
LOWER PLENUM VOLUME	(m^3)	29.6	1.38	1/21.44
UPPER PLENUM VOLUME	(m^3)	43.6	2.04	1/21.44
FUEL (HEATER ROD) ASSEMBLY				
NUMBER OF BUNDLES	(—)	193	32	
ROD ARRAY	(—)	15 × 15	8 × 8	
ROD HEATED LENGTH	(mm)	3660	3660	1/1
ROD PITCH	(mm)	14.3	14.3	1/1
FUEL ROD OUTSIDE DIAMETER	(mm)	10.72	10.7	1/1
THIMBLE TUBE DLAMETER	(mm)	13.87	13.8	1/1
INSTRUMENT TUBE DIAMETER	(mm)	13.87	13.8	1/1
NUMBER OF HEATER RODS	(—)	39372	1824	1/21.58
NUMBER OF NON-HEATED RODS	(—)	4053	224	1/18.09
CORE FLOW AREA	(m^2)	5.29	0.25	1/21.2
CORE FLUID VOLUME	(m^3)	17.95	0.915	1/19.6
PRIMARY LOOP				
HOT LEG INSIDE DIAMETER	(mm)	736.6 (29")	155.2	1/4.75
HOT LEG FLOW AREA	(m^2)	0.426	0.019	1/22.54
HOT LEG LENGTH	(mm)	3940	3940	1/1
PUMP SUCTION INSIDE DIAMETER	(mm)	787.4 (31")	155.2	1/5.07
PUMP SUCTION FLOW AREA	(m^2)	0.487	0.019	1/25.77
PUMP SUCTION LENGTH	(mm)	7950	7950	1/1

Table 1 - (cont'd)

COMPONENT		PWR	JAERI	RATIO
COLD LEG INSIDE DIAMETER	(mm)	698.5 (27.5")	155.2	1/4.50
COLD LEG FLOW AREA	(m^2)	0.383	0.019	1/20.26
COLD LEG LENGTH	(mm)	5600	5600	1/1
STEAM GENERATOR SIMULATOR				
NUMBER OF TUBES	(—)	3388	158	1/21.44
TUBE LENGTH (AVERAGE)	(m)	20.5	15.2	1/1.35
TUBE OUTSIDE DIAMETER	(mm)	22.225 (0.875")	25.4	
TUBE INSIDE DIAMETER	(mm)	19.7 (0.05")	19.6	1/1
TUBE WALL THICKNESS	(mm)	1.27	2.9	
HEAT TRANSFER AREA	(m^2)	4784 (51500 ft^2)	192	1/24.92
TUBE FLOW AREA	(m^2)	1.03	0.048	1/21.44
INLET PLENUM VOLUME	(m^3)	4.25	0.198	1/21.44
OUTLET PLENUM VOLUME	(m^3)	4.25	0.198	1/21.44
PRIMARY SIDE VOLUME	(m^3)	30.50 (1077 ft^3)	1.2	1/25.41
SECONDARY SIDE VOLUME	(m^3)	157.33 (5556 ft^3)	2.5	1/62.93
CONTAINMENT TANK - I	(m^3)		30	
CONTAINMENT TANK - II	(m^3)		50	
STORAGE TANK	(m^3)		25	
ACC. TANK	(m^3)		5	
SATURATED WATER TANK	(m^3)		3.5	
ELEVATION				
BOTTOM OF HEATED REGION IN CORE	(mm)	0	0	
TOP OF HEATED REGION IN CORE	(mm)	3660	3660	0
TOP OF DOWNCOMER	(mm)	4849	4849	0
BOTTOM OF DOWNCOMER	(mm)	0	0	0
CENTERLINE OF COLD LEG	(mm)	5198	4927	- 271
BOTTOM OF COLD LEG (INSIDE)	(mm)	4849	4849	0
CENTERLINE OF LOOP SEAL LOWER END	(mm)	2056	2047	- 9
BOTTOM OF LOOP SEAL LOWER END	(mm)	1662	1959	+ 297

Table 1 (cont'd)

COMPONENT		PWR	JAERI	RATIO
CENTER OF HOT LEG	(mm)	5198	4927	- 271
BOTTOM OF HOT LEG (INSIDE)	(mm)	4830	4849	+ 19
BOTTOM OF UPPER CORE PLATE	(mm)	3957	3957	0
TOP OF LOWER CORE PLATE	(mm)	- 108	- 50	+ 58
BOTTOM OF TUBE SHEET OF STEAM GENERATOR SIMULATOR	(mm)	7308	7307	- 1
LOWER END OF STEAM GENERATOR SIMULATOR PLENUM	(mm)	5713	5712	- 1
TOP OF TUBES OF STEAM GENERATOR SIMULATOR (avg)	(mm)	17952.7	14820	

Table 2 Comparisons of the measured test conditions among the tests C1-5, C1-10 and C1-12.

Item	Test C1-10	Test C1-5	Test C1-12
Total power (MW)	9.39	9.36	9.40
Averaged linear power (kW/m)	1.41	1.40	1.41
Radial power distribution	1.15:1.08:0.88	1.16:1.08:0.89	1.15:1.08:0.88
Containment pressure (MPa)	0.152	0.195	0.299
Initial superheat of downcomer wall (K)	60	63	57
Primary piping wall temperature (K)	388	393	406
SG secondary side temperature (K)	540	535	538
Peak clad temperature			
at ECC injection (K)	802	775	797
at reflood initiation (K)	879	888	874
Lower plenum fluid temperature (K)	379	387	399
ECC water temperature (K)	312	312	313
Lower plenum water level (m)	0.89	0.87	0.86
SG secondary side water level (m)	7.3	7.3	7.4
Acc injection rate (m^3/s)	7.47×10^{-2}	7.72×10^{-2}	8.02×10^{-2}
LPCI injection rate (m^3/s)	8.44×10^{-3}	8.39×10^{-3}	8.52×10^{-3}

Table 3 Comparisons of test conditions of the FLECHT LOW FLOODING TEST, the FLECHT SET Phase B1 tests, the CCTF pressure effect tests and the CCTF FLECHT-coupling tests

Item \ Test name	FLECHT LOW FLOODING TEST	FLECHT-SET Phase B1 test	CCTF pressure effect tests	CCTF FLECHT-coupling tests
Peak power (kW/m)	3.12	2.76	2.66	2.80
Initial clad surface temperature (K)	1144	866	880	866
Core inlet subcooling(*) (K)	77.8	43 (0.15 MPa) 78 (0.41 MPa)	12	54 (0.15 MPa) 74 (0.41 MPa)
Core inlet velocity(*) (m/s)	2.03	∿1.89(0.15 MPa) ∿2.78(0.41 MPa)	∿2.05(0.15 MPa) ∿2.47(0.30 MPa)	∿2.2 (0.15 MPa) ∿3.5 (0.41 MPa)
Water supply method	Forced-feed	Gravity-feed	Gravity-feed	Gravity-feed
Injection location of ECC water	Lower plenum	Downcomer (Bottom)	Cold leg	Lower plenum

(*) Time averaged value in the LPCI injection period

Table 4 Comparison of the time-averaged core inlet mass flow rate among the tests C1-5, C1-10 and C1-12

Averaging period \ Test name	Test C1-10 (P = 0.15 MPa)	Test C1-5 (P = 0.20 MPa)	Test C1-12 (P = 0.30 MPa)
0 ∿ 20 (seconds)	13.76	16.25	17.39
20 ∿ 80 (seconds)	5.29	5.88	6.49
80 ∿ 300 (seconds)	5.02	5.28	5.94

note: The unit of the core inlet mass flow rates is kg/s

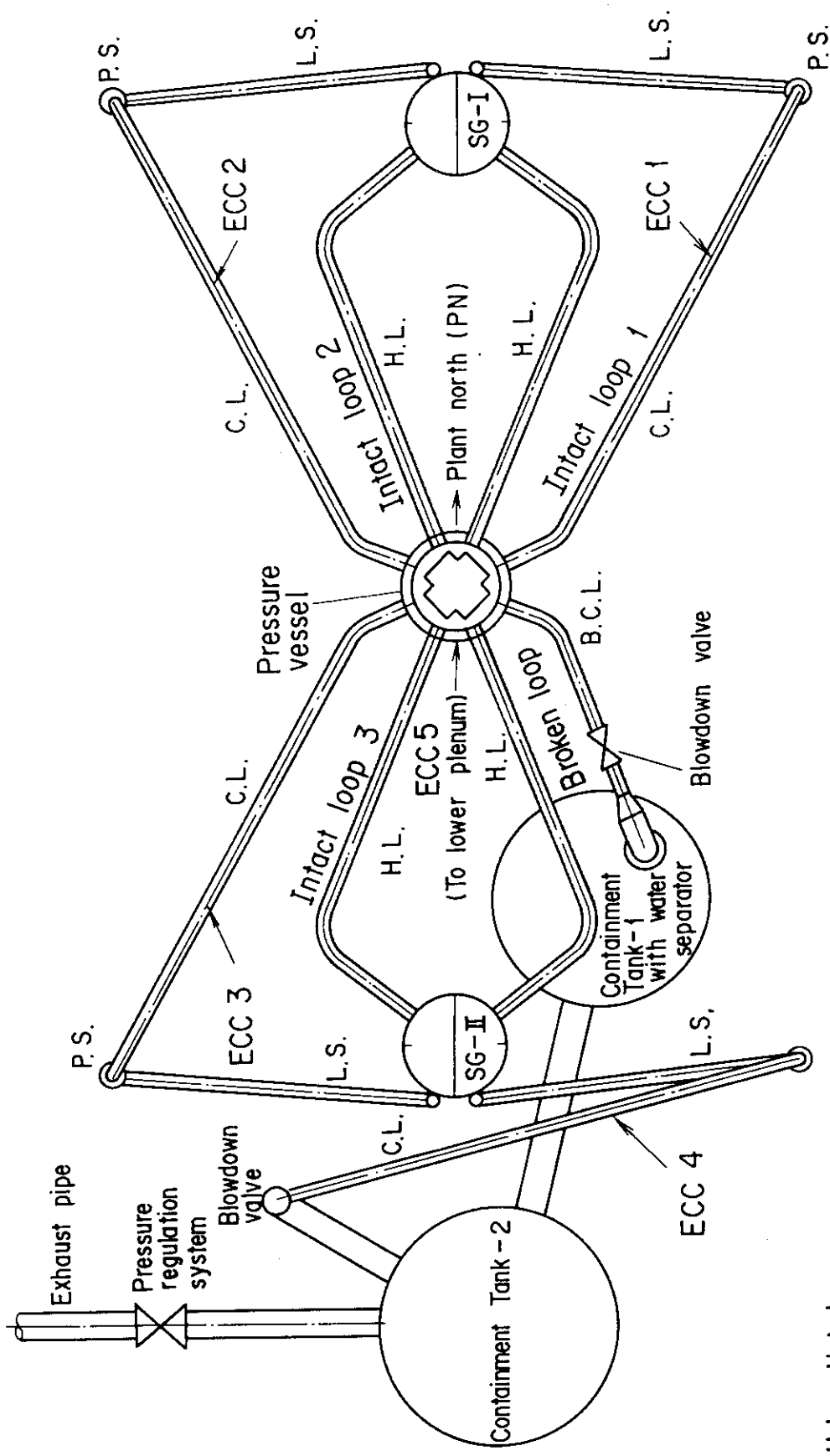

H.L. : Hot leg
S.G. : Steam generator
L.S. : Loop seal
P.S. : Pump simulator
C.L. : Cold leg

Fig. 1 Schematic of the Cylindrical Core Test Facility.

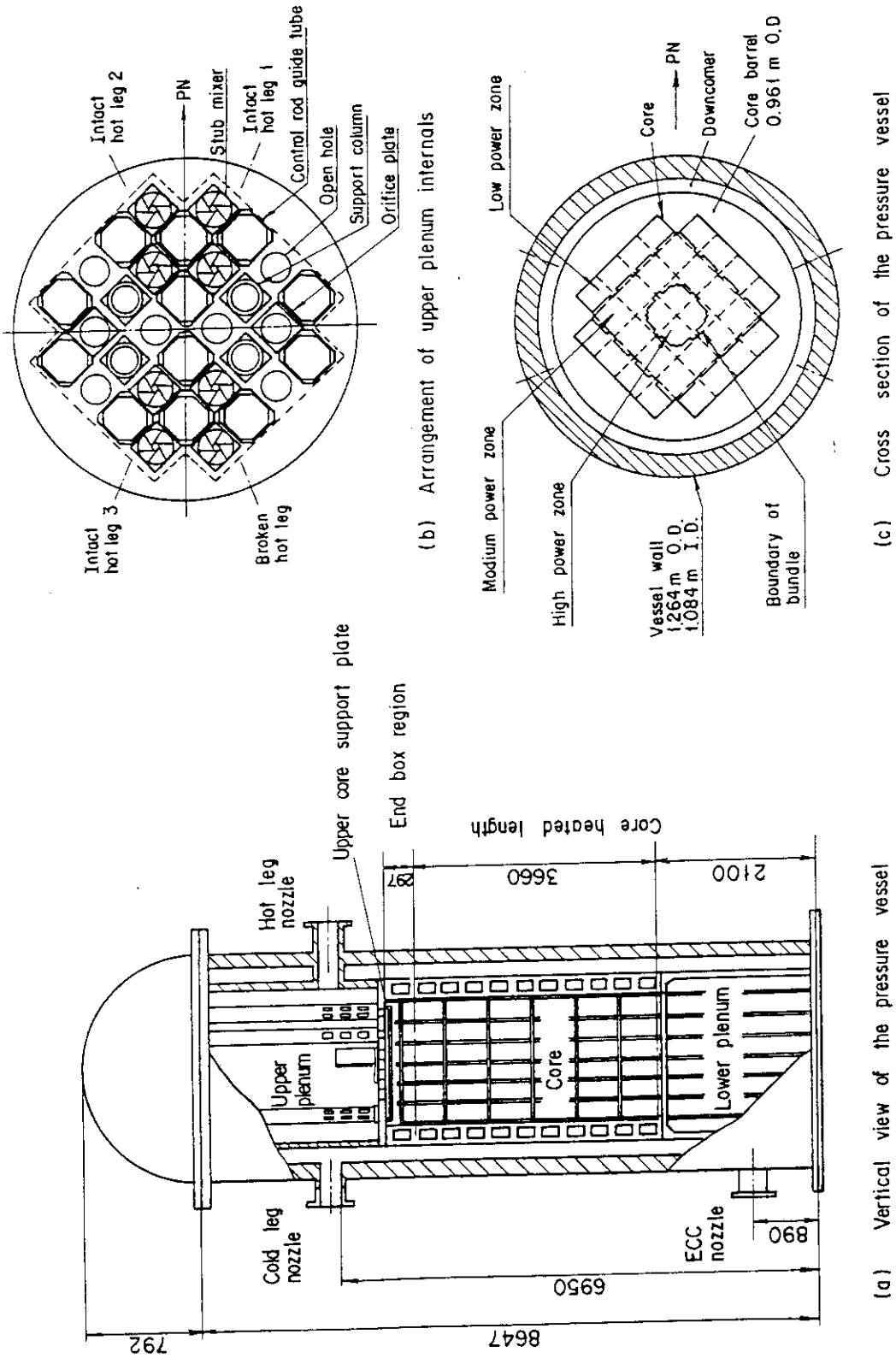

Fig. 2 Schematic of the pressure vessel of the Cylindrical Core Test Facility.

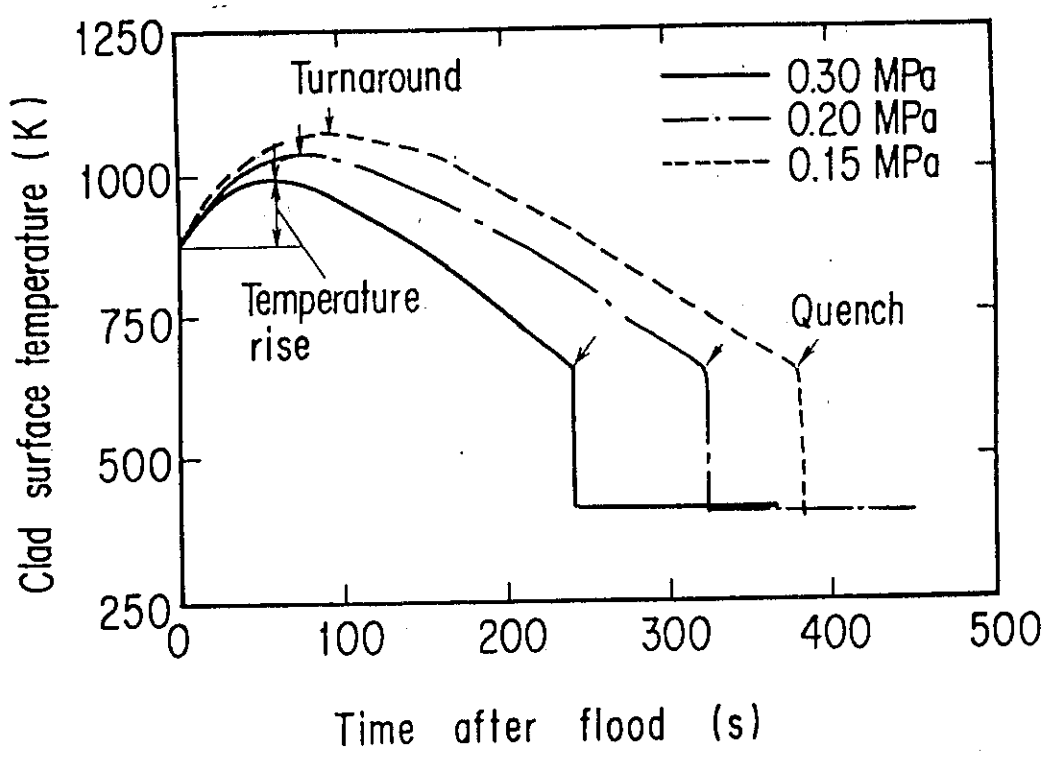

Fig. 3 Comparison of the clad surface temperature at the midplane of a peak power rod.

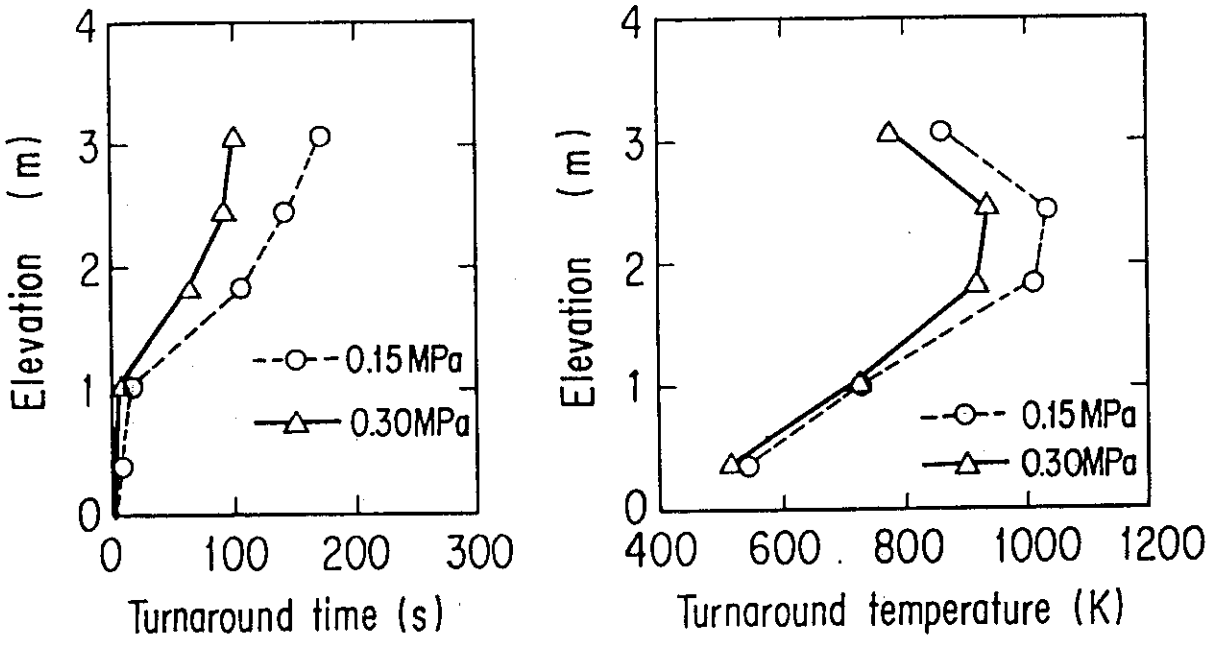

Fig. 4 Containment pressure effect on the turnaround time and temperature along the average power rods.

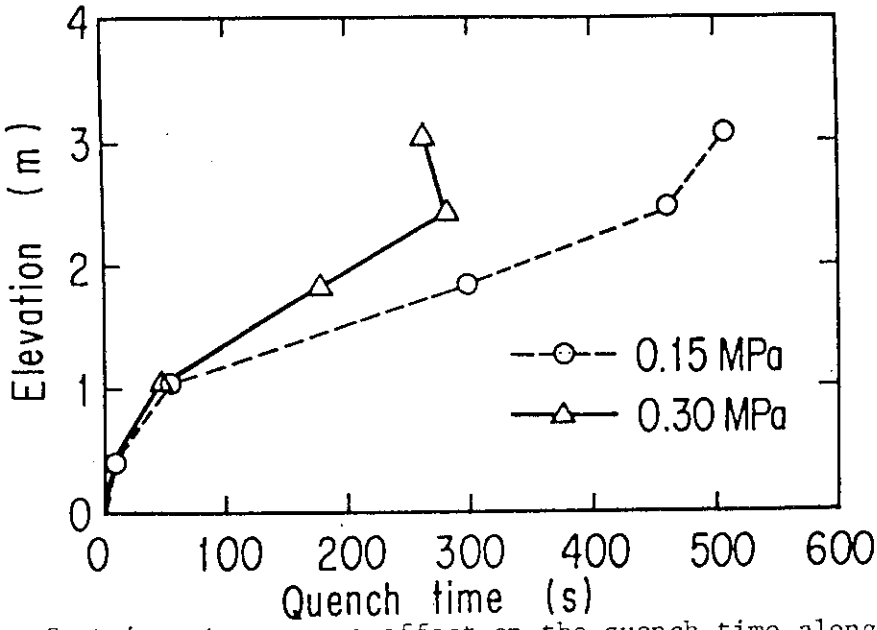

Fig. 5 Containment pressure effect on the quench time along the average power rods.

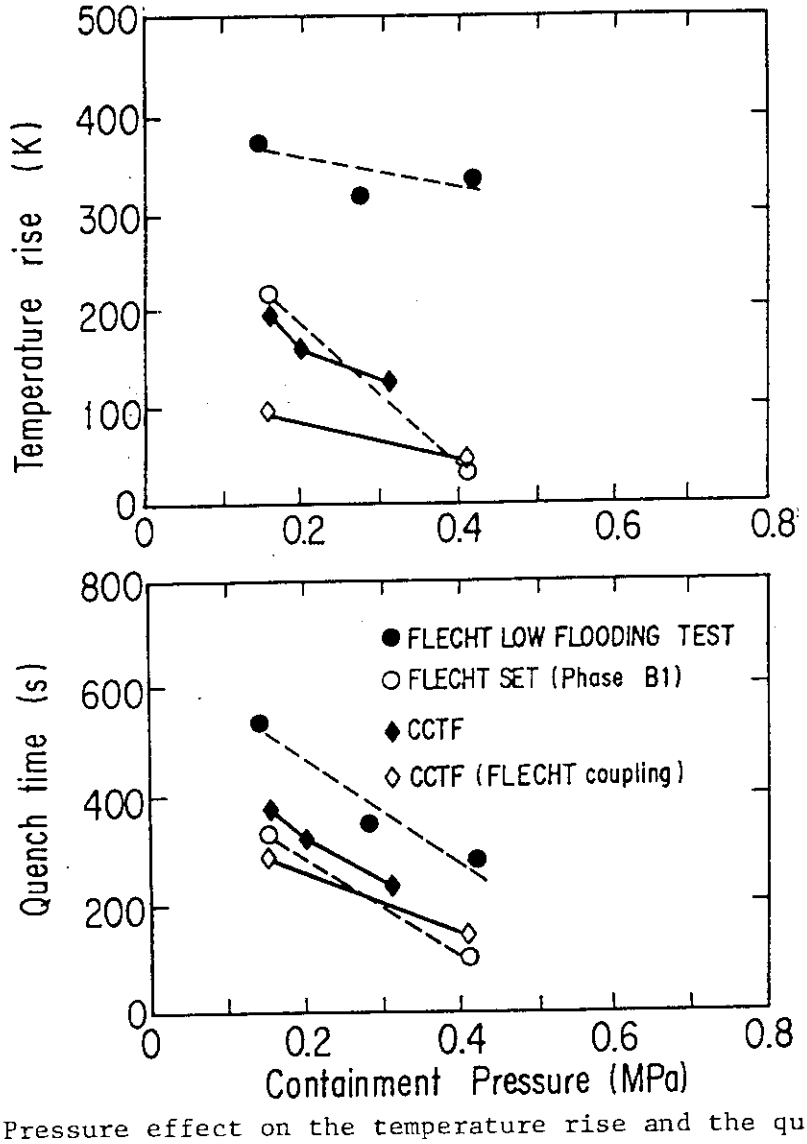

Fig. 6 Pressure effect on the temperature rise and the quench time at the midplane of the peak power rod in the CCTF, the FLECHT-SET and the FLECHT LOW FLOODING TEST.

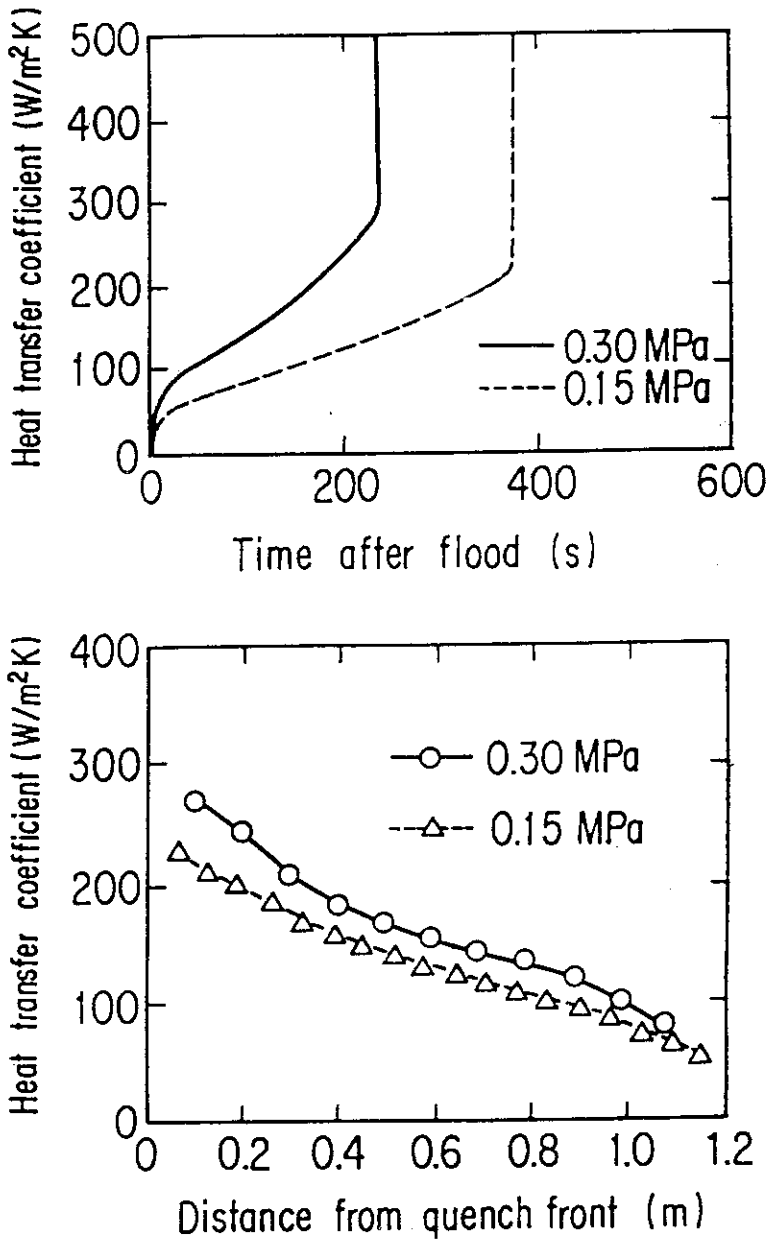

Fig. 7 Containment pressure effect on the heat transfer coefficient.

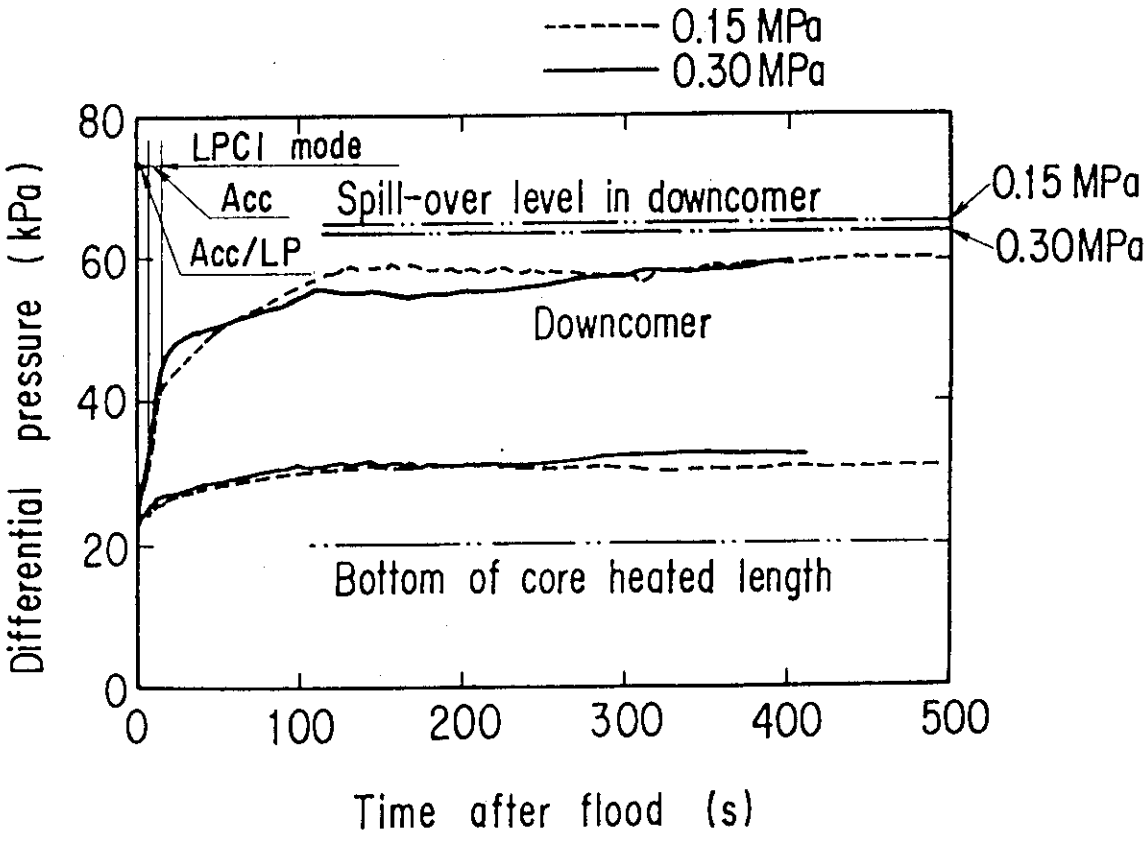

Fig. 8 Comparison of the core and downcomer water-heads between the 0.15 and 0.30 MPa tests.

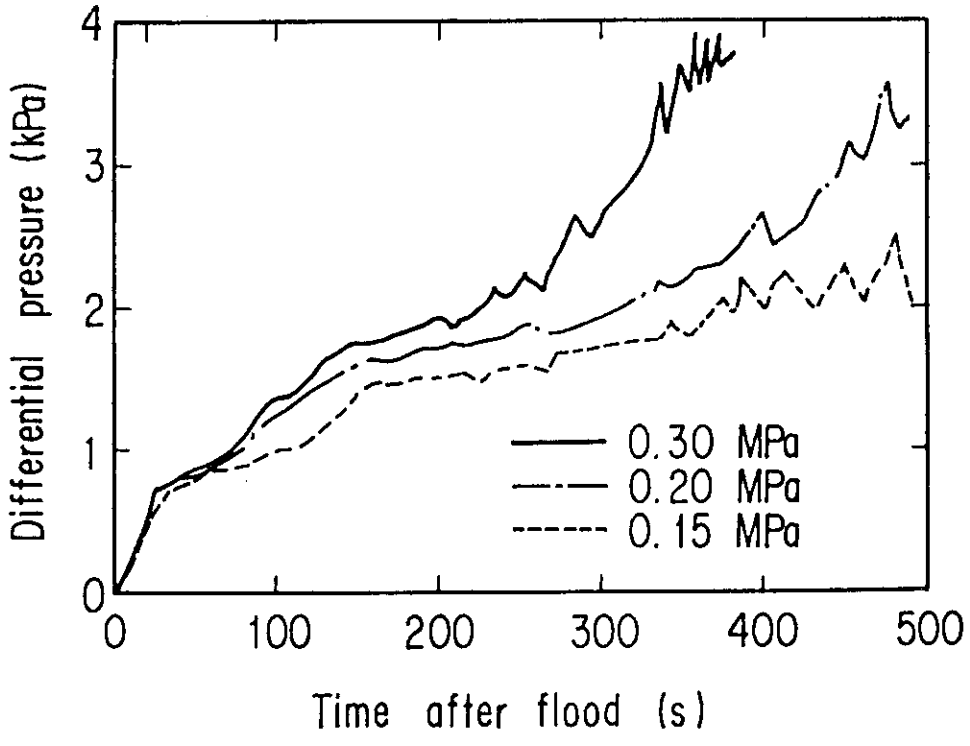

Fig. 9 Comparison of the upper plenum water head in the upper plenum between the 0.15, 0.20 and 0.30 MPa tests.

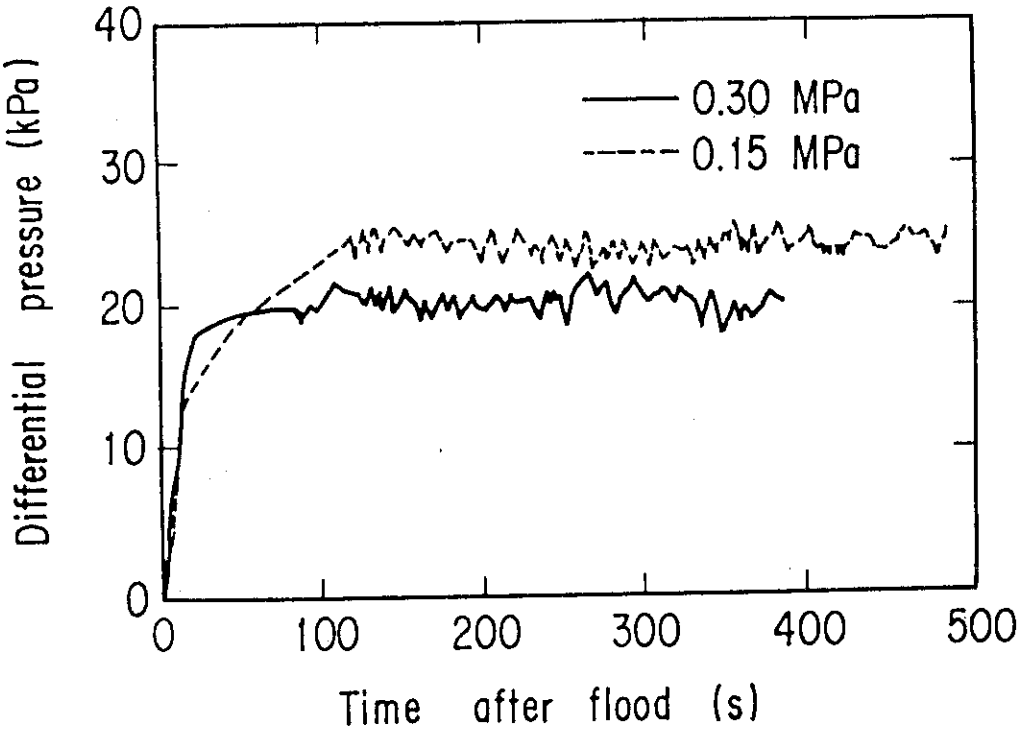

Fig. 10 Comparison of the pressure drop through the intact loop between the 0.15 and 0.30 MPa tests.

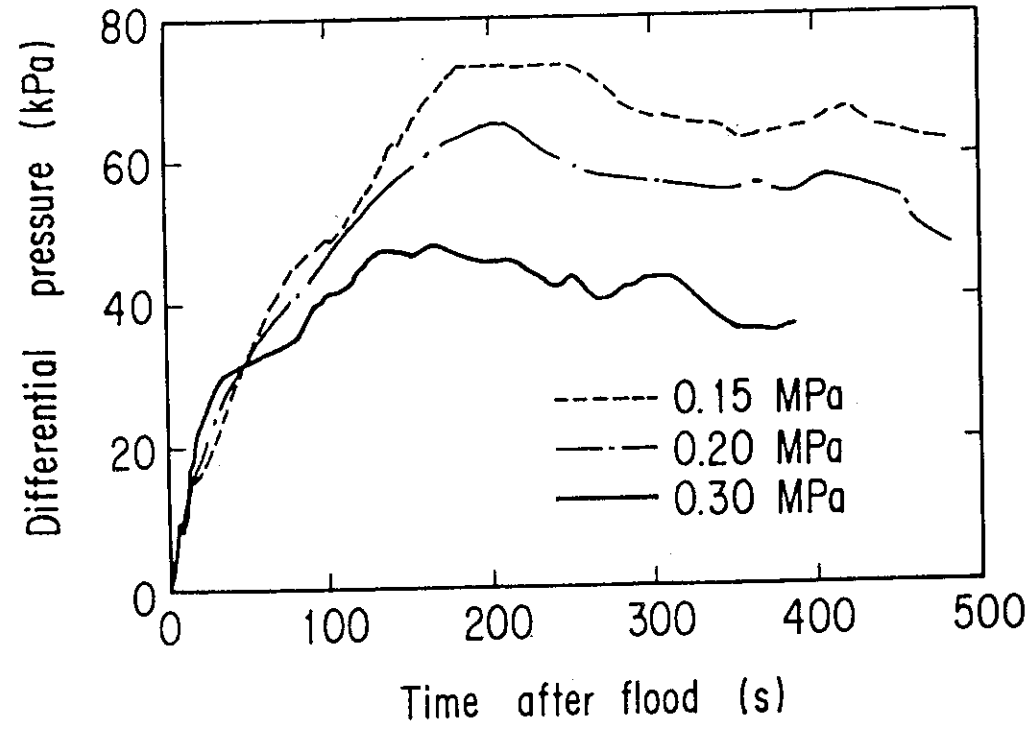

Fig. 11 Comparison of the pressure drop through the broken loop between the 0.15 and 0.30 MPa tests.

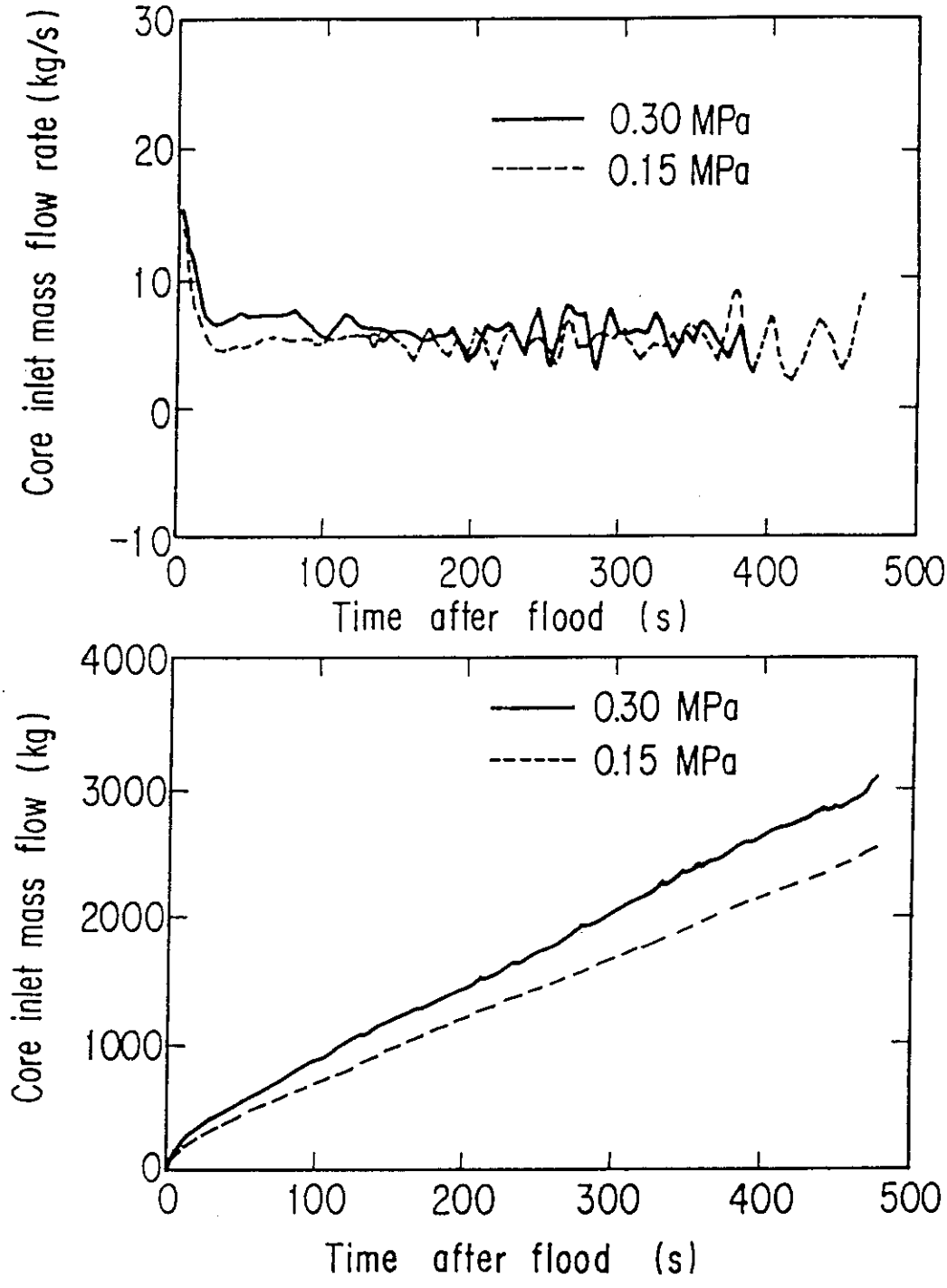

Fig. 12 Comparison of the core inlet mass flow rate and the core inlet mass flow between the 0.15 and 0.30 MPa test.

Appendix A

Definition of Tag. IDs in Appendix B through Appendix D

Figure list

1. Definition of Tag.ID for clad surface temperatures

Notation : TENNWAM

NN : Bundle number

WA : Power zone

WA = X1, X2 : High power (Local power factor 1.1)

WA = Y1, Y2 : Medium power (Local power factor 1.0)

WA = Z1, Z2 : Low power (Local power factor 0.95)

M : Elevation

	Elevation (m)	Axial power factor
1	0.38	0.568
2	1.015	1.176
3	1.83	1.492
4	2.44	1.312
5	3.05	0.815

2. Definition of power zone and bundle number

See Fig. A-1

3. Definition of Tag.ID for void fraction

See Fig. A-2

4. Definition of Tag.ID for average linear power of heater rod in each power unit zone

See Fig. A-3

5. Definition of carry-over rate fraction (C.R.F)

$$CRF = \frac{\dot{m}_{UP} + \dot{m}_{L}}{\dot{m}_{CR} + \dot{m}_{UP} + \dot{m}_{L}}$$

The calculated data within ±25 s are averaged:

$$(CRF)_i = \frac{1}{101} \sum_{k=i-50}^{i+50} (CRF)_k$$

where

ΔP_{UP} : Average of measured data at four orientations

ΔP_{CR} : Same as above

$$\dot{m}_{UP} = A_{up} \frac{d}{dt} (\Delta P_{UP})$$

$$\dot{m}_{CR} = A_{CR} \frac{d}{dt} (\Delta P_{CR})$$

$$\dot{m}_L = \sum_{k=1}^{4} \dot{m}_{pk}$$

$\dot{m}$: mass flow rate or mass accumulation rate

ΔP: differential pressure

suffix

UP: upper plenum

CR: core

L : loop

p : primary pump

6. Definition of Tag.ID for differential pressure through downcomer, upper plenum, core and lower plenum

   See Fig. A-4

7. Definition of Tag.ID for differential pressure through intact and broken loop and broken cold leg nozzle

   See Fig. A-5

8. Definition of Tag.ID for fluid temperature in inlet and outlet plenum and secondary of steam generator

   See Fig. A-6

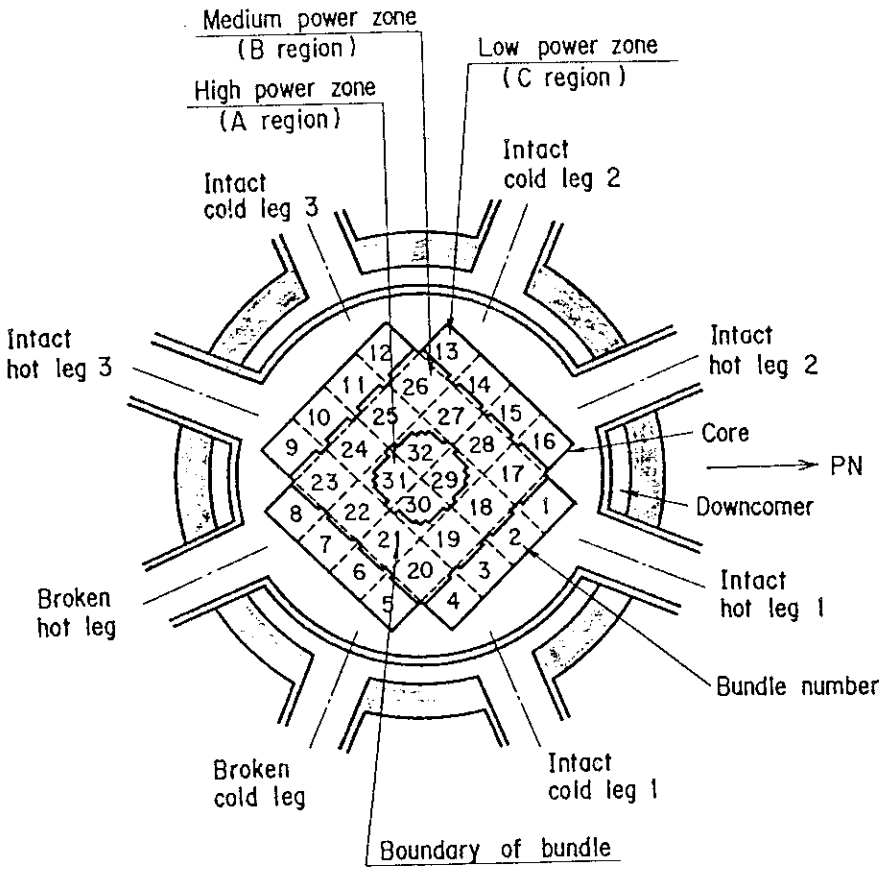

Fig.A-1 Definition of power zones and bundle numbers

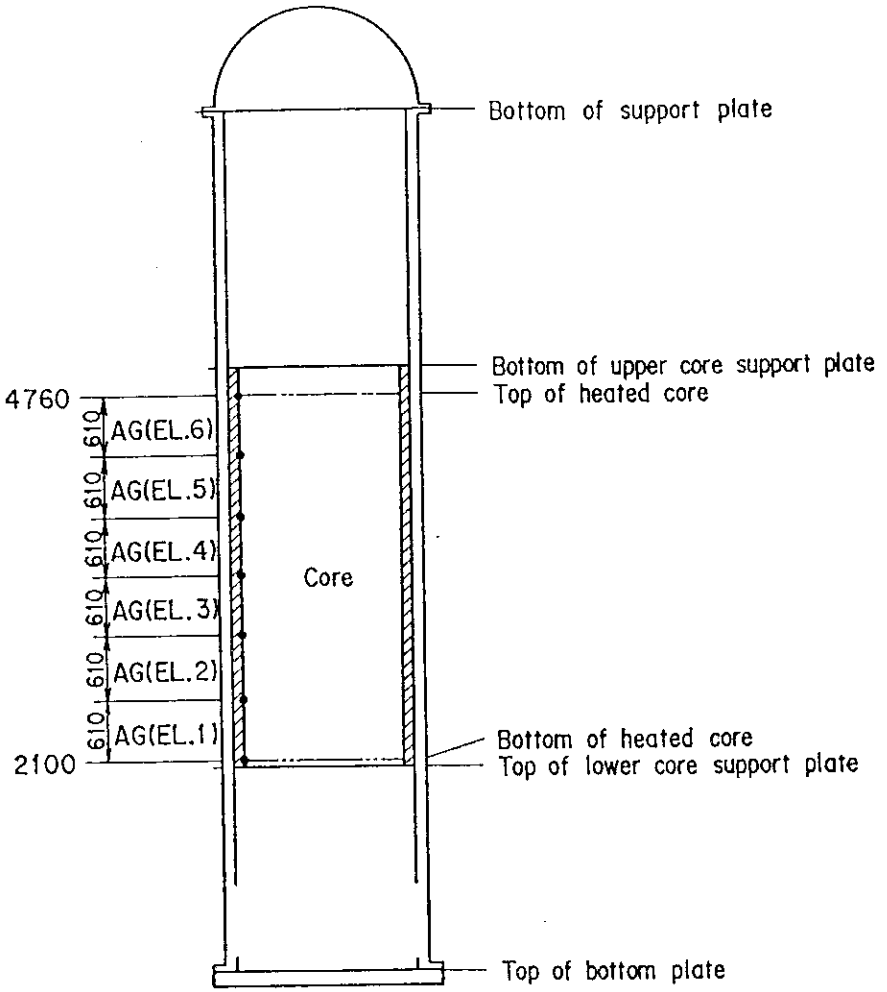

Fig.A-2 Definition of Tag.ID for void fraction (AG(EL.1)～AG(EL.6))

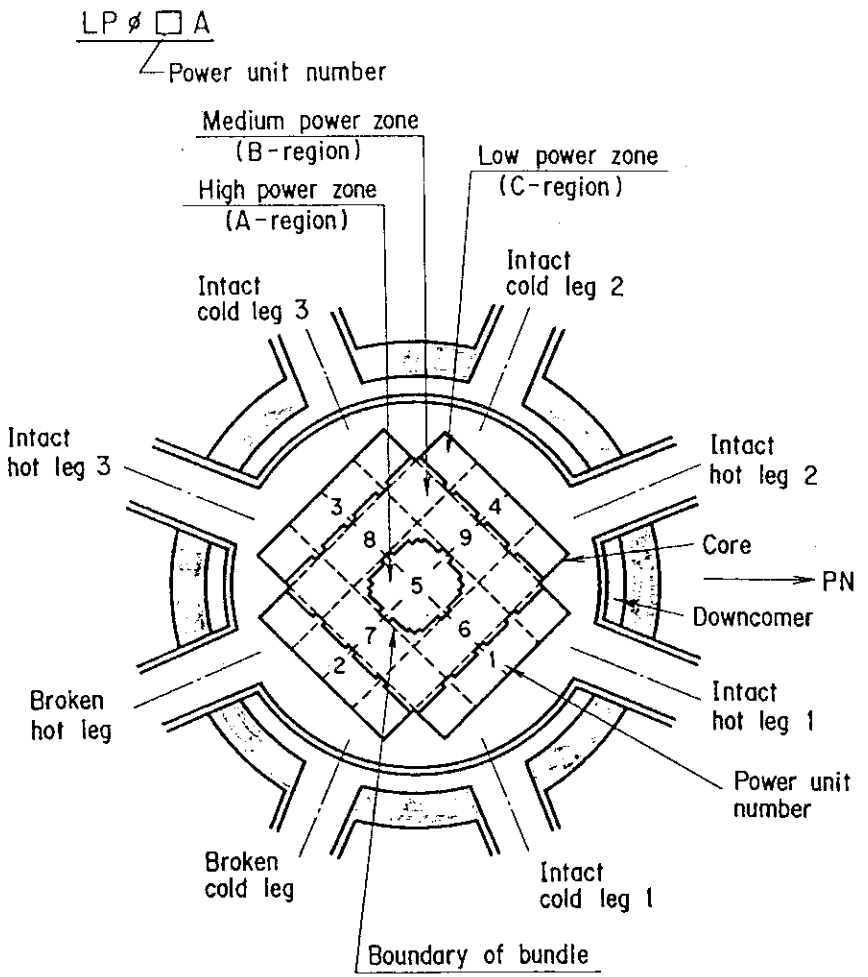

Fig. A-3 Definition of Tag. ID for average linear power of heater rod in each power unit zone (LP01A ~ LP09A)

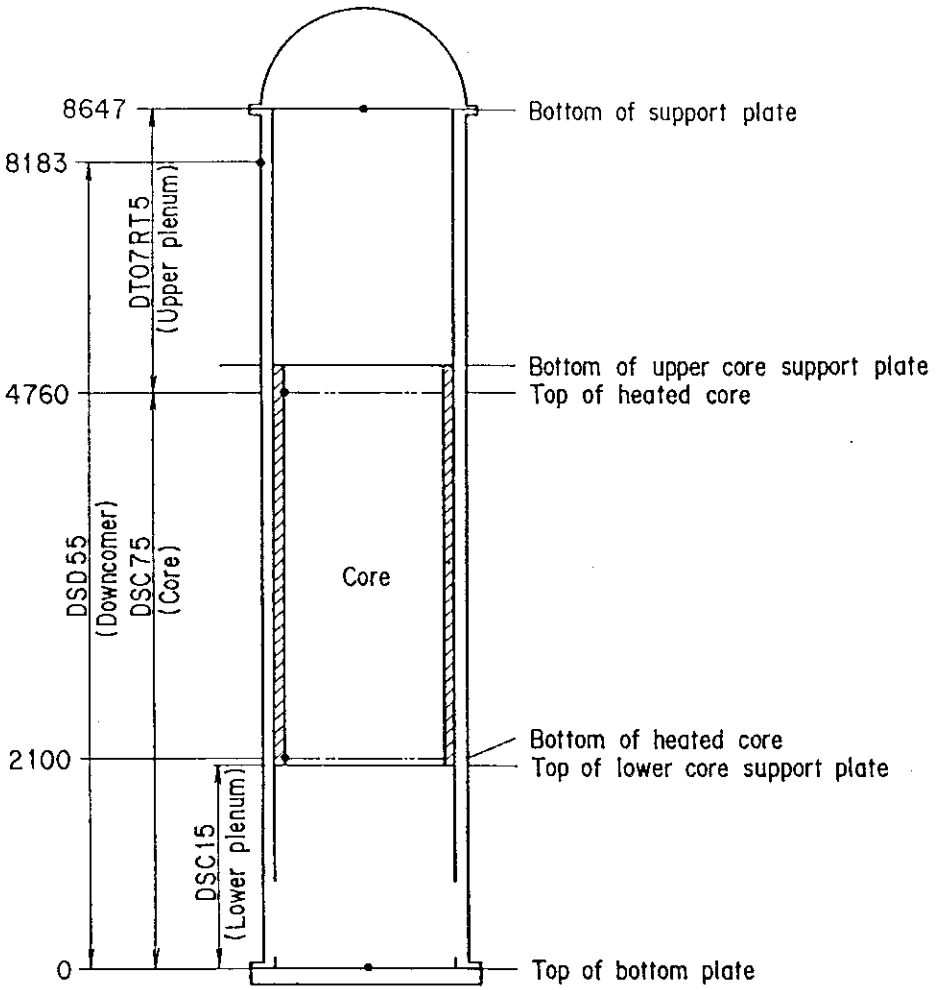

Fig. A-4 Definition of Tag. ID for differential pressure through downcomer, upper plenum, core, and lower plenum (DSD55, DT07RT5, DSC75, DSC15)

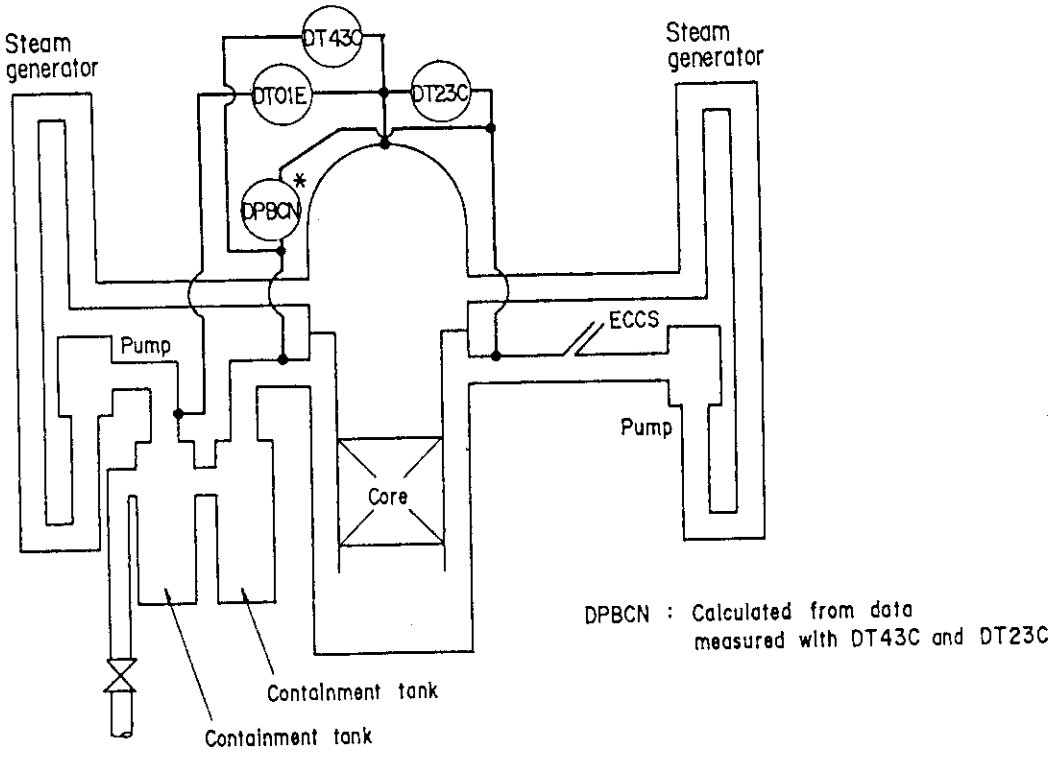

Fig. A-5 Definition of Tag. ID for differential pressure through intact and broken loop and broken cold leg nozzle (DT23C, DT01B, DPBCN)

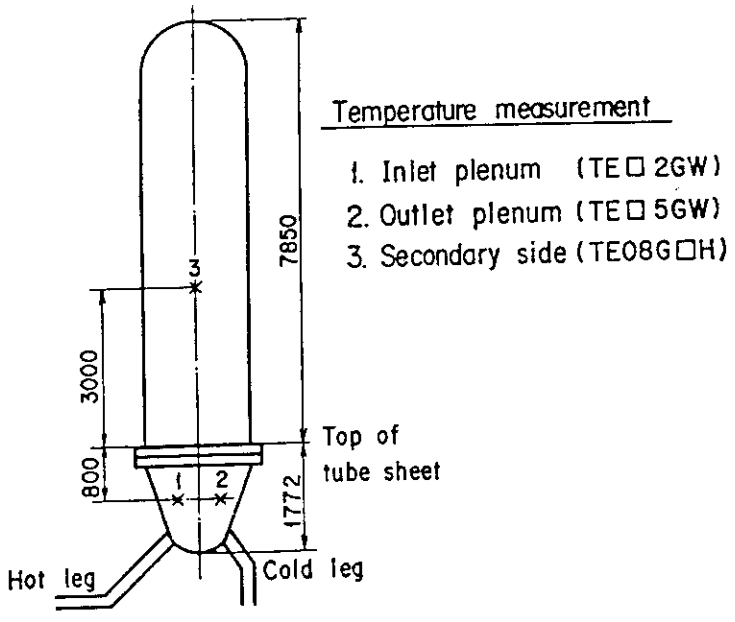

Fig. A-6 Definition of Tag. ID for fluid temperature in inlet and outlet plenum and secondary of steam generator (TE□2GW, TE□5GW, TE08G□H)

Appendix B

Main results of Test C1-5 (Run 14)

Table and Figure List

Table B-1 Summary of test conditions

1. TEST TYPE : Low System Pressure Test
2. TEST NUMBER : RUN 019 3. DATE : Dec.20, 1979
4. POWER : A: TOTAL: 9.39 MW; B:LINEAR: 1.4 KW/M
5. RELATIVE RADIAL POWER SHAPE :

   A: ZONE: A B C

   B: RATIO: 1.07 : 1.0 : 0.82
6. AXIAL POWER SHAPE : CHOPPED COSINE
7. PRESSURE (KG/CM^2A) :

   A: SYSTEM: 1.57, B: CONTAINMENT 1.55,

   C: STEAM GENERATOR SECONDARY: 54
8. TEMPERATURE (DEG.C) :

   A: DOWNCOMER WALL 172, B: VESSEL INTERNALS 108,

   C: PRIMARY PIPING WALL 115, D: LOWER PELNUM LIQUID 106,

   E: ECC LIQUID 39, F: STEAM GENERATOR SECONDARY 267,

   G: CORE TEMPERATURE AT ECC INITIATION 529
9. ECC INJECTION TYPE: C

   A: COLD LEG, B: LOWER PLENUM, C: LOWER PLENUM + COLD LEG
10. PUMP K-FACTOR : ~15
11. ECC FLOW RATES AND DURATION :

    A: ACCUMULATOR 269 M^3/HR FROM 0 TO 23 SECONDS

    B: LPCI 30.4 M^3/HR FROM 23 TO 858 SECONDS

    C: ECC INJECTION TO LOWER PLENUM : FROM 0 TO 17.5 SECONDS

    (VALVE OPENING AND CLOSING TIMES ARE INCLUDED IN THE INJECTION DURATION)
12. INITIAL WATER LEVEL IN LOWER PLENUM : 0.89 M.
13. POWER CONTROL : ANS x 1.2 + ACTINIDE (30 SEC AFTER SCRAM)
14. EXPECTED BOCREC TIME FROM ECC INITIATION 12 , SEC
15. EXPECTED PEAK TEMPERATURE AT BOCREC 600 C

Table B-2 Chronology of events

EVENT	TIME (sec)
Test Initiated (Heater Rods Power on) (Data Recording Initiated)	0.0
Accumulator Injection Initiated	55
Power Decay Initiated (Bottom of Core Recovery)	66.5
Accumulator Injection Switched from Lower Plenum to Cold Leg	72.5
Accumulator Injection Ended and LPCI Injection Initiated	78
All Heater Rods Quenched	695
Power Off	770
LPCI Injection Ended	858
Test Ended (Data Recording Ended)	1071

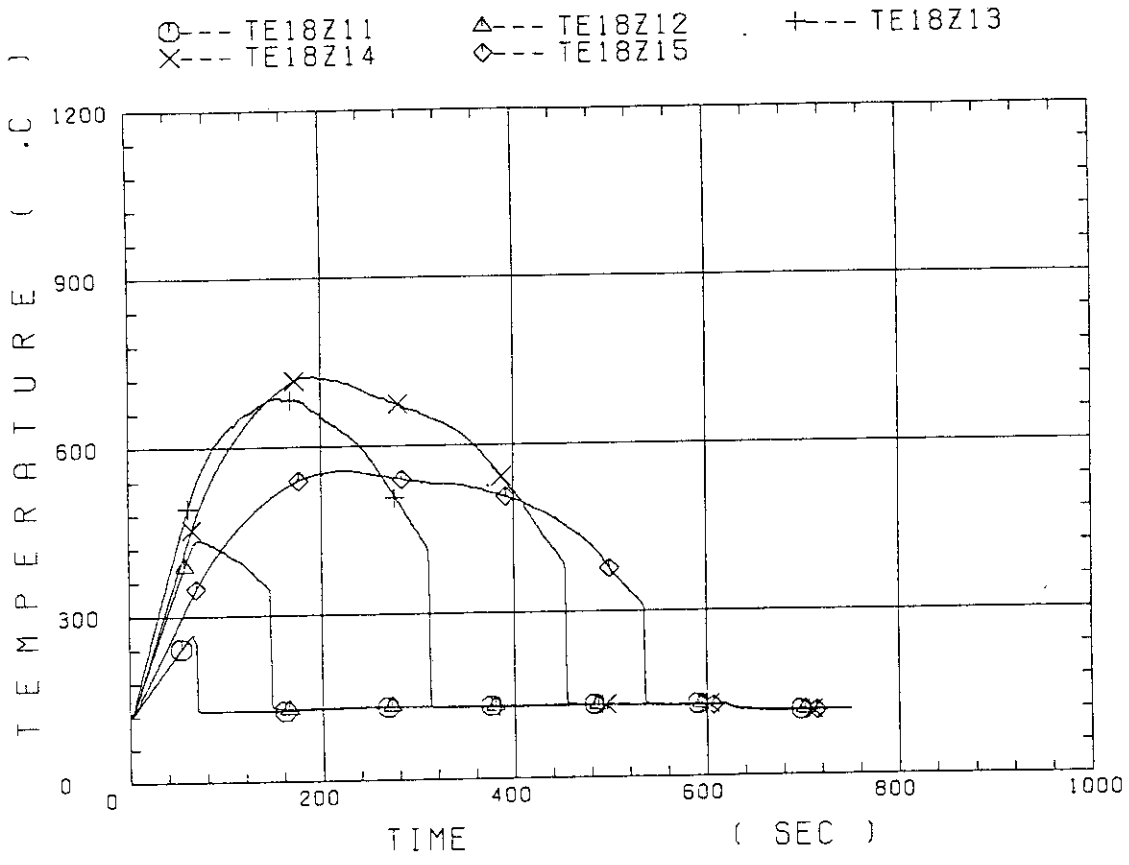

Fig. B-1 Surface temperature on low power rod (Z-rod) in medium power region (B region) (average power rod)

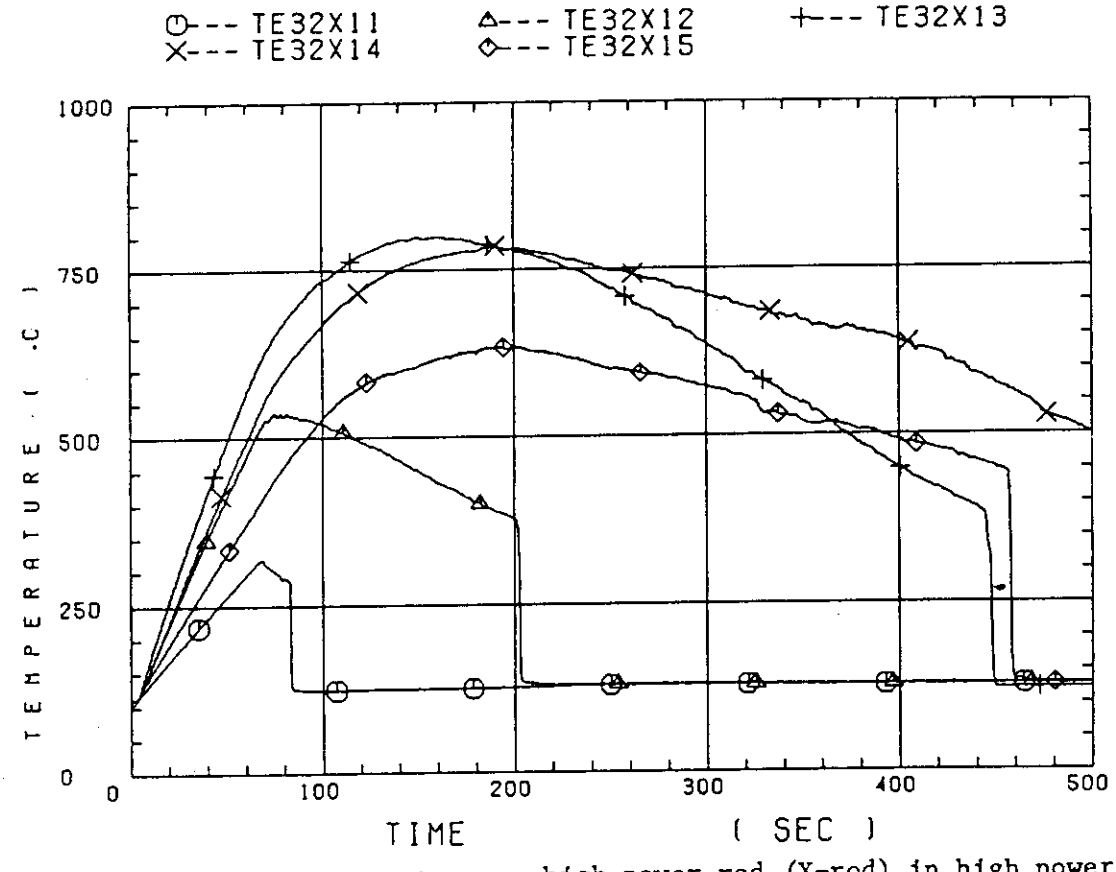

Fig. B-2 Surface temperature on high power rod (X-rod) in high power region (A region) (peak power rod)

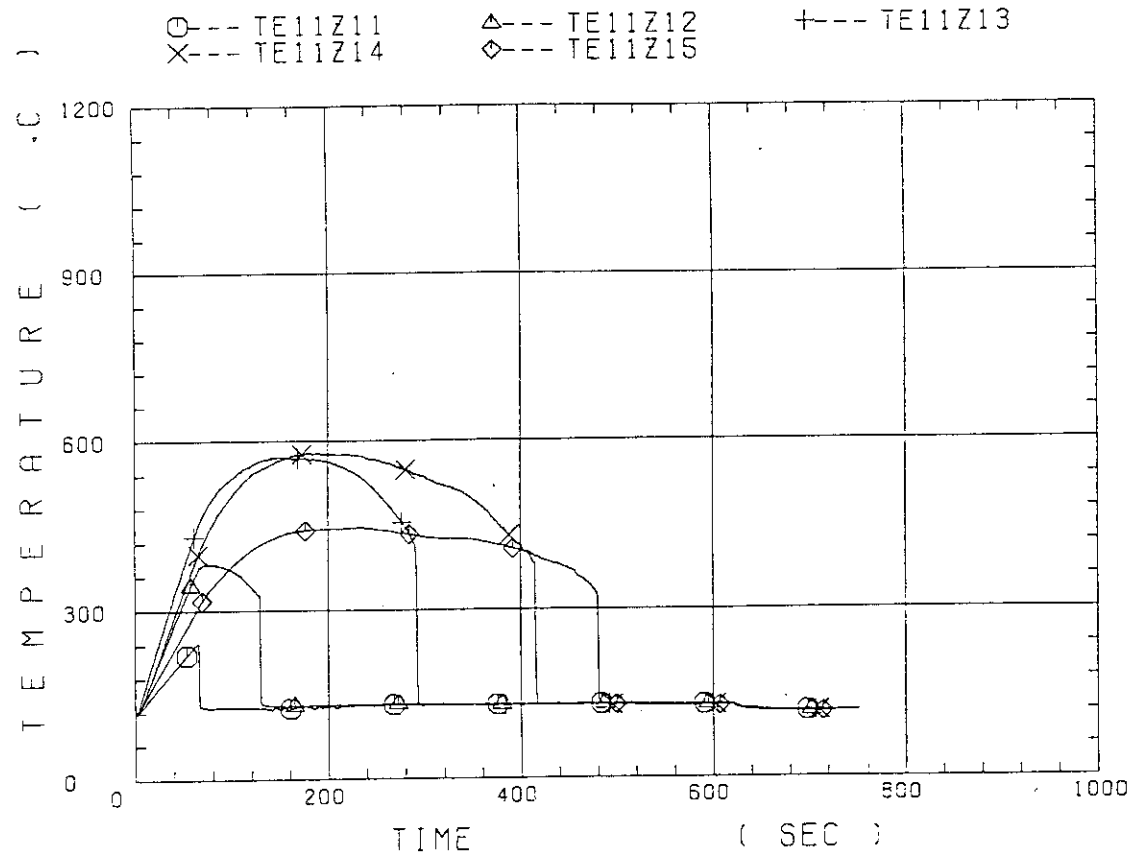

Fig. B-3 Surface temperature on low power rod (Z-rod) in low power region (C region) (lowest power rod)

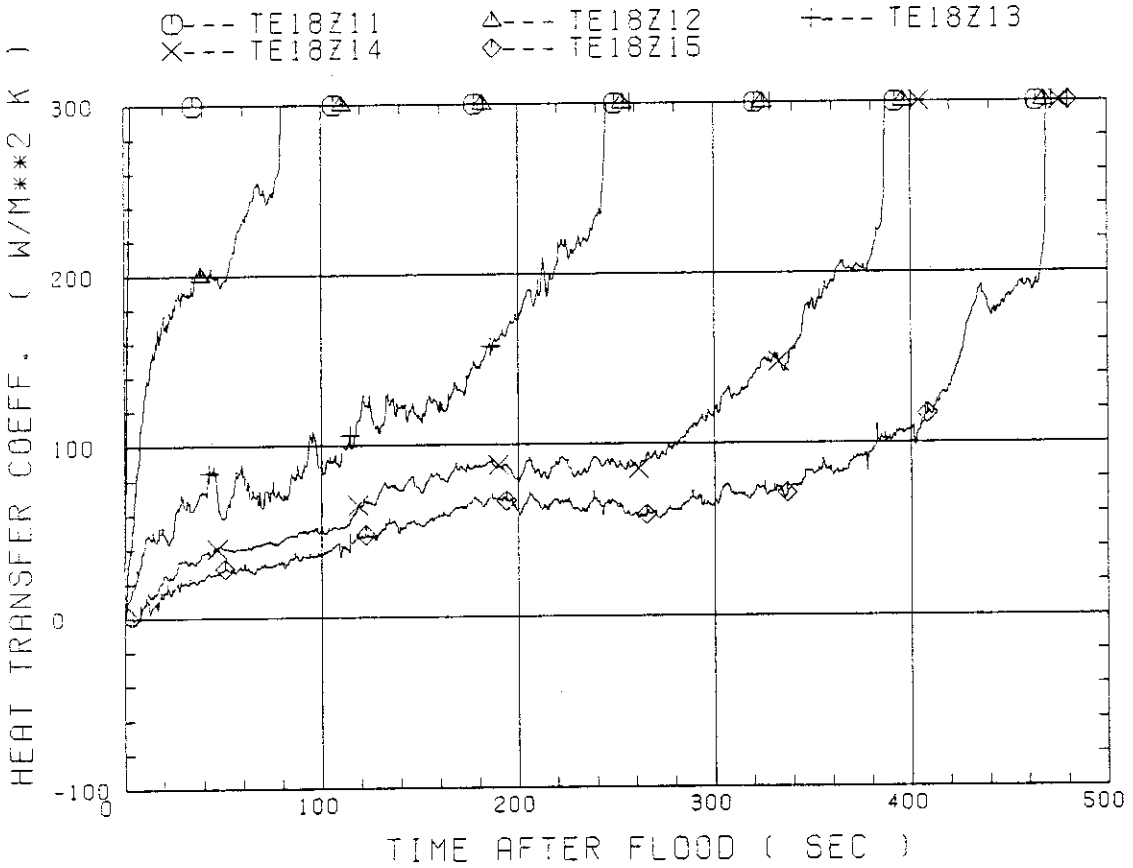

Fig. B-4 Heat transfer coefficient along a low power rod (Z-rod) in medium power region (B region) (average power rod)

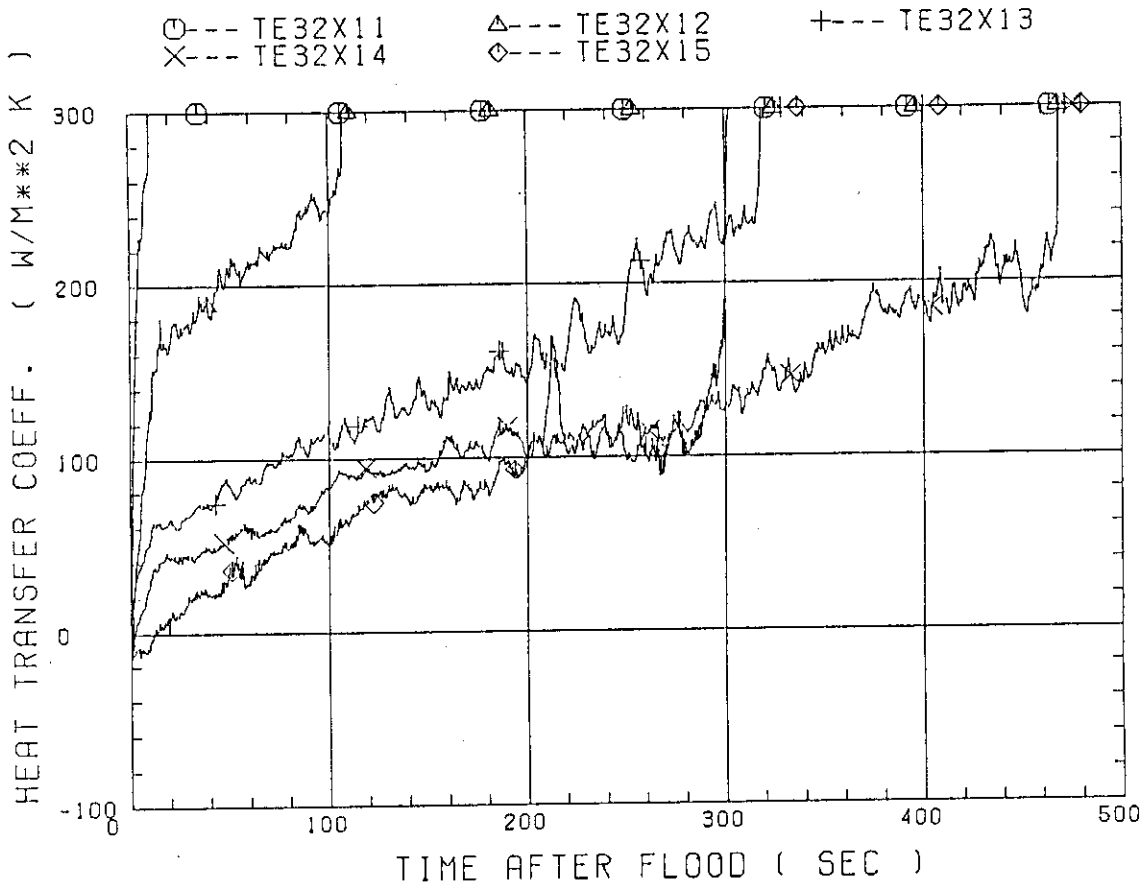

Fig. B-5 Heat transfer coefficient along a high power rod (X-rod) in high power region (A region) (peak power rod)

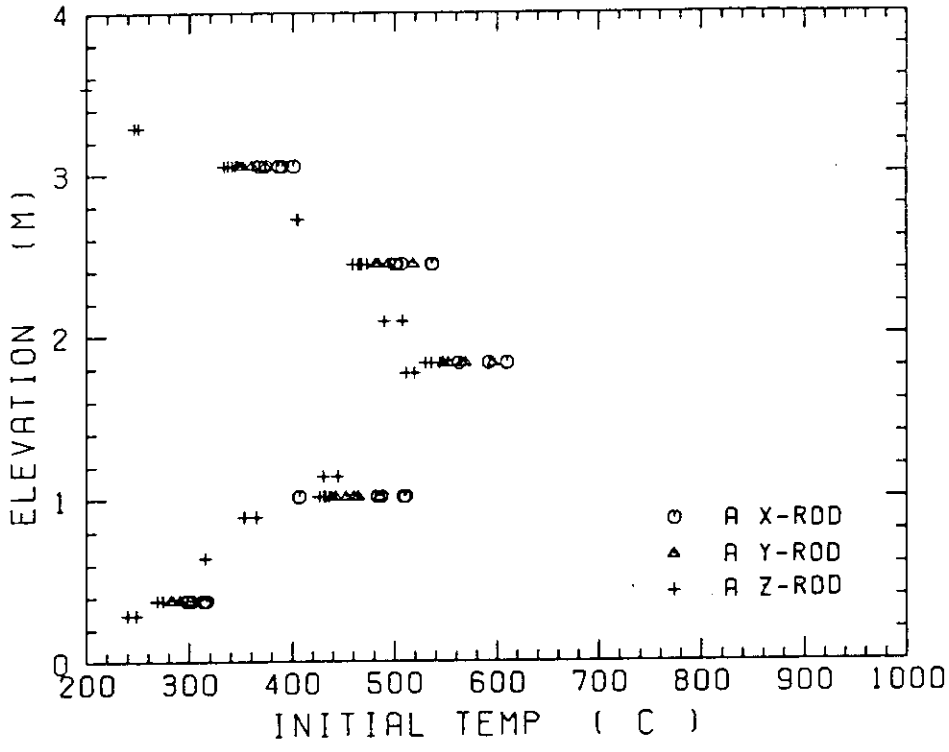

Fig. B-6 Initial rod surface temperature in high power region (A region)

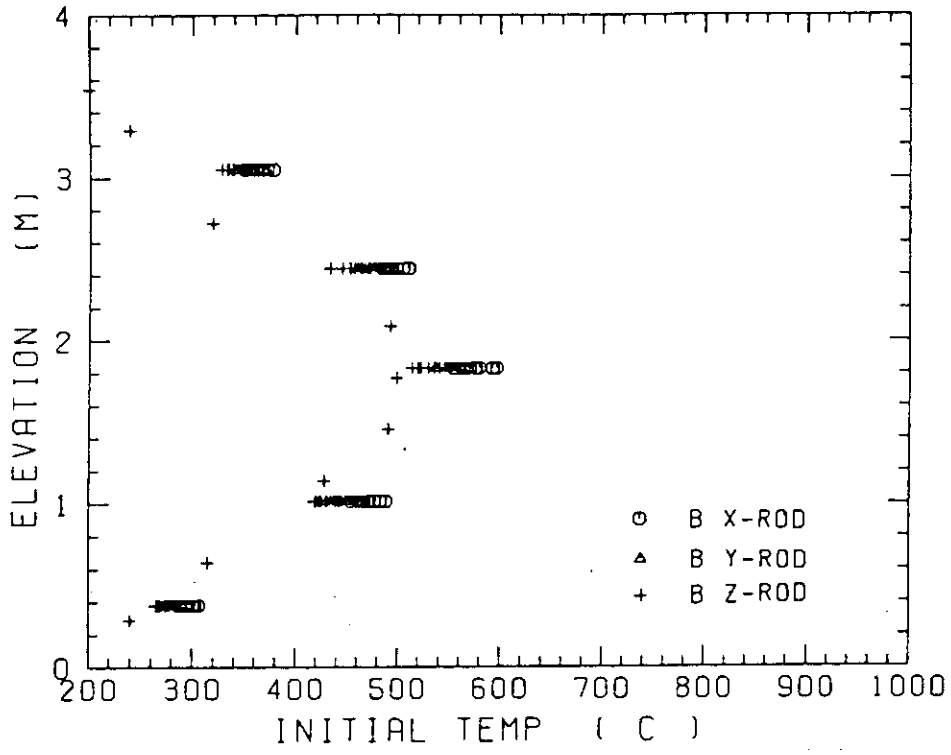

Fig. B-7 Initial rod surface temperature in medium power region (B region)

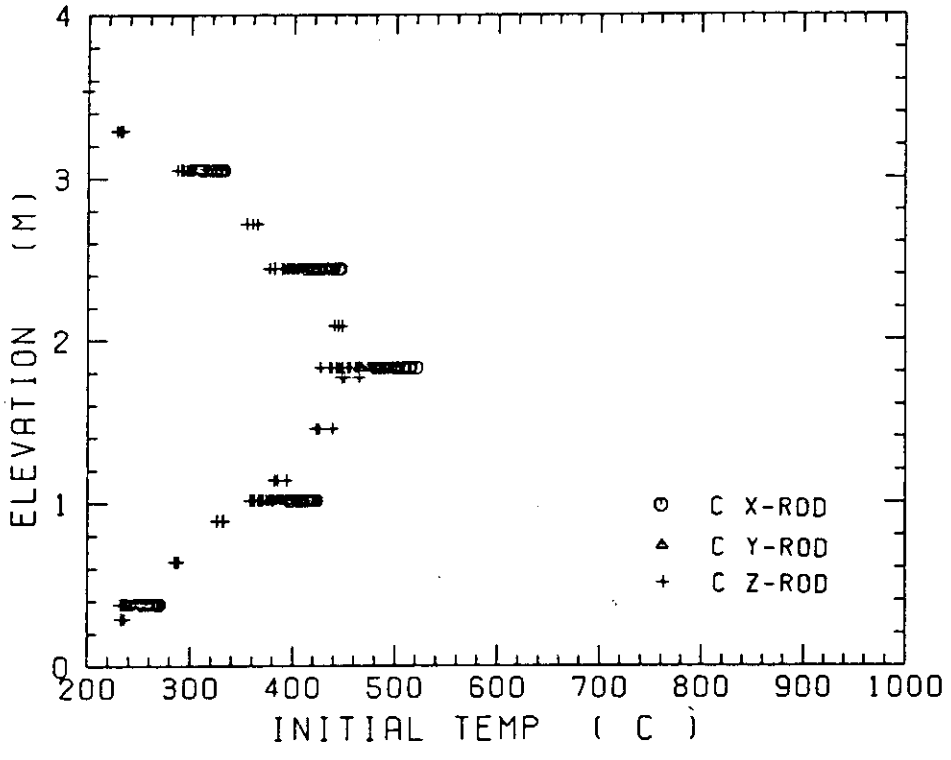

Fig. B-8 Inital rod surface temperature in low power region (C region)

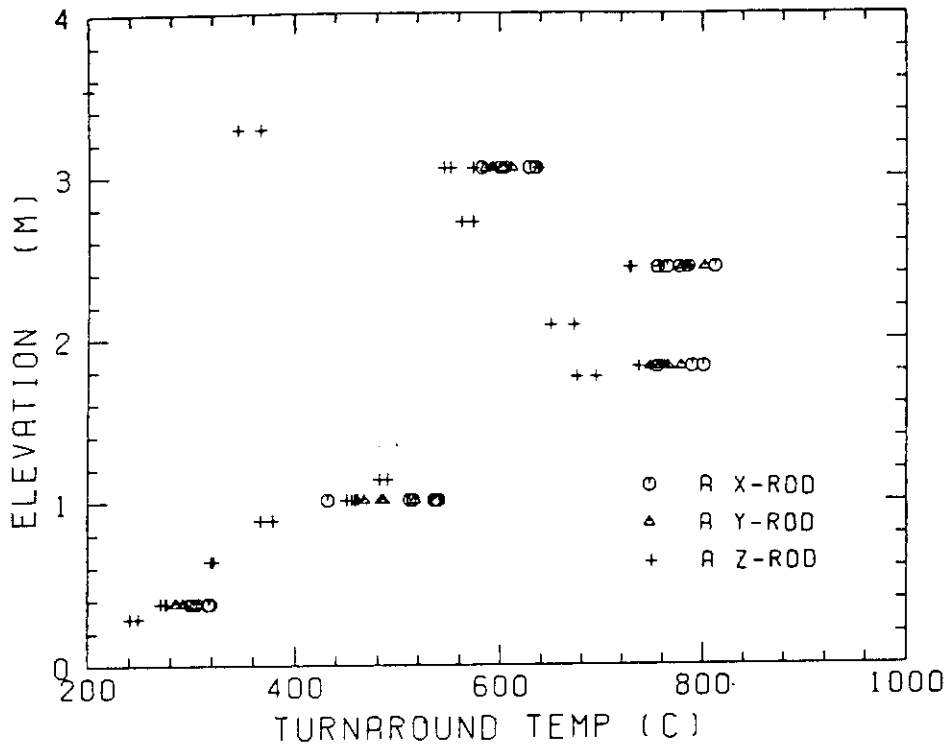

Fig. B-9 Turnaround temperature in high power region (A region)

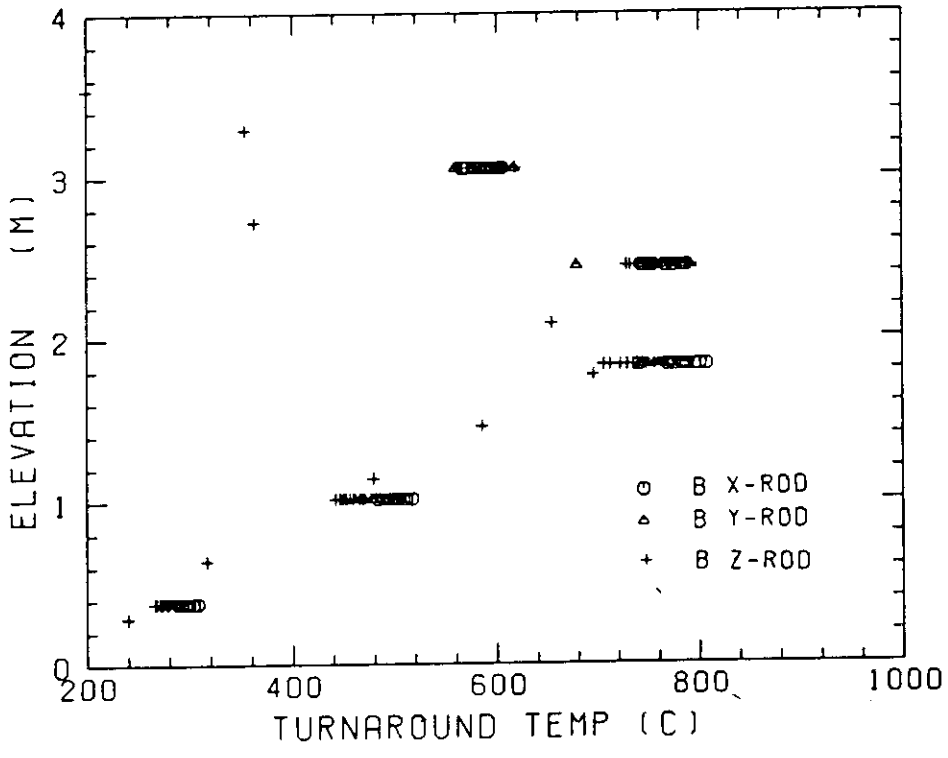

Fig. B-10 Turnaround temperature in medium power region (B region)

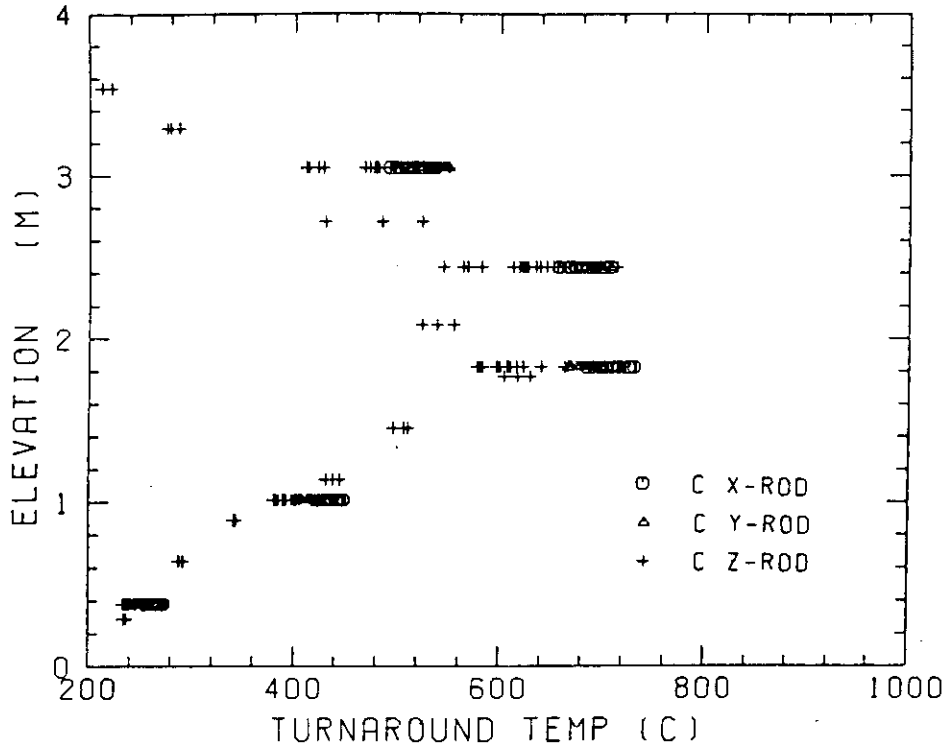

Fig. B-11 Turnaround temperature in low power region (C region)

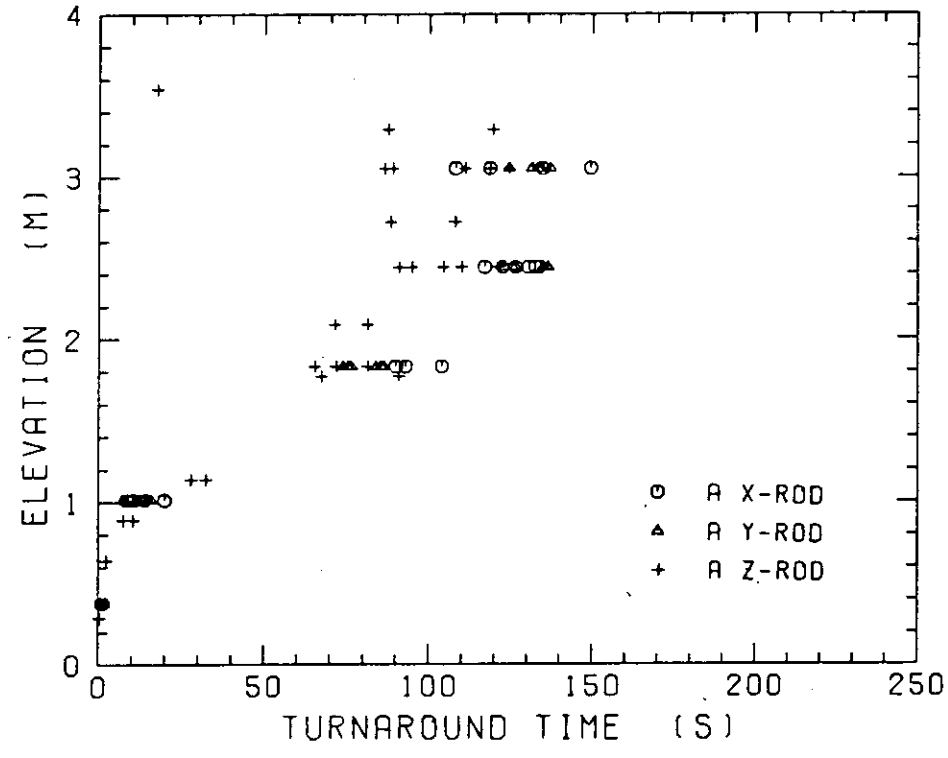

Fig. B-12 Turnaround time in high power region (A region)

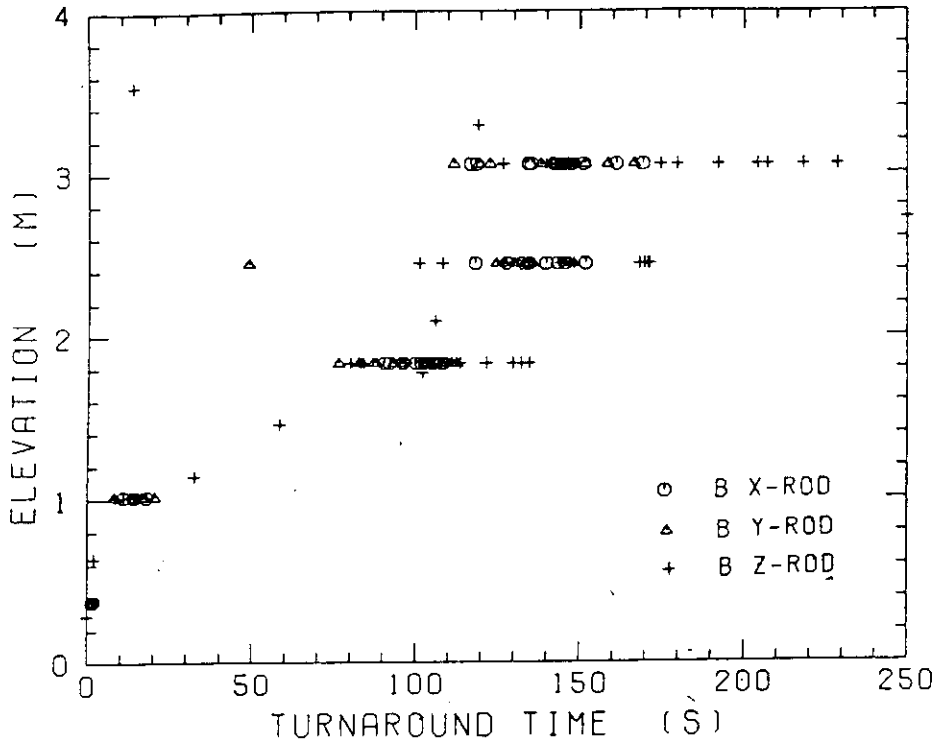

Fig. B-13 Turnaround time in medium power region (B region)

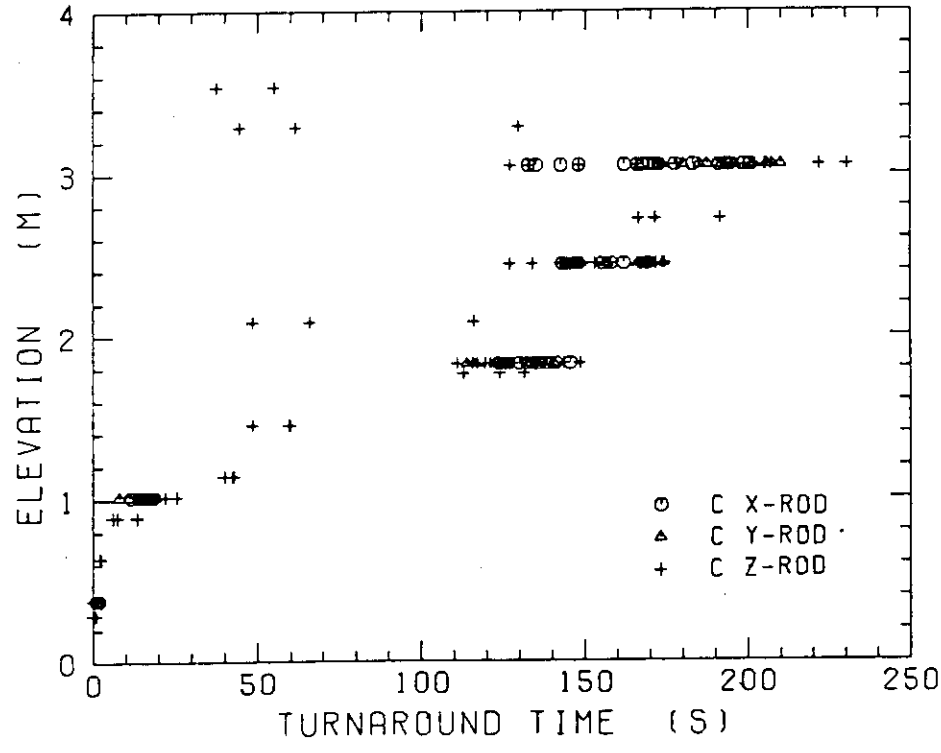

Fig. B-14 Turnaround time in low power region (C region)

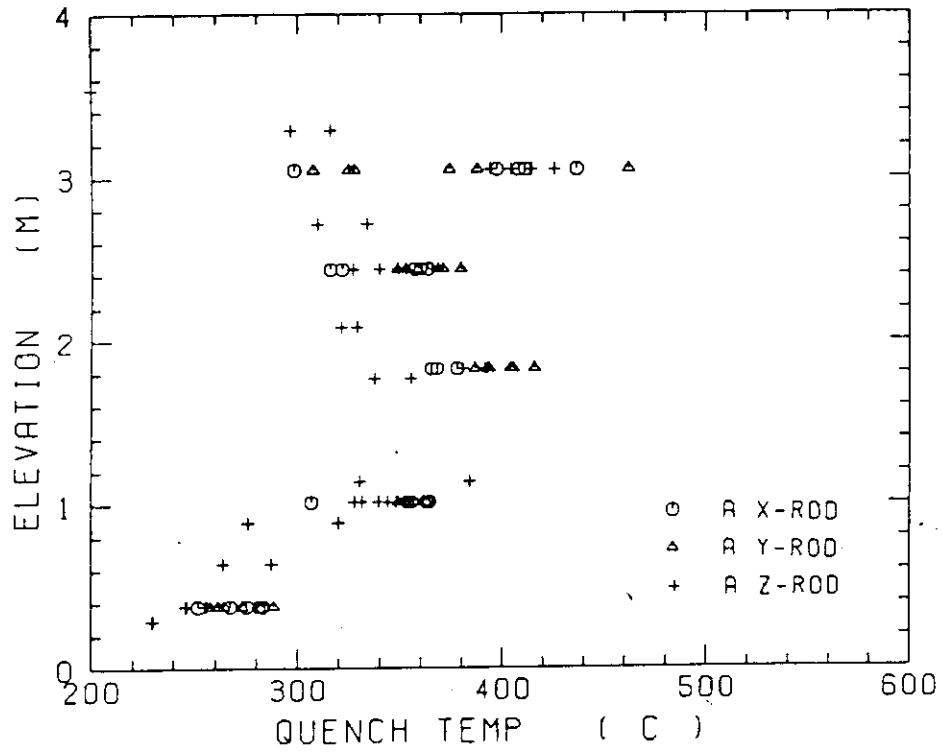

Fig. B-15 Quench temperature in high power region (A region)

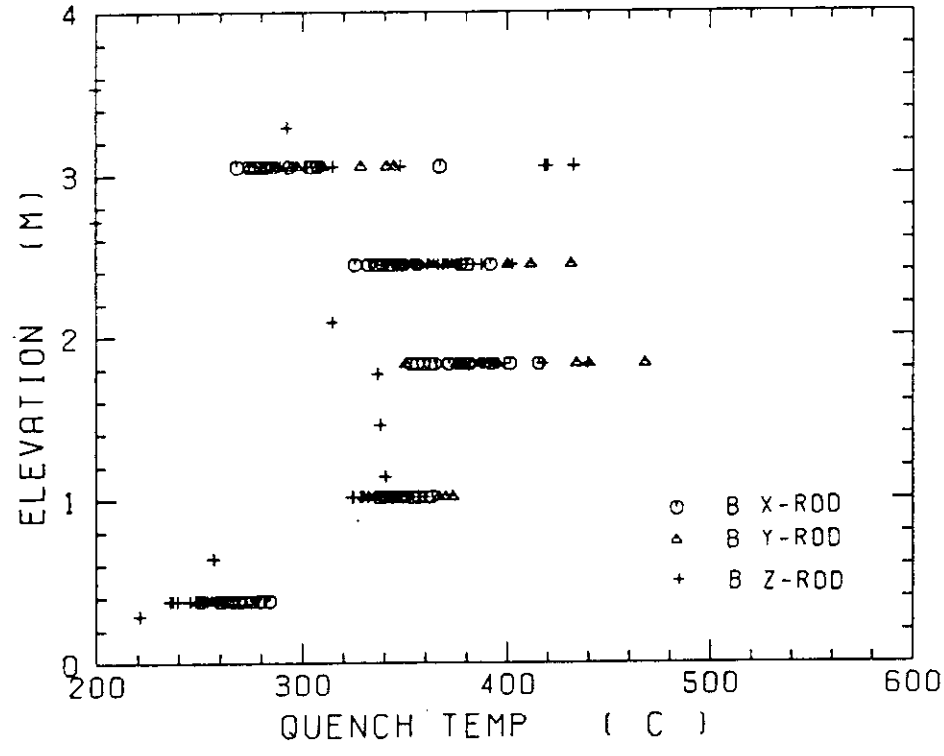

Fig. B-16 Quench temperature in medium power region (B region)

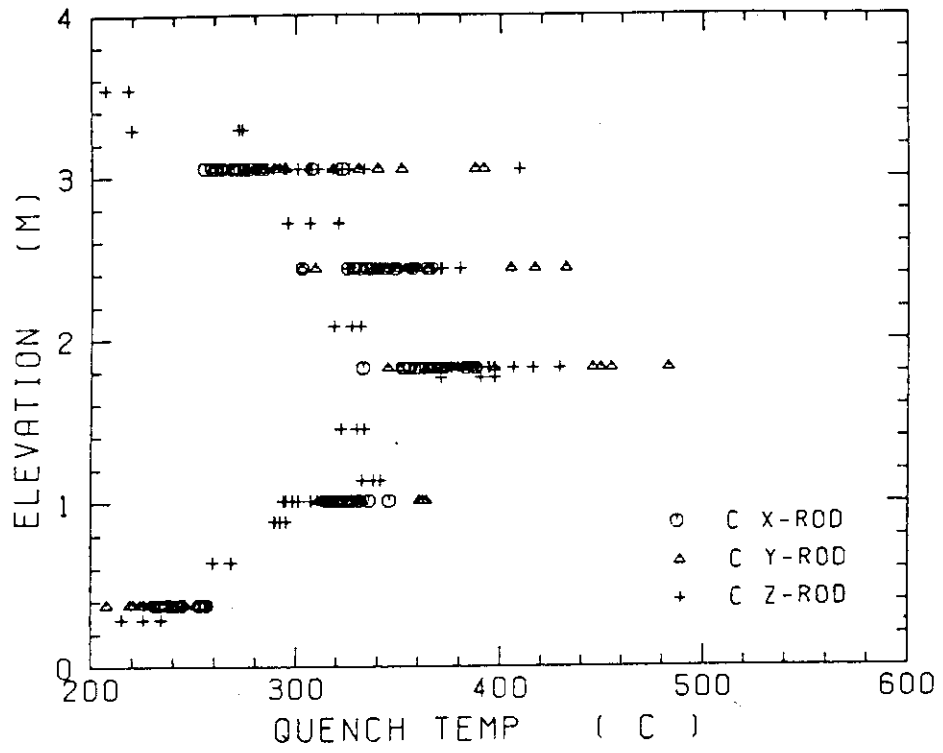

Fig. B-17 Quench temperature in low power region (C region)

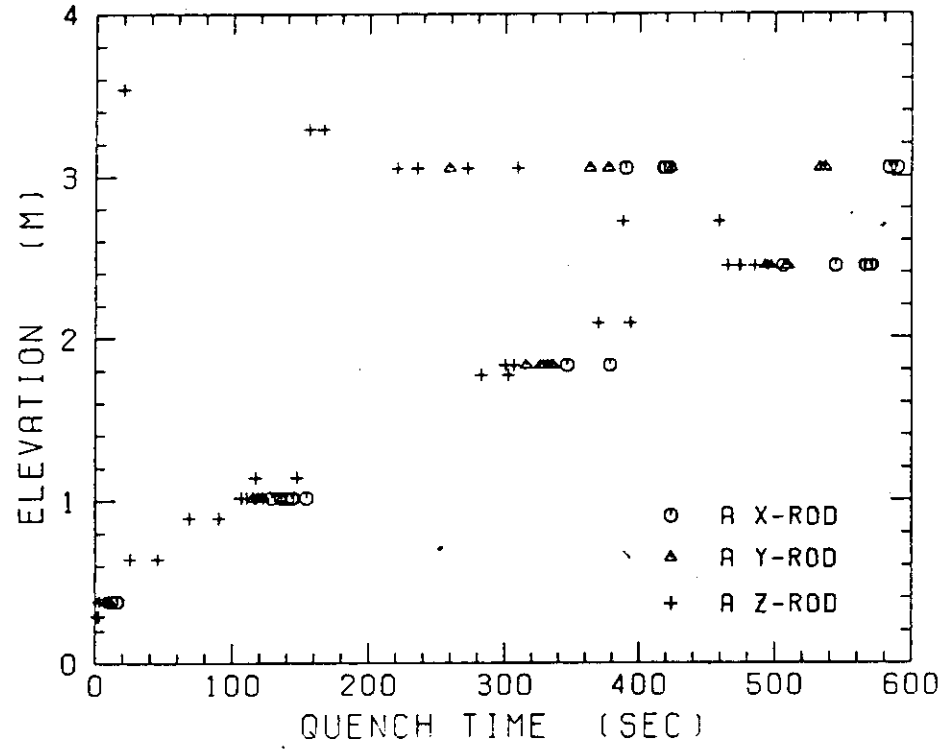

Fig. B-18 Quench time in high power region (A region)

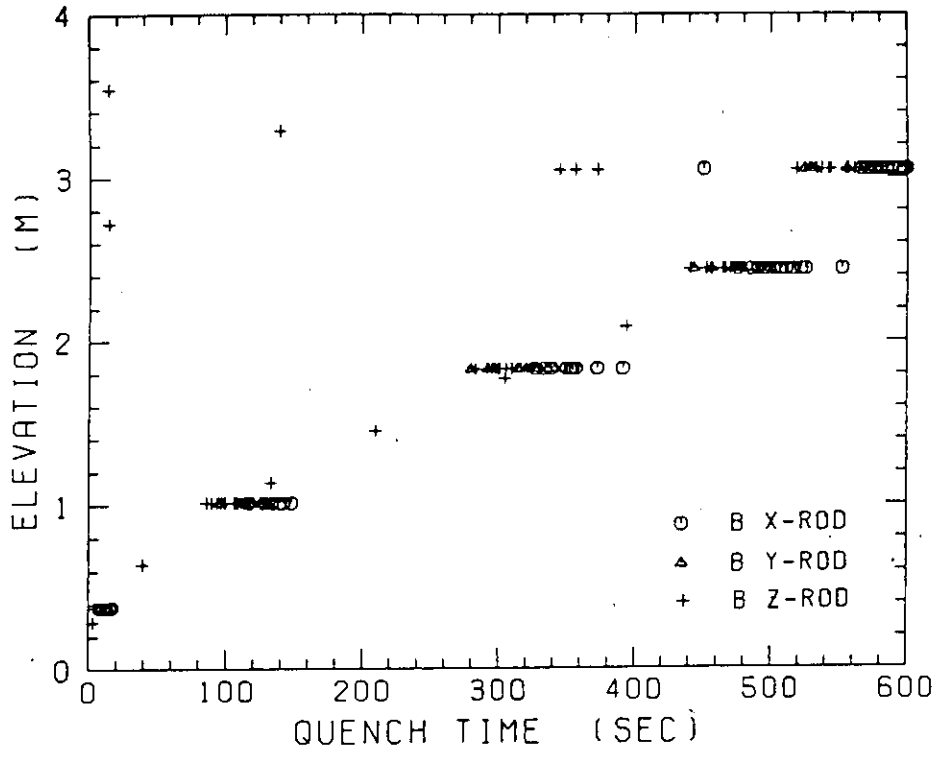

Fig. B-19 Quench time in medium power region (B region)

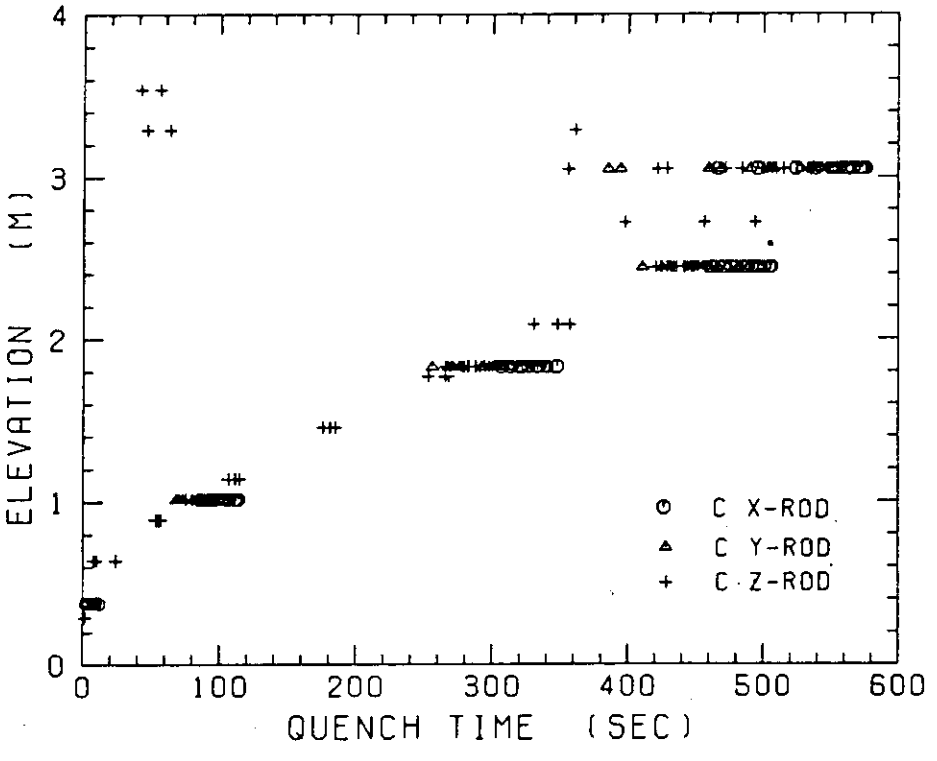

Fig. B-20 Quench time in low power region (C region)

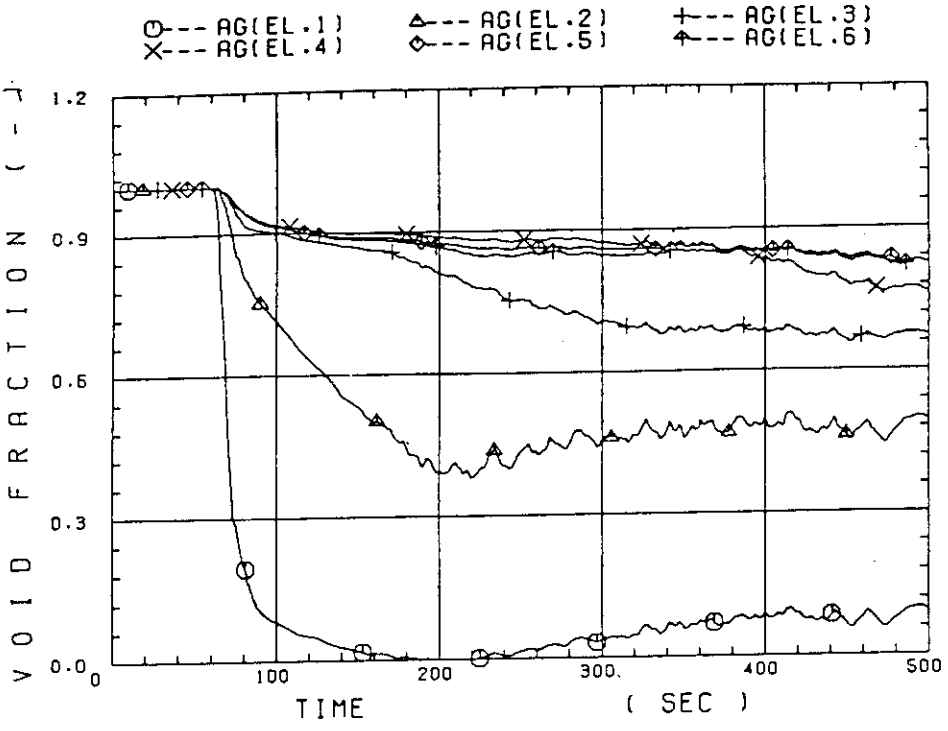

Fig. B-21 Void fraction in core

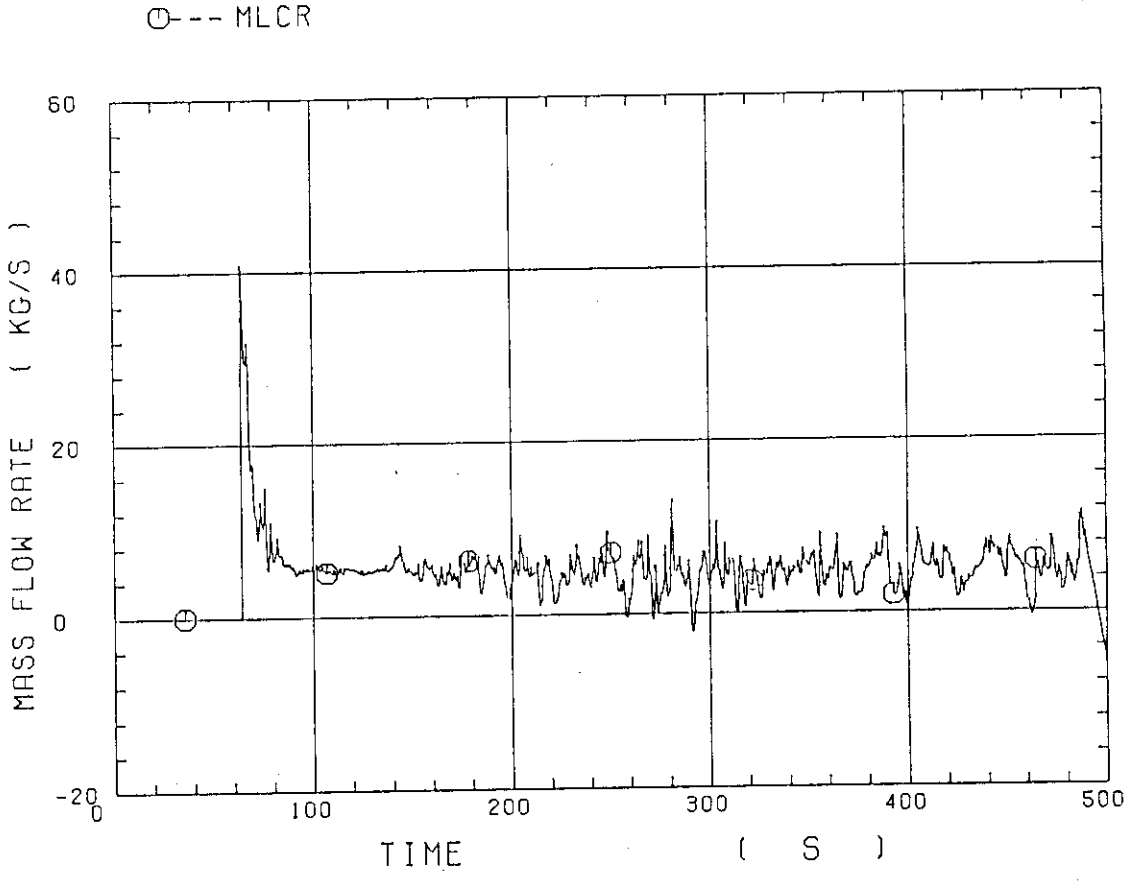

Fig. B-22 Evaluated core inlet mass flow rate

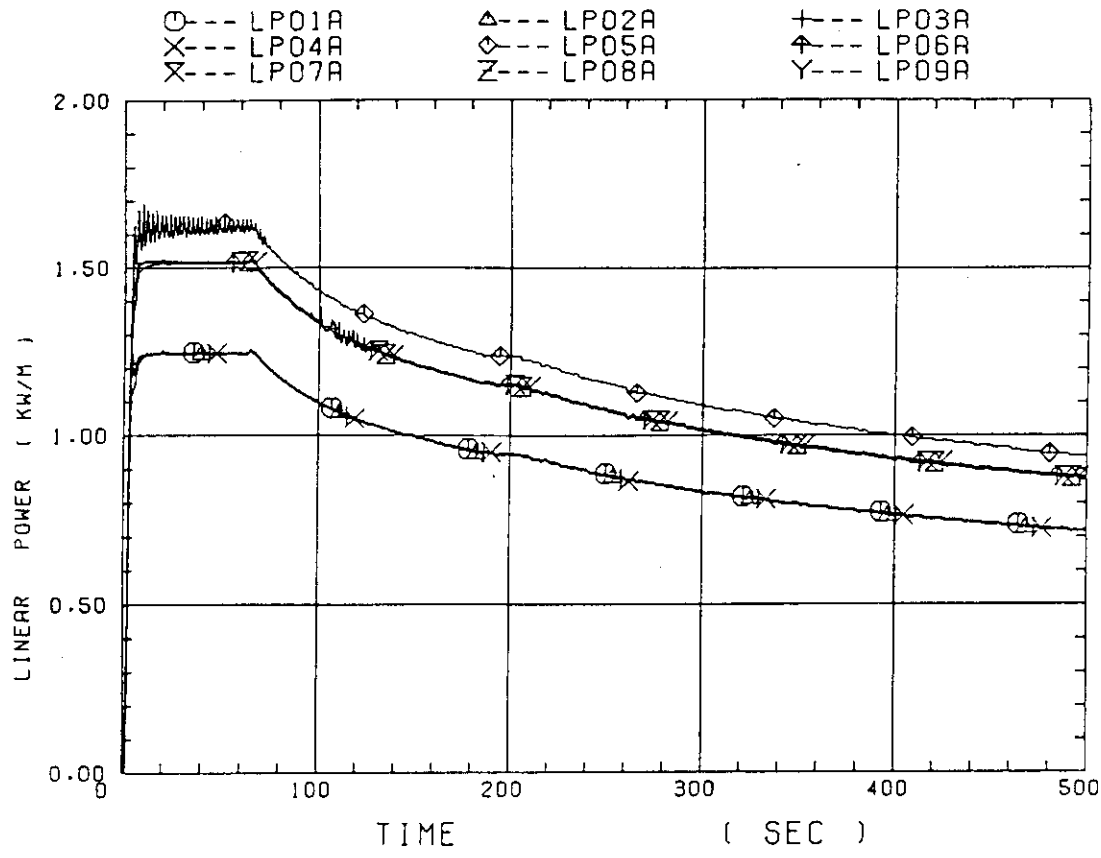

Fig. B-23 Average linear power of heater rod in each power unit zone

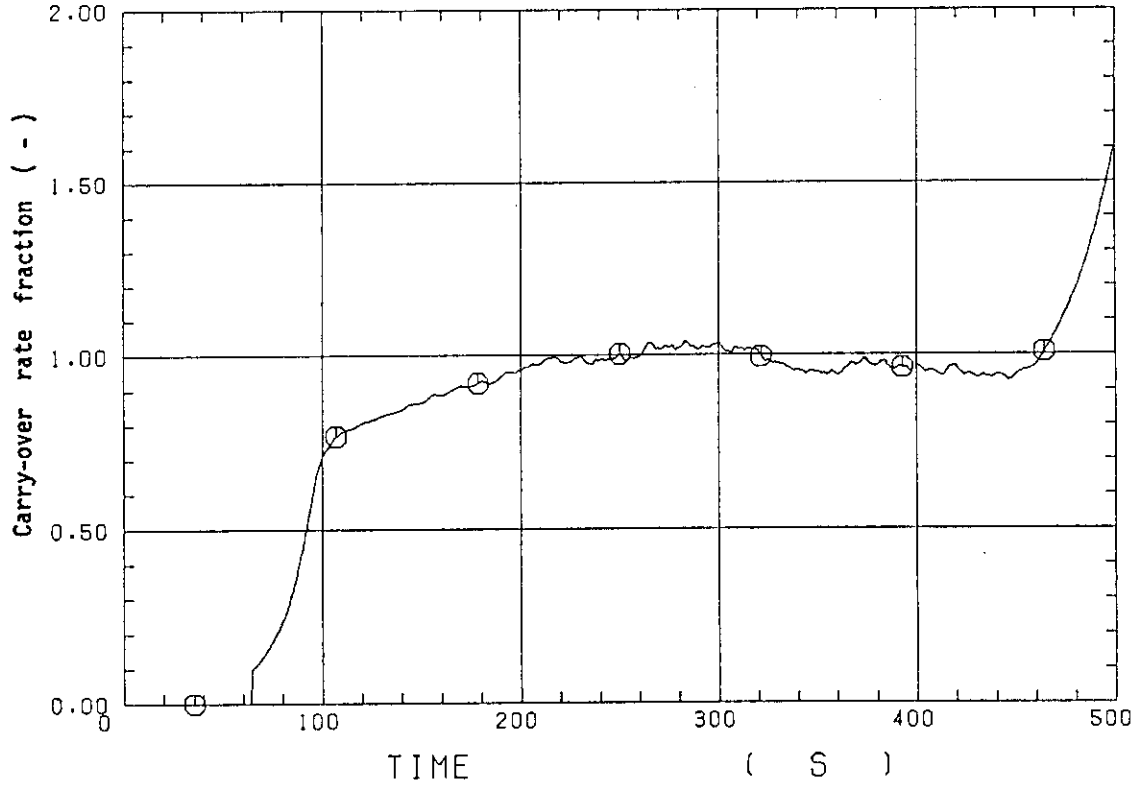

Fig. B-24 Carry-over rate fraction

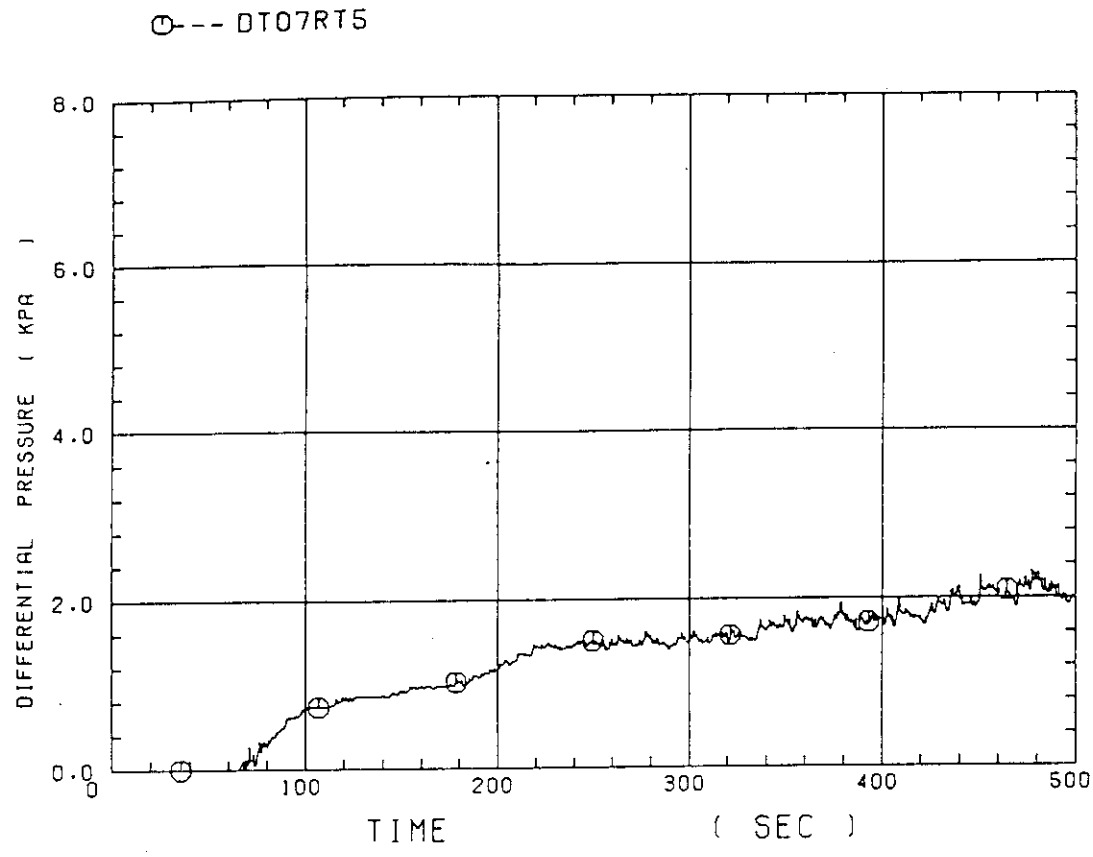

Fig. B-25 Differential pressure through upper plenum

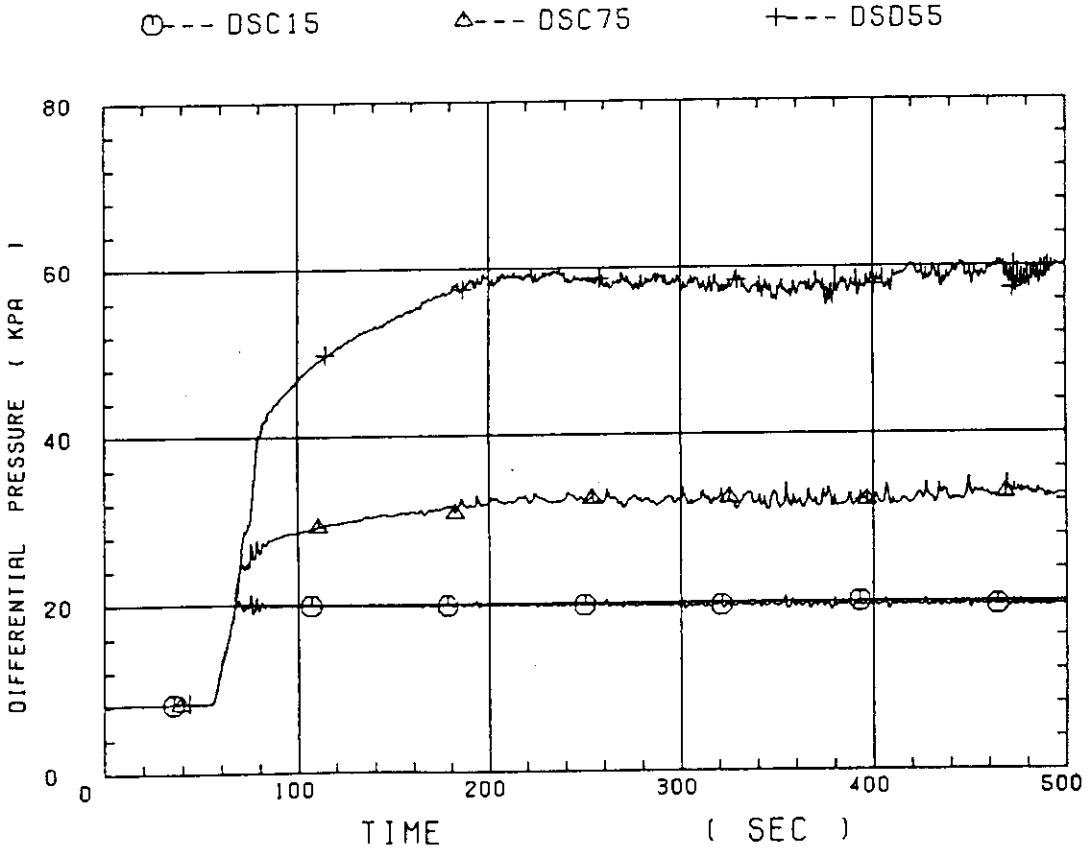

Fig. B-26 Differential pressure through downcomer, core, and lower plenum

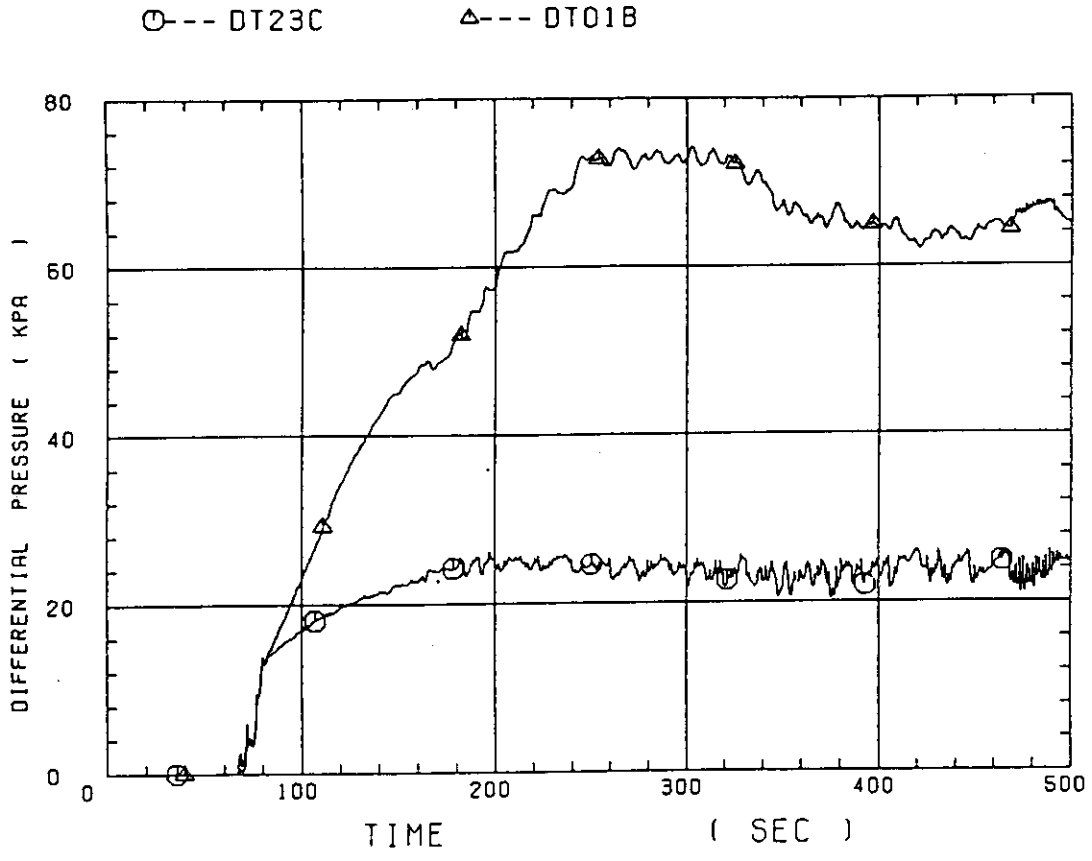

Fig. B-27 Differential pressure through intact and broken loops

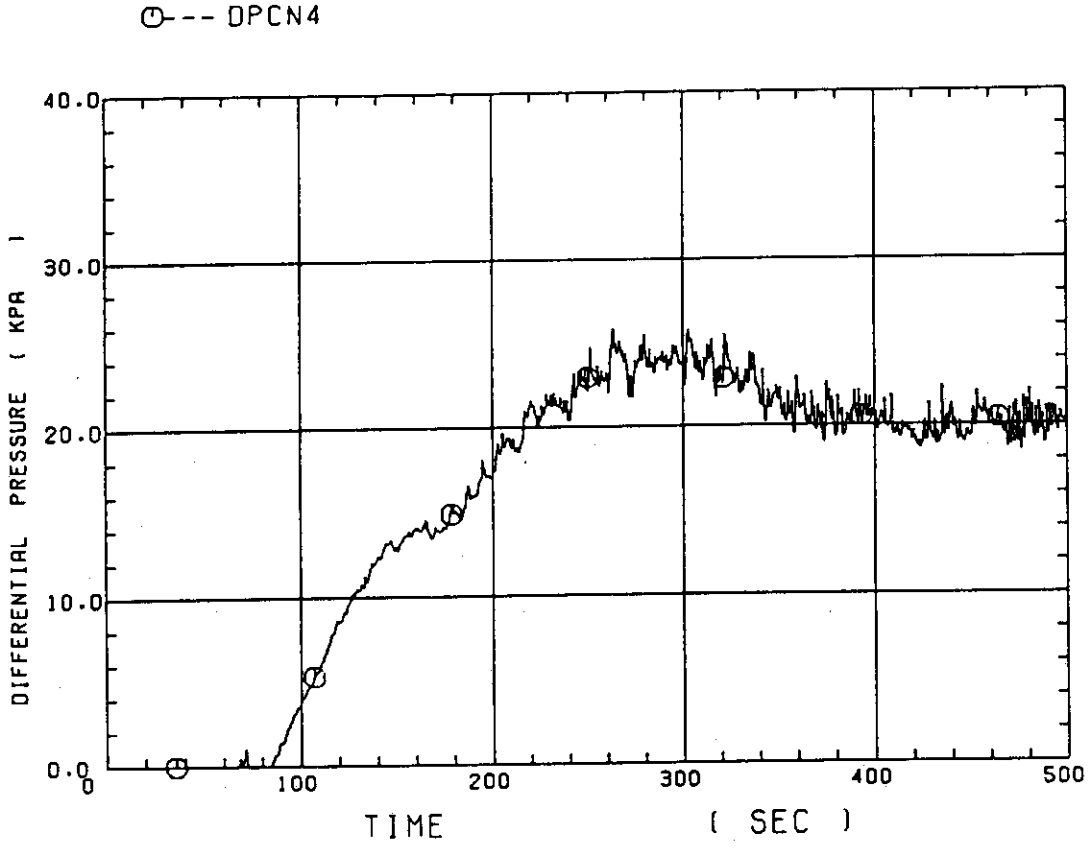

Fig. B-28 Differential pressure through broken cold leg nozzle

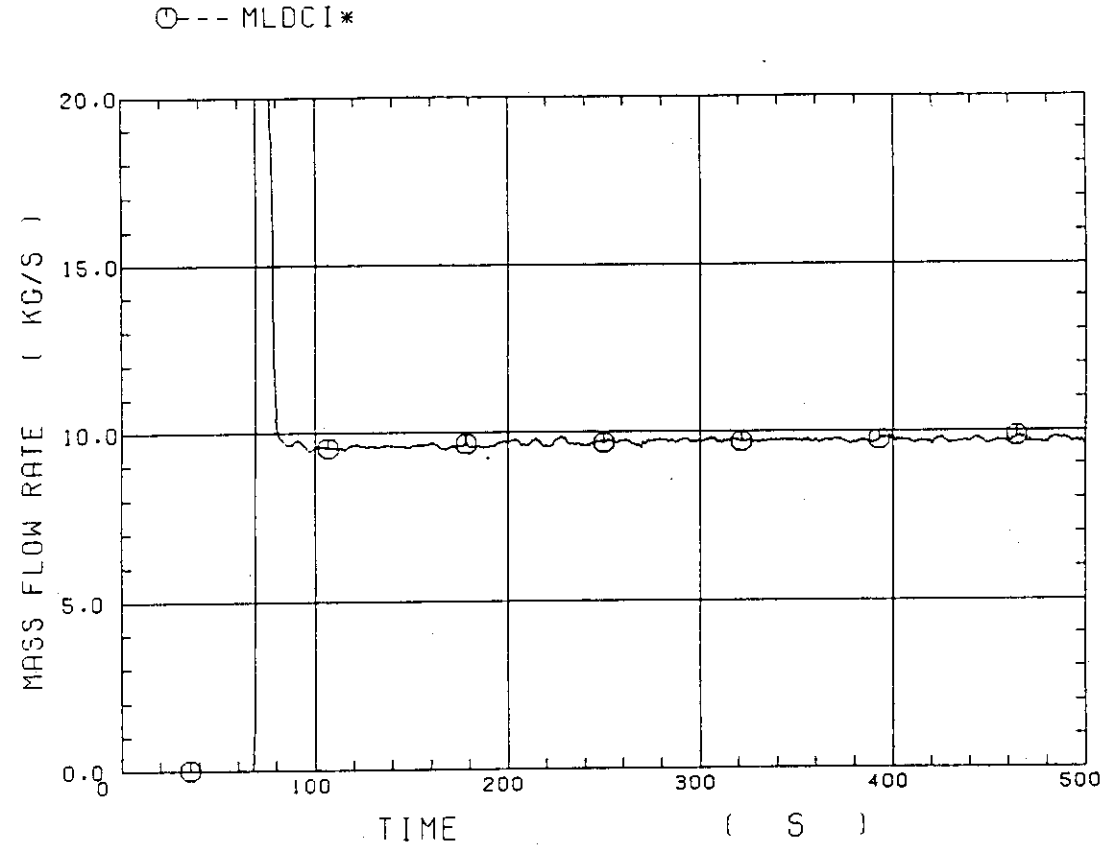

Fig. B-29 Total water mass flow rate from intact loops to downcomer

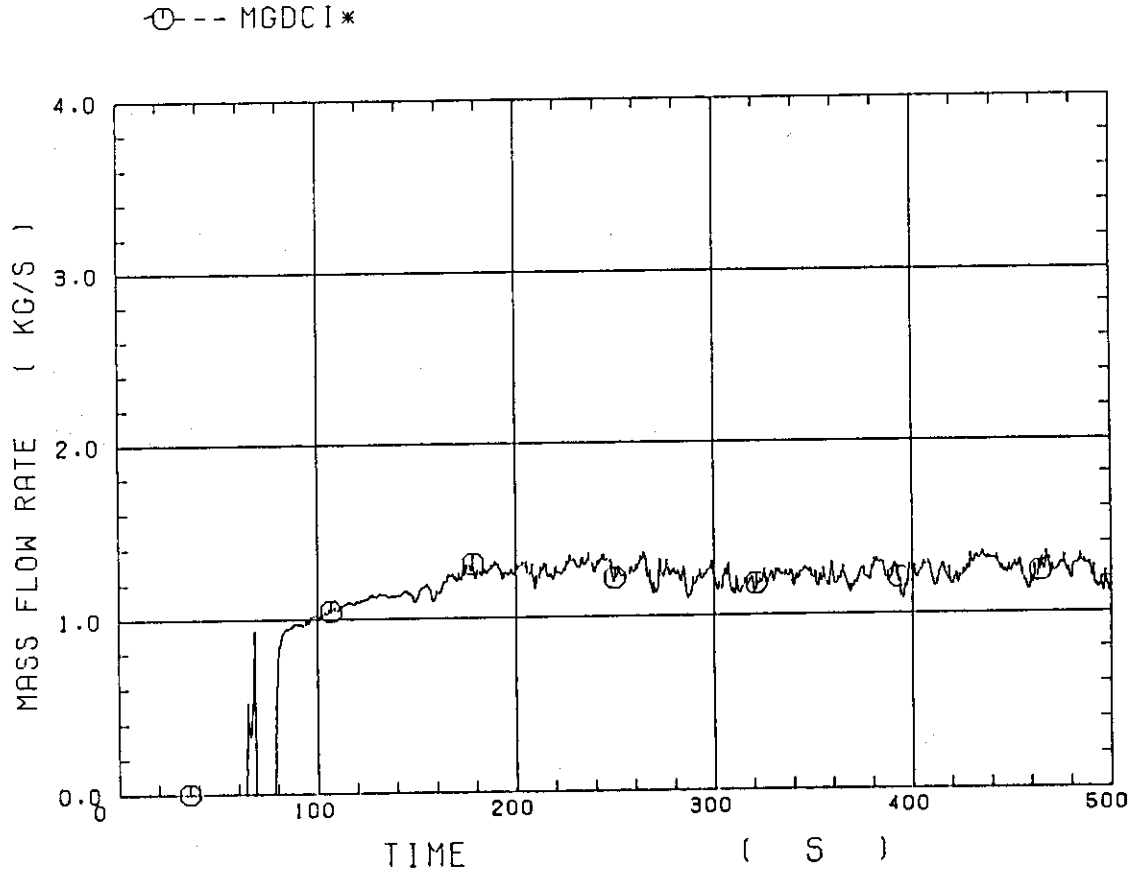

Fig. B-30 Total steam mass flow rate from intact loops to downcomer

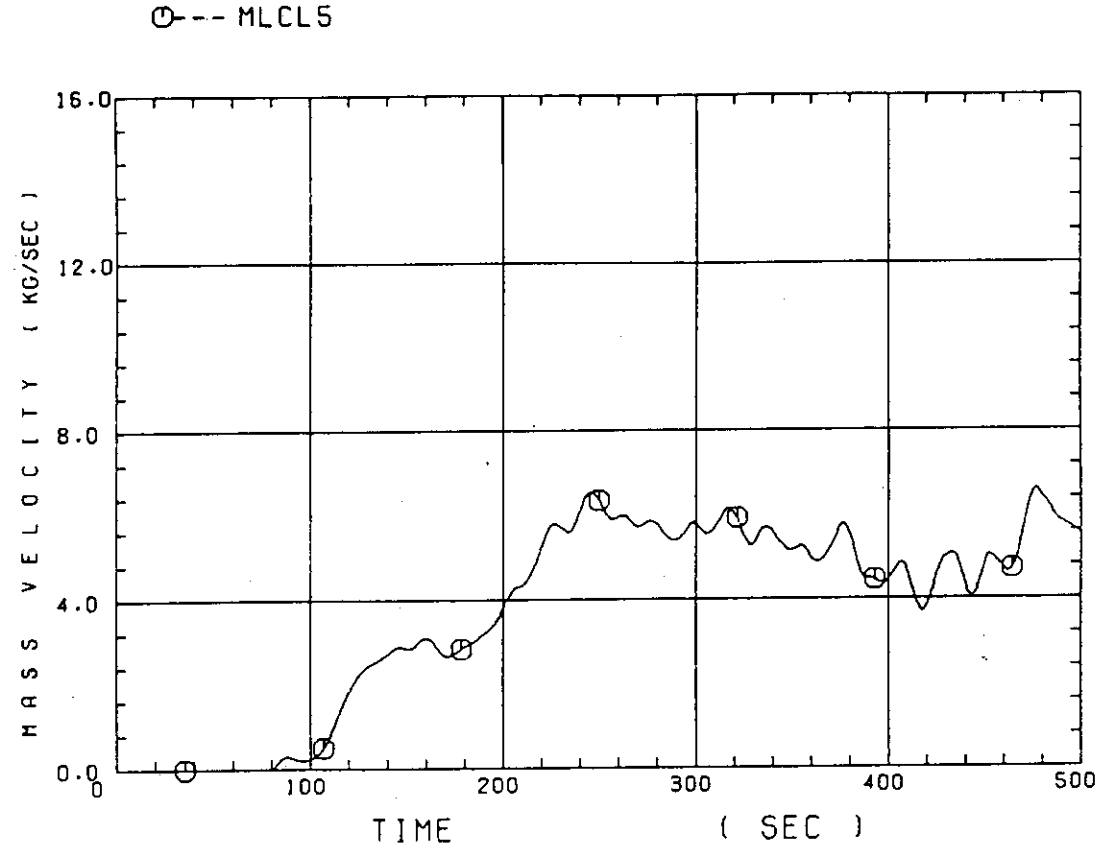

Fig. B-31 Water mass flow rate through broken cold leg nozzle

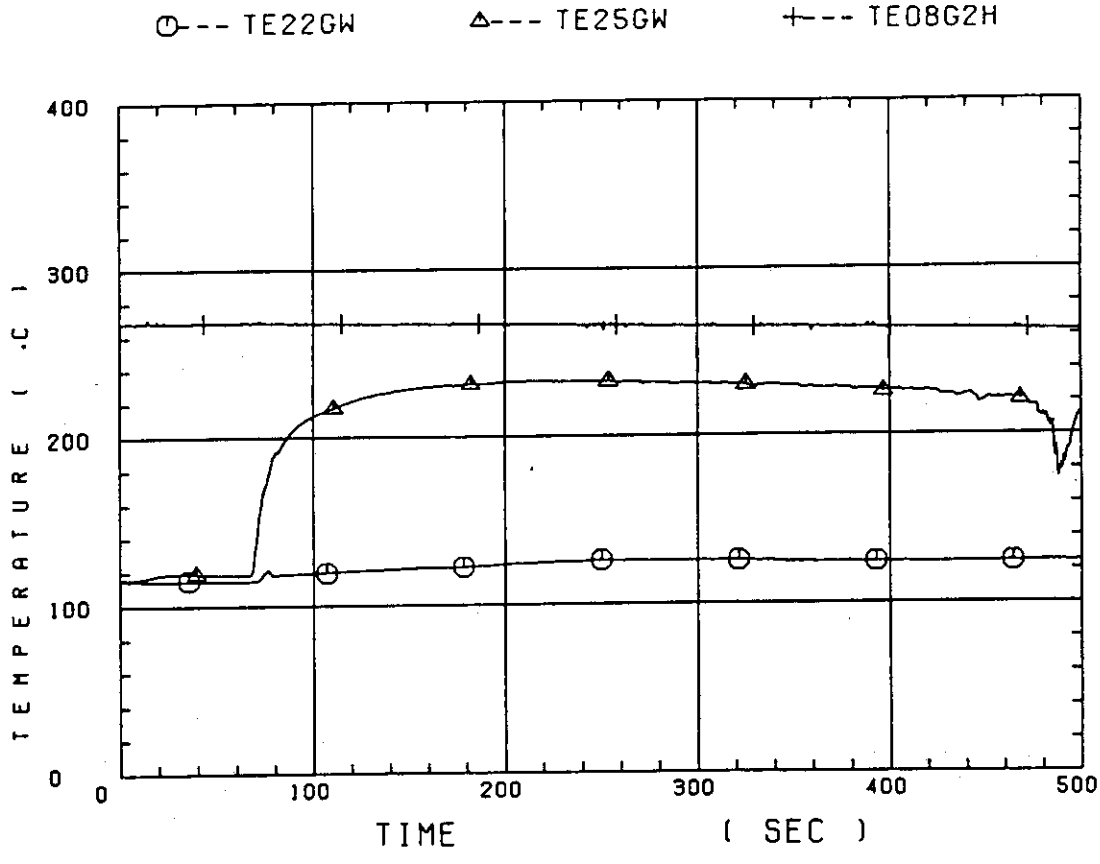

Fig. B-32 Fluid temperature in inlet plenum, outlet plenum, and secondary of steam generator 1

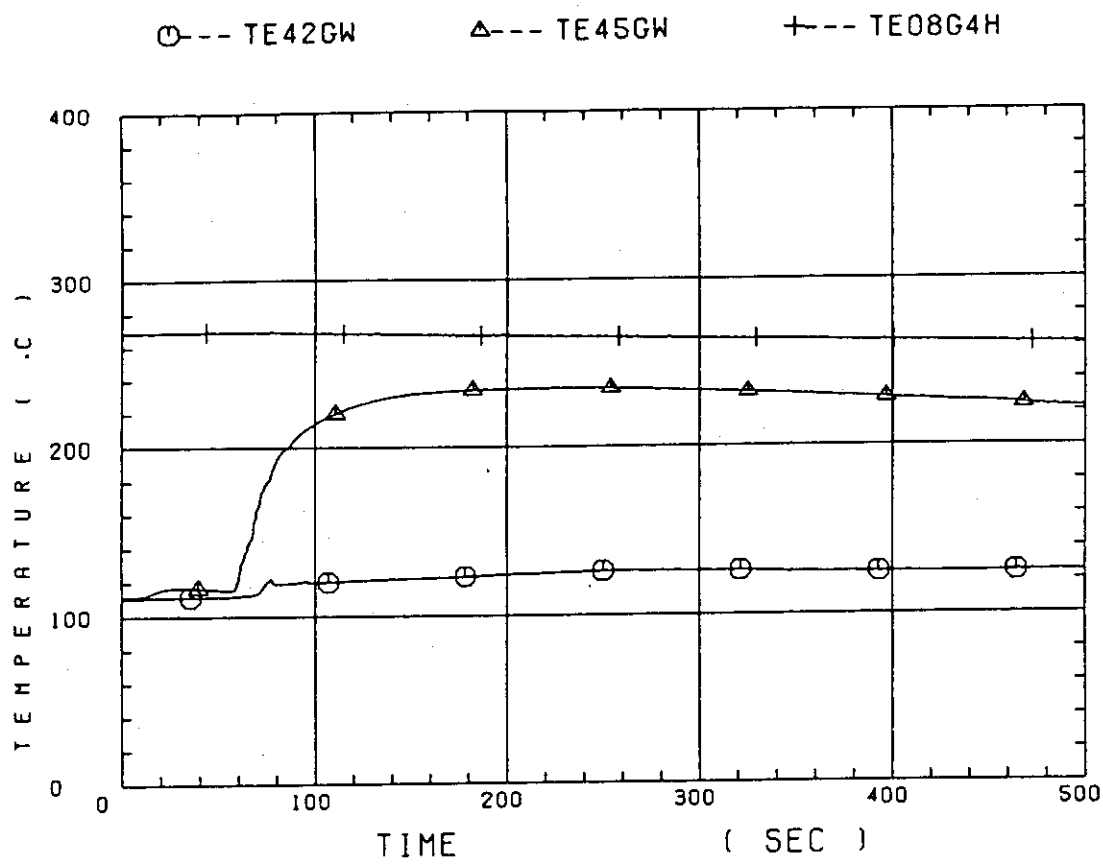

Fig. B-33 Fluid temperature in inlet plenum, outlet plenum, and secondary of steam generator 2

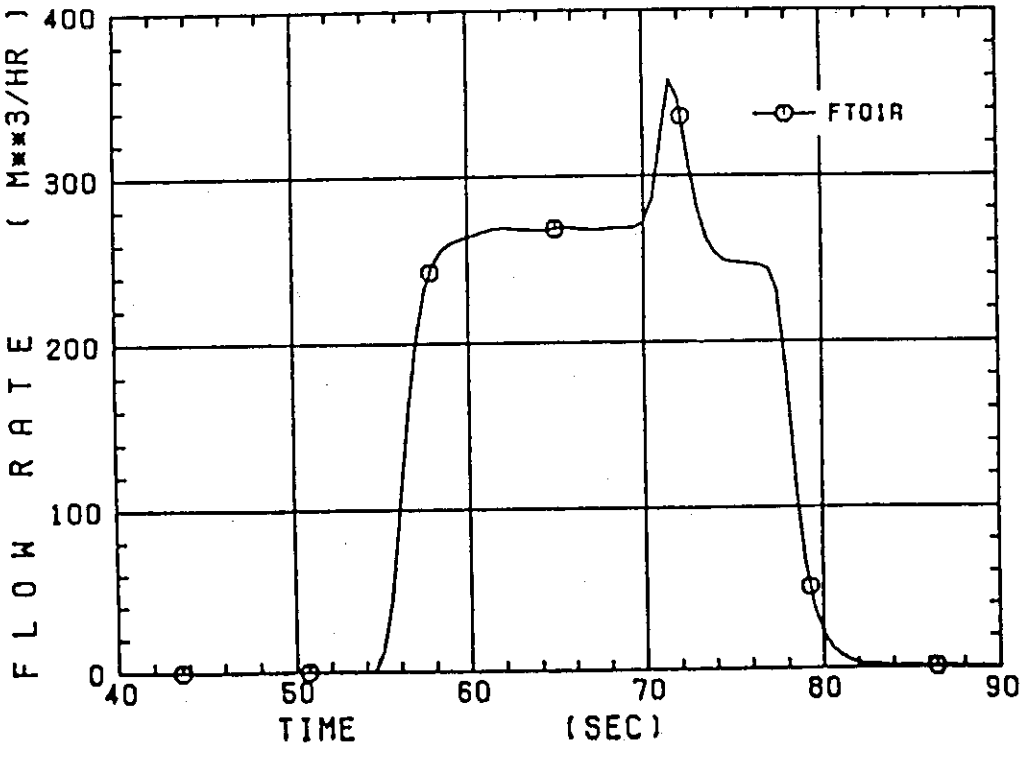

Fig. B-34 Total accumulator injection rate

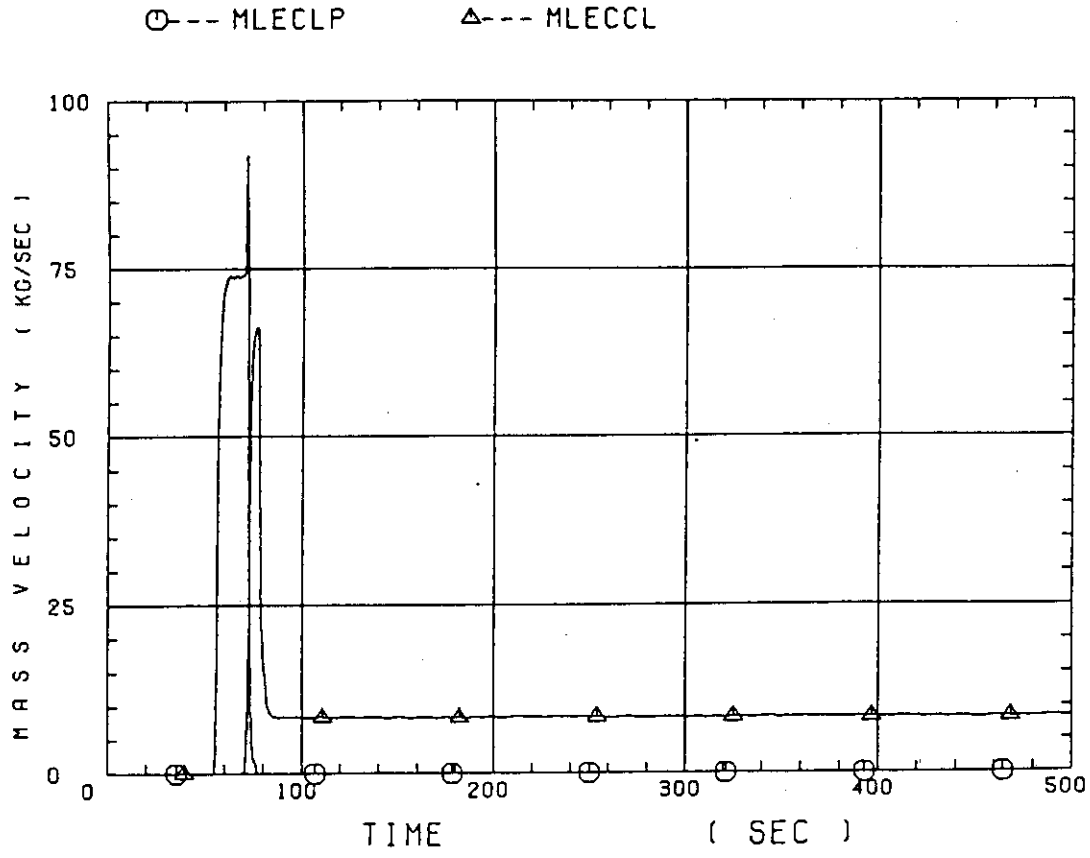

Fig. B-35 ECC water injection rates to lower plenum and to cold legs

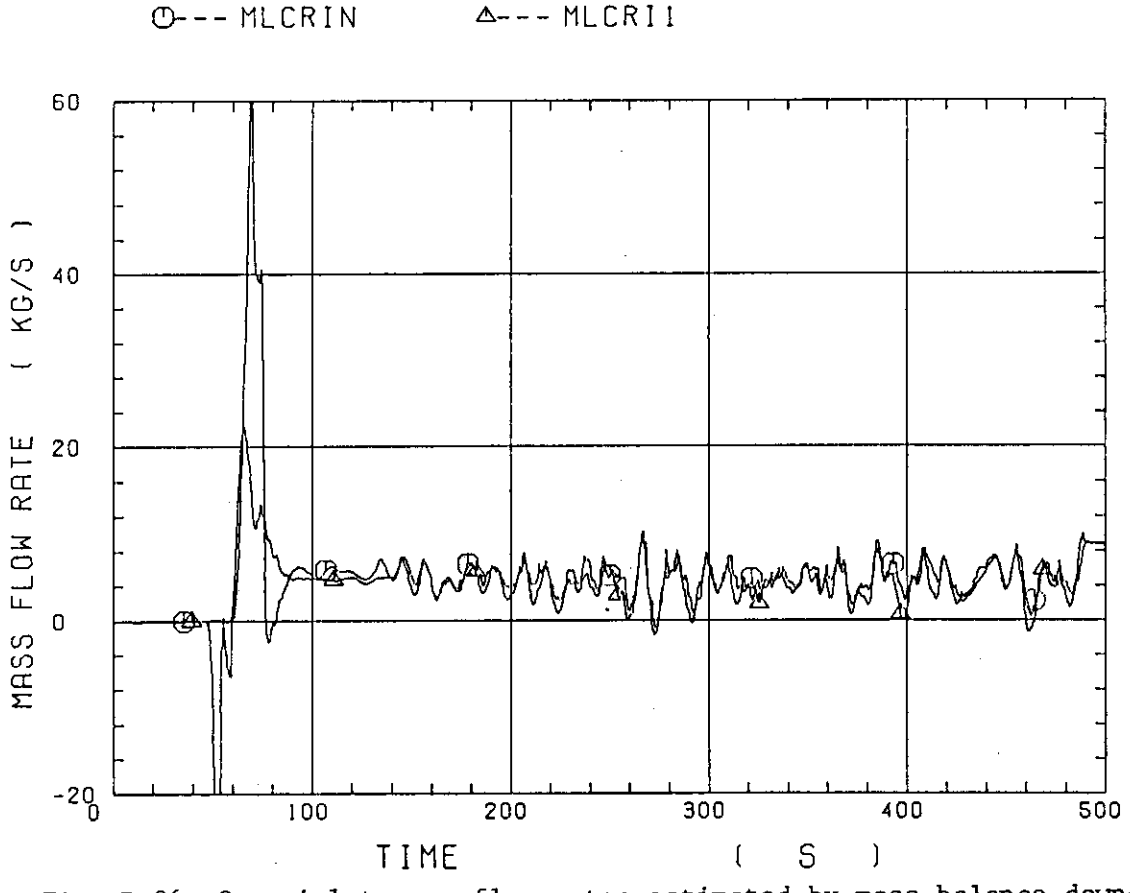

Fig. B-36 Core inlet mass flow rates estimated by mass balance downstream and upstread of core inlet

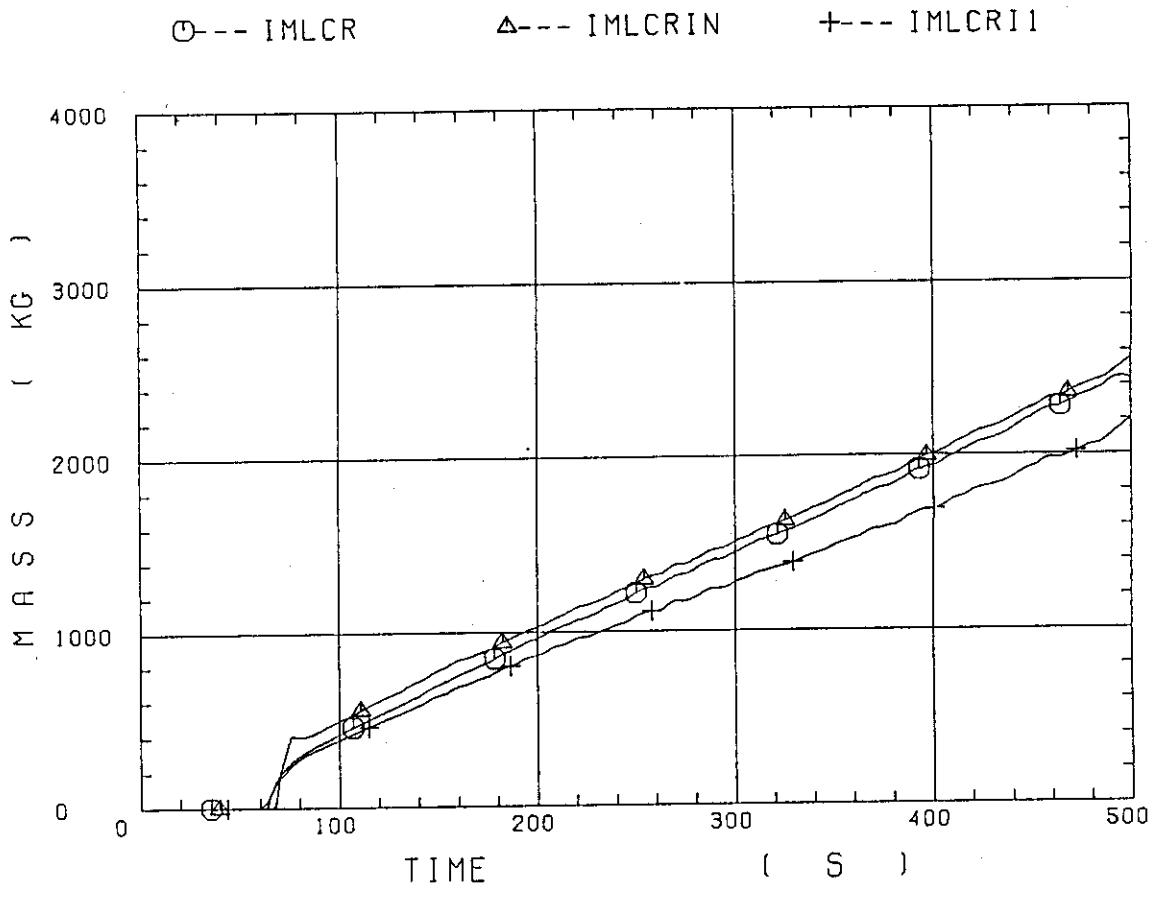

Fig. B-37 Comparison of injected mass into core among two estimation methods and evaluated mass

Appendix C

Main results of the test C1-10

Table and Figure List

Table C-1 Summary of test conditions

1. TEST TYPE : Low System Pressure Test

2. TEST NUMBER : RUN 019 3. DATE : Dec.20, 1979

4. POWER : A: TOTAL: 9.39 MW; B:LINEAR: 1.4 KW/M

5. RELATIVE RADIAL POWER SHAPE :

   A: ZONE: A B C

   B: RATIO: 1.07 : 1.0 : 0.82

6. AXIAL POWER SHAPE : CHOPPED COSINE

7. PRESSURE (KG/CM^2A) :

   A: SYSTEM: 1.57, B: CONTAINMENT 1.55,

   C: STEAM GENERATOR SECONDARY: 54

8. TEMPERATURE (DEG.C) :

   A: DOWNCOMER WALL 172, B: VESSEL INTERNALS 108,

   C: PRIMARY PIPING WALL 115, D: LOWER PELNUM LIQUID 106,

   E: ECC LIQUID 39, F: STEAM GENERATOR SECONDARY 267,

   G: CORE TEMPERATURE AT ECC INITIATION 529

9. ECC INJECTION TYPE: C

   A: COLD LEG, B: LOWER PLENUM, C: LOWER PLENUM + COLD LEG

10. PUMP K-FACTOR : $\sim$ 15

11. ECC FLOW RATES AND DURATION :

   A: ACCUMULATOR 269 M^3/HR FROM 0 TO 23 SECONDS

   B: LPCI 30.4 M^3/HR FROM 23 TO 858 SECONDS

   C: ECC INJECTION TO LOWER PLENUM : FROM 0 TO 17.5 SECONDS

   (VALVE OPENING AND CLOSING TIMES ARE INCLUDED IN THE INJECTION DURATION)

12. INITIAL WATER LEVEL IN LOWER PLENUM : 0.89 M.

13. POWER CONTROL : ANS x 1.2 + ACTINIDE (30 SEC AFTER SCRAM)

14. EXPECTED BOCREC TIME FROM ECC INITIATION 12 SEC

15. EXPECTED PEAK TEMPERATURE AT BOCREC 600 C

Table C-2 Chronology of events

EVENT	TIME (sec)
Test Initiated (Heater Rods Power on) (Data Recording Initiated)	0.0
Accumulator Injection Initiated	55
Power Decay Initiated (Bottom of Core Recovery)	66.5
Accumulator Injection Switched from Lower Plenum to Cold Leg	72.5
Accumulator Injection Ended and LPCI Injection Initiated	78
All Heater Rods Quenched	695
Power Off	770
LPCI Injection Ended	858
Test Ended (Data Recording Ended)	1071

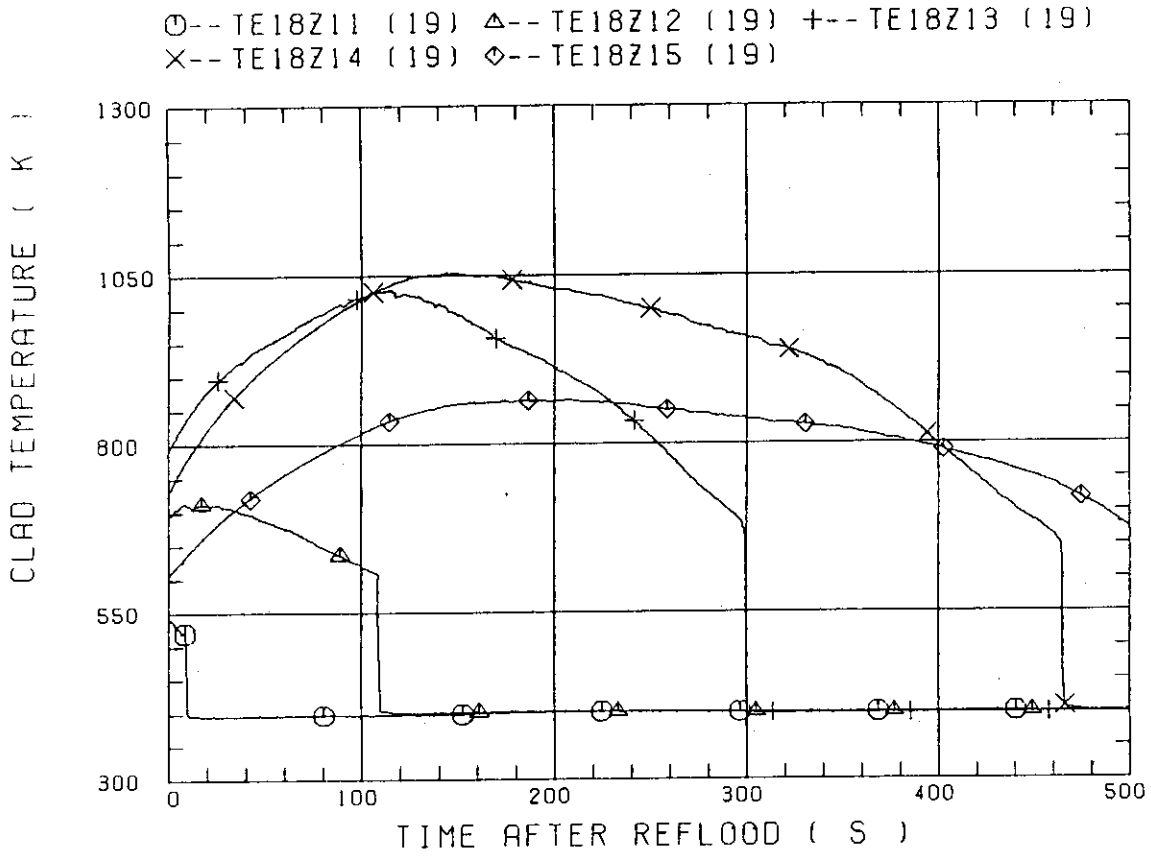

Fig. C-1 **Surface temperature on low power rod (Z-rod) in medium power region (B region) (average power rod)**

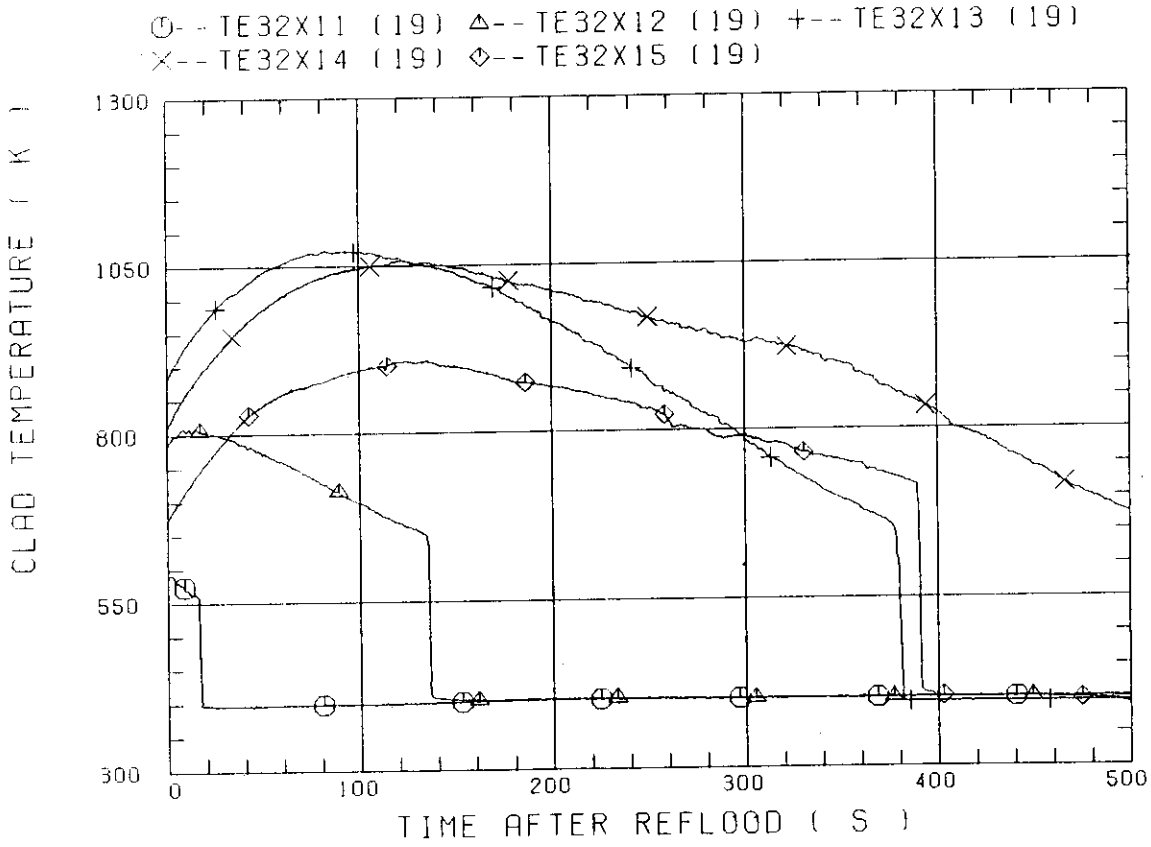

Fig. C-2 **Surface temperature on high power rod (X-rod) in high power region (A region) (peak power rod)**

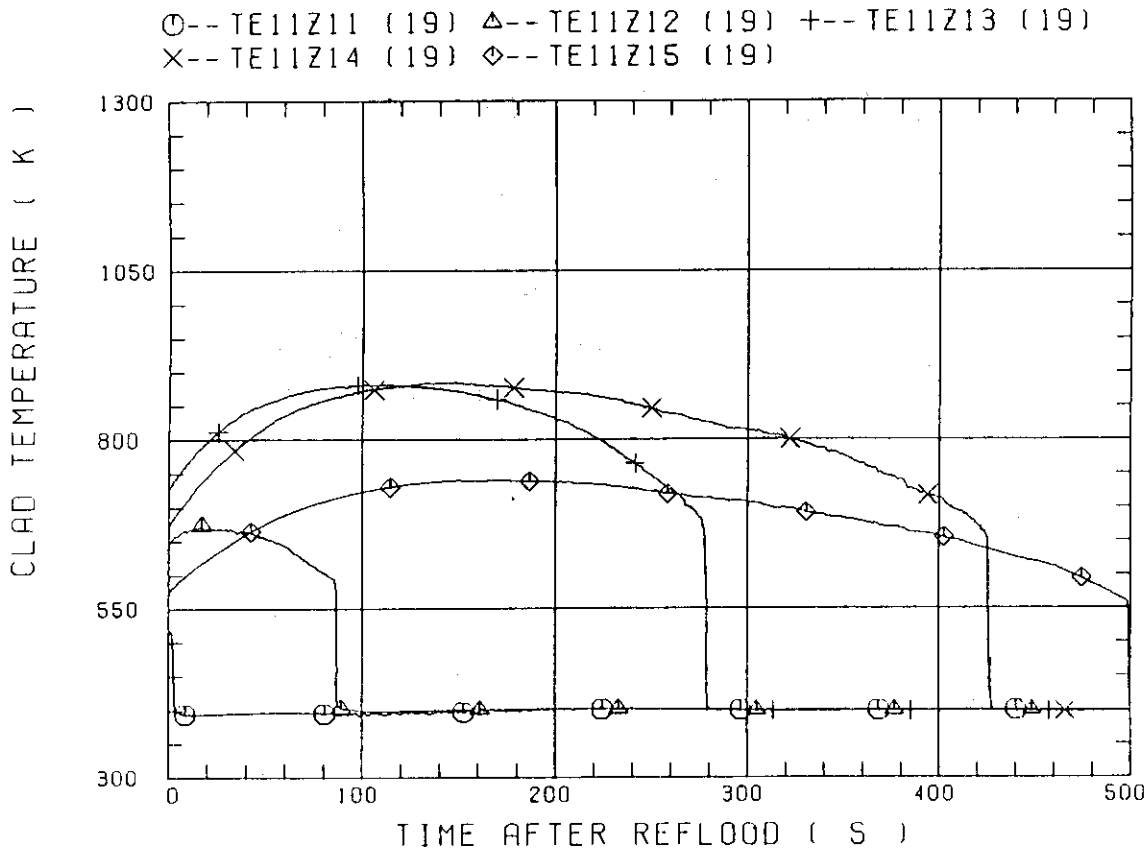

Fig. C-3 **Surface temperature on low power rod (Z-rod) in low power region (C region) (lowest power rod)**

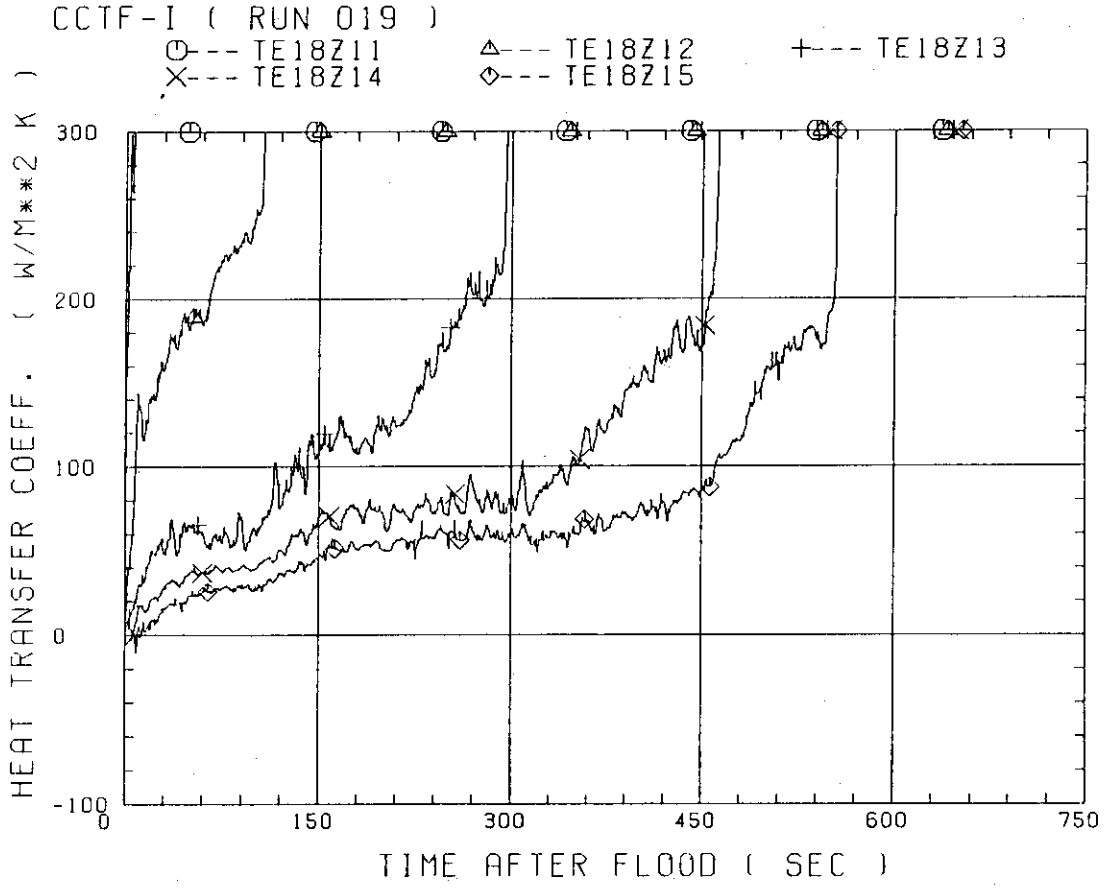

Fig. C-4 **Heat transfer coefficient along a low power rod (Z-rod) in medium power region (B region) (average power rod)**

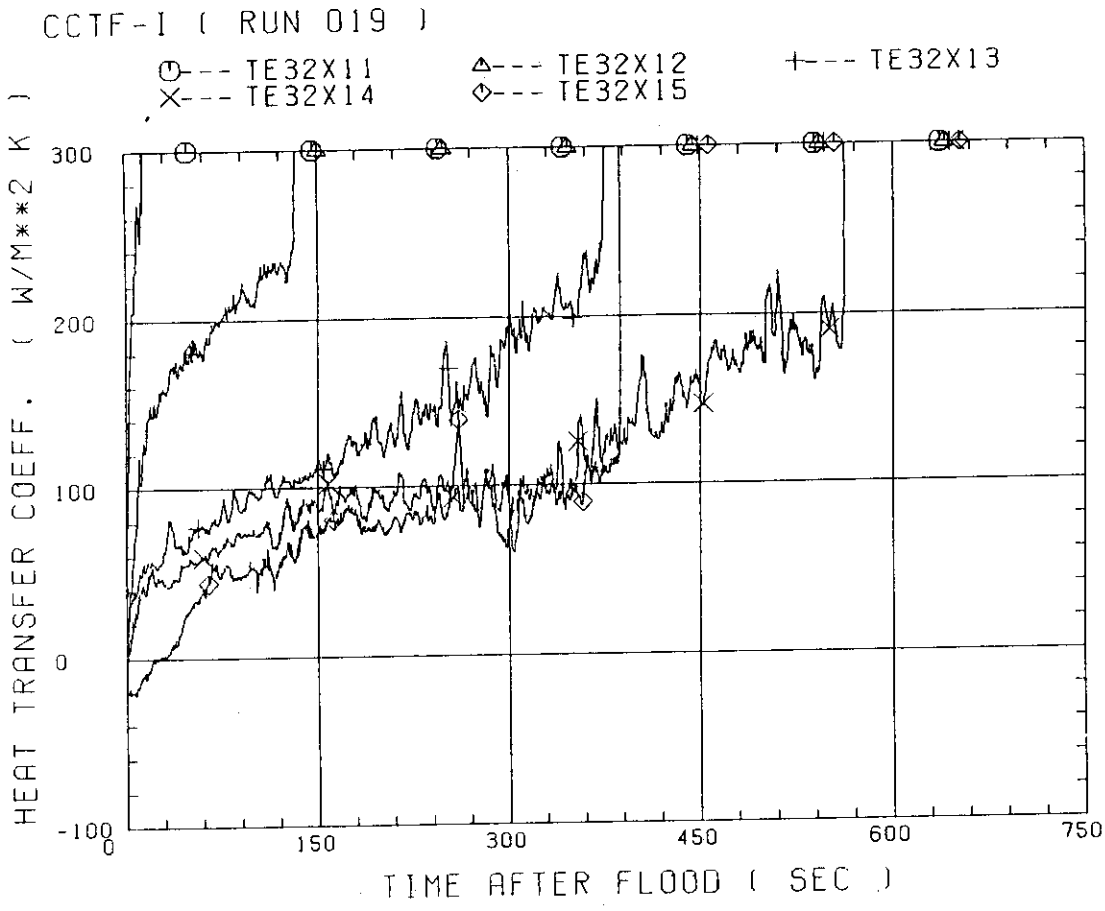

Fig. C-5 Heat transfer coefficient along a high power rod (X-rod) in high power region (A region) (peak power rod)

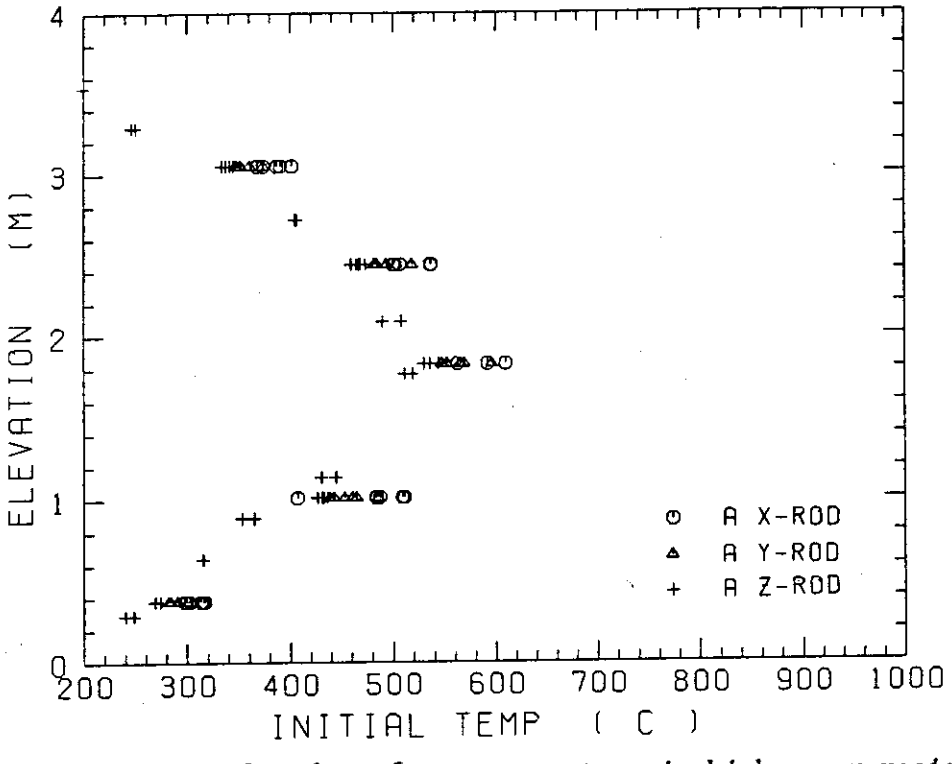

Fig. C-6 Initial rod surface temperature in high power region (A region)

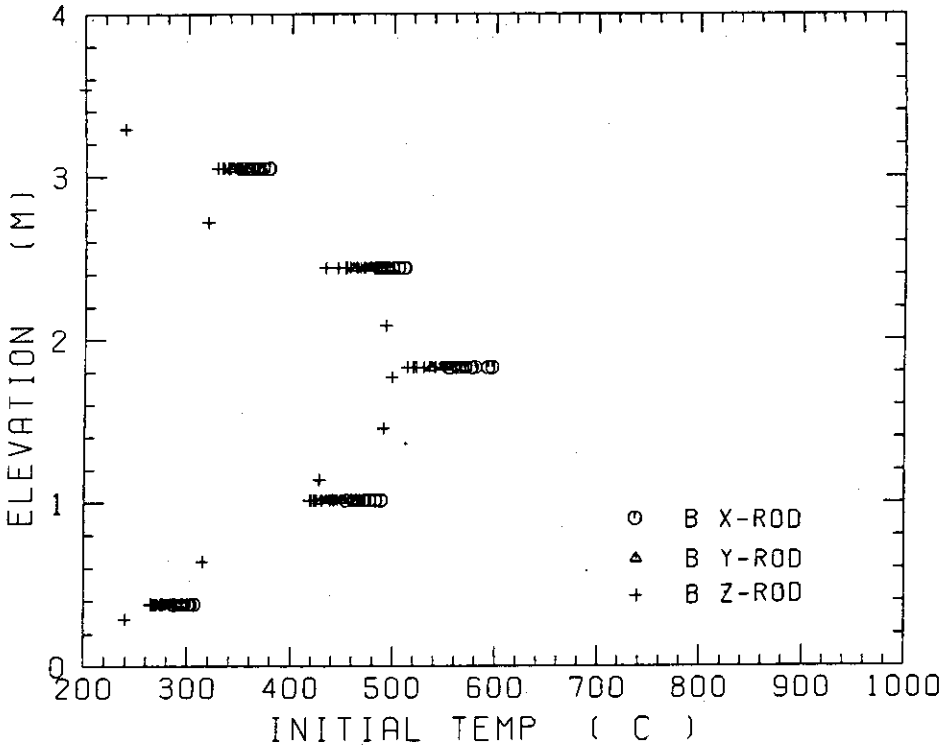

Fig. C-7 **Initial rod surface temperature in medium power region (B region)**

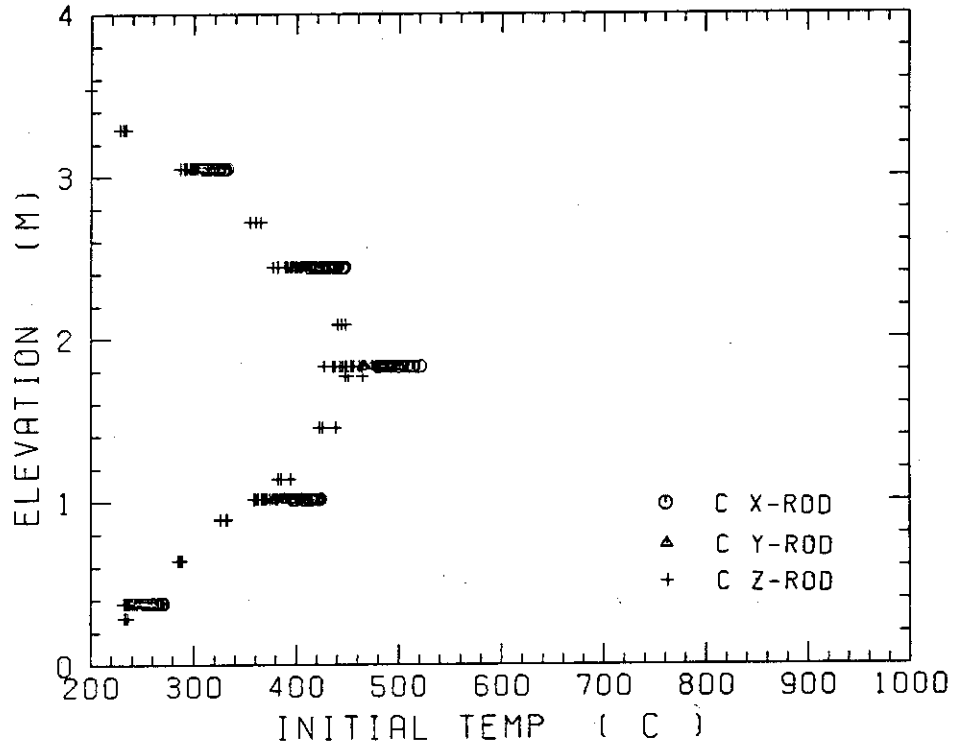

Fig. C-8 **Inital rod surface temperature in low power region (C region)**

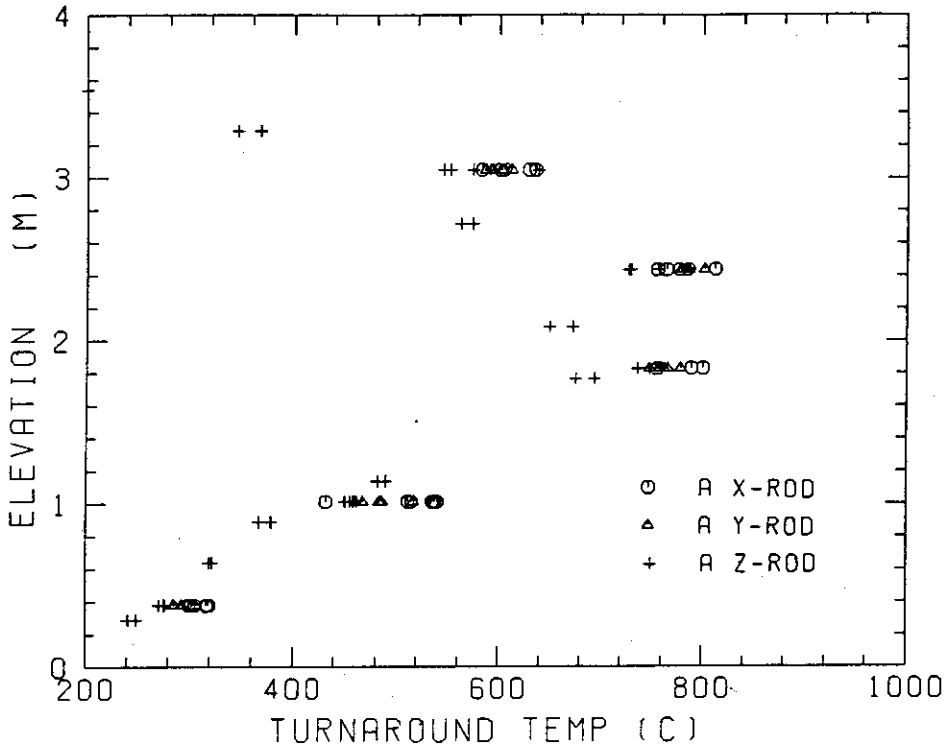

Fig. C-9 Turnaround temperature in high power region (A region)

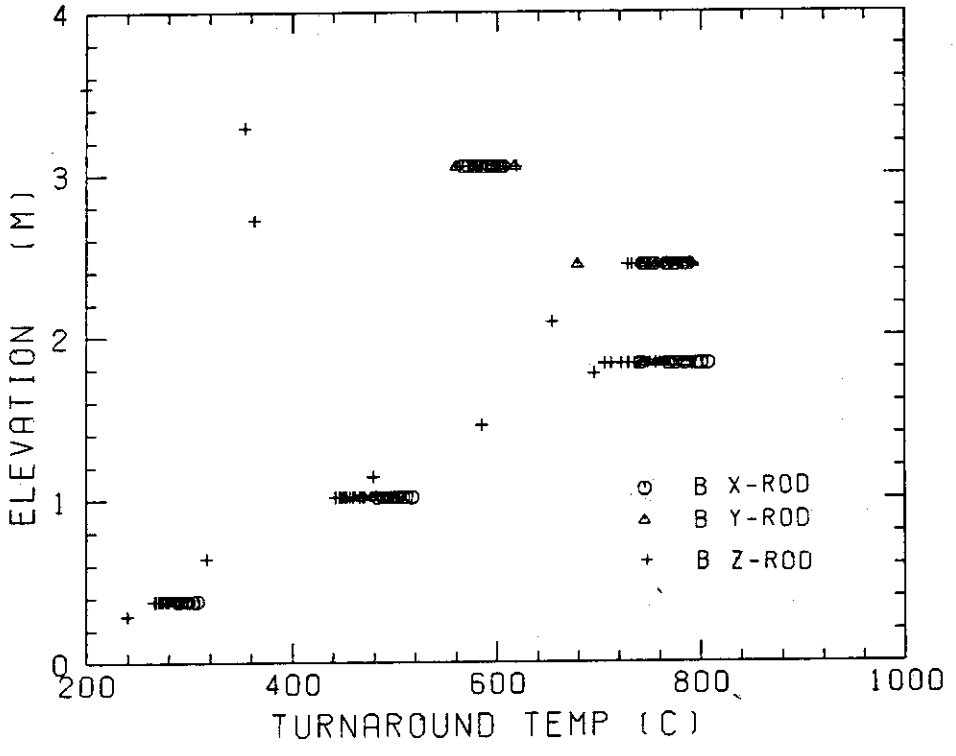

Fig. C-10 Turnaround temperature in medium power region (B region)

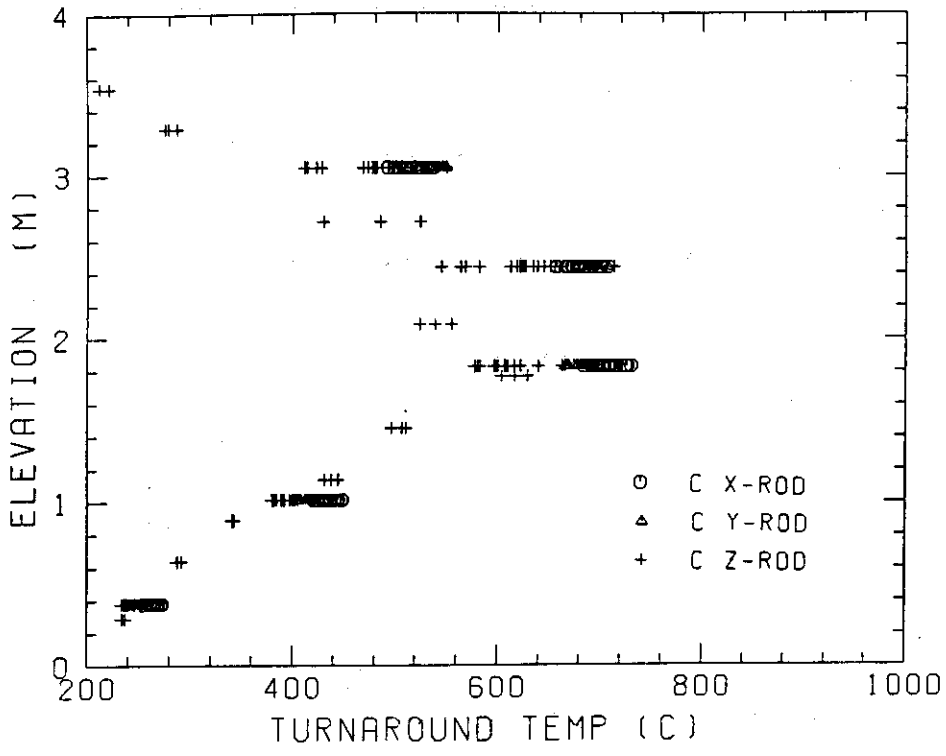

Fig. C-11 Turnaround temperature in low power region (C region)

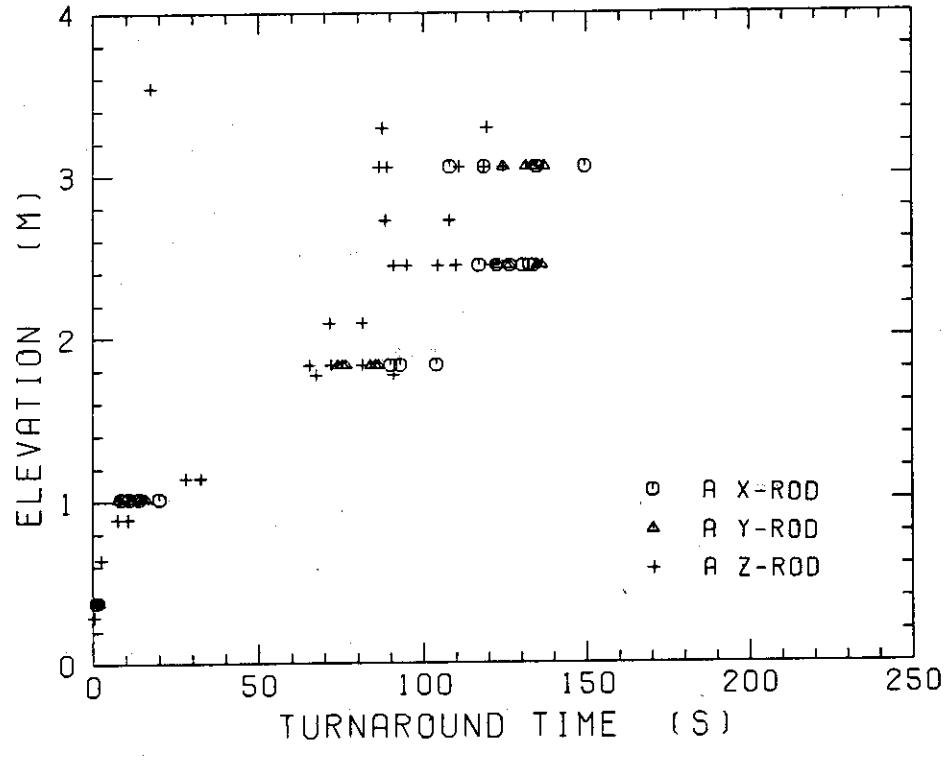

Fig. C-12 Turnaround time in high power region (A region)

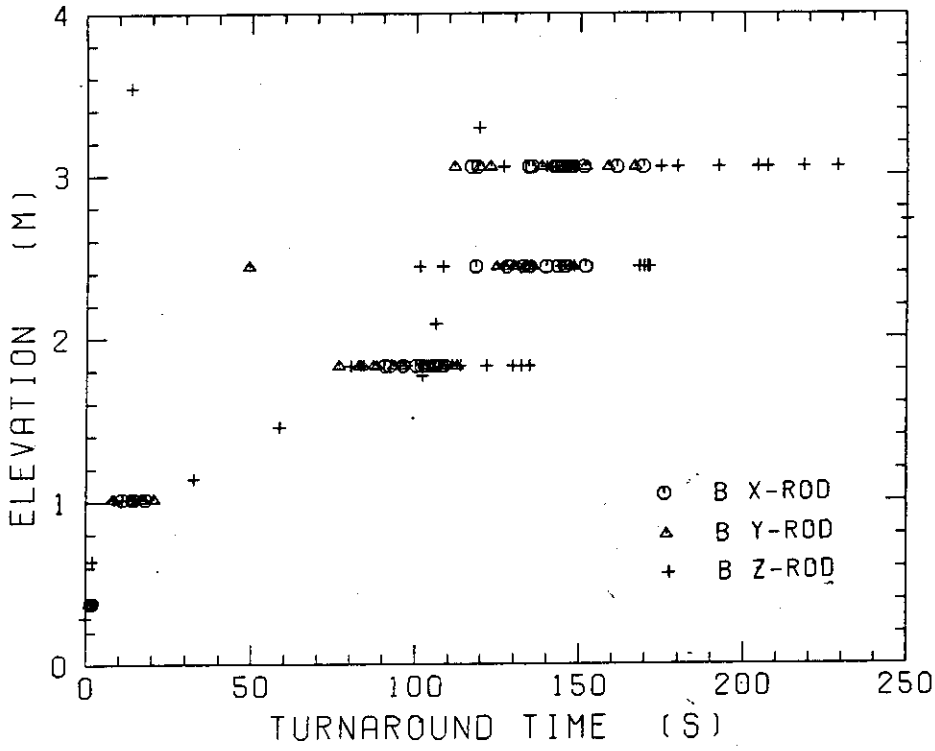

Fig. C-13 Turnaround time in medium power region (B region)

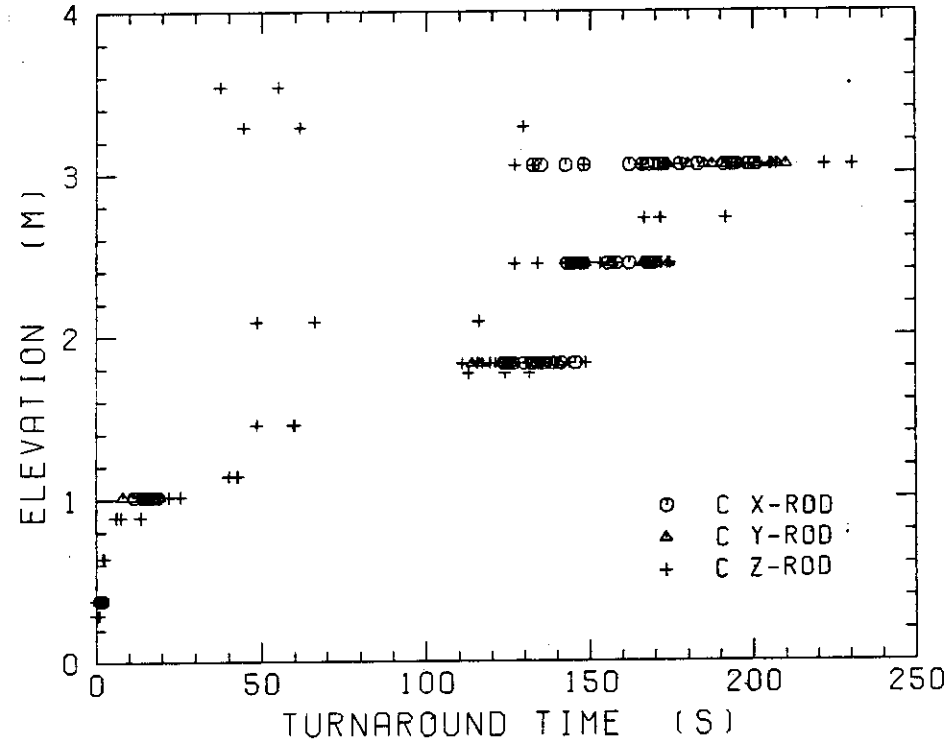

Fig. C-14 Turnaround time in low power region (C region)

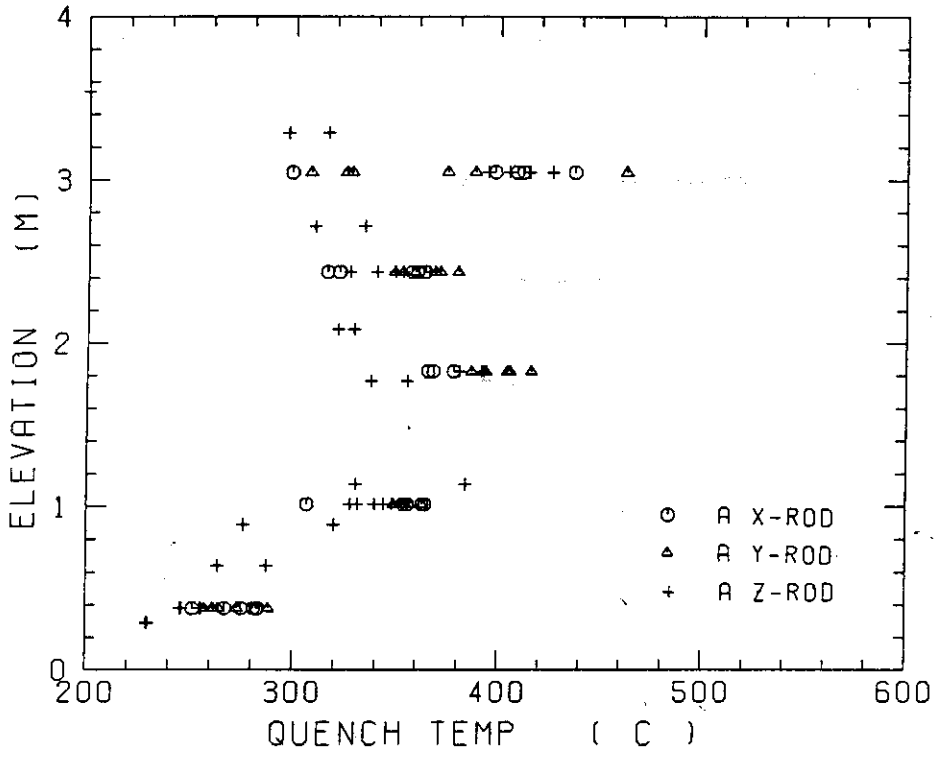

Fig. C-15 Quench temperature in high power region (A region)

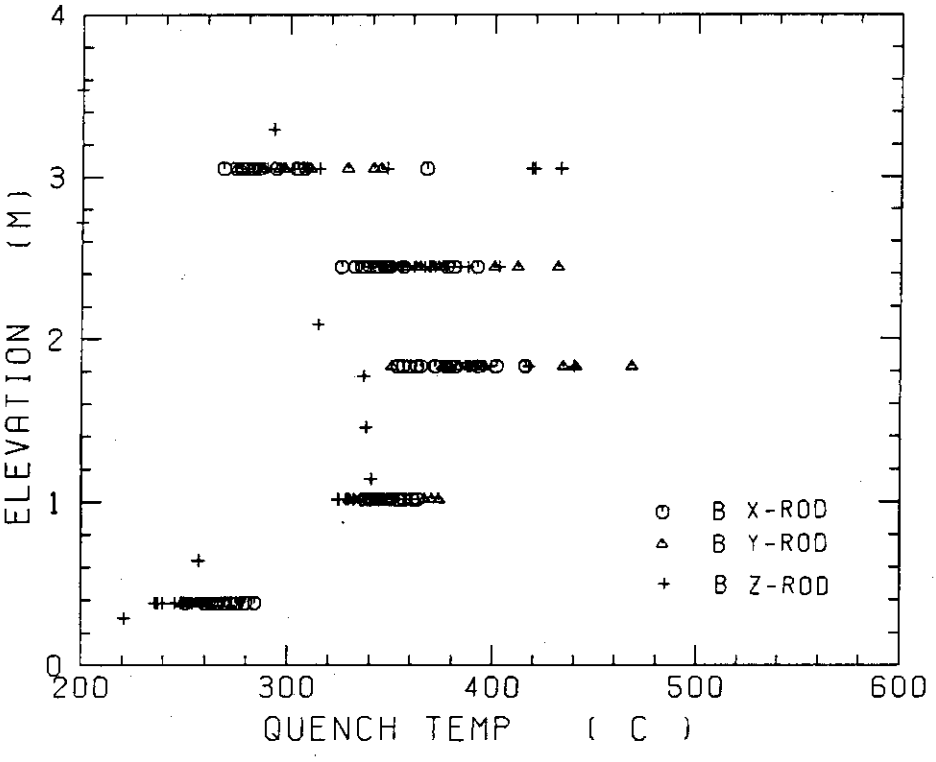

Fig. C-16 Quench temperature in medium power region (B region)

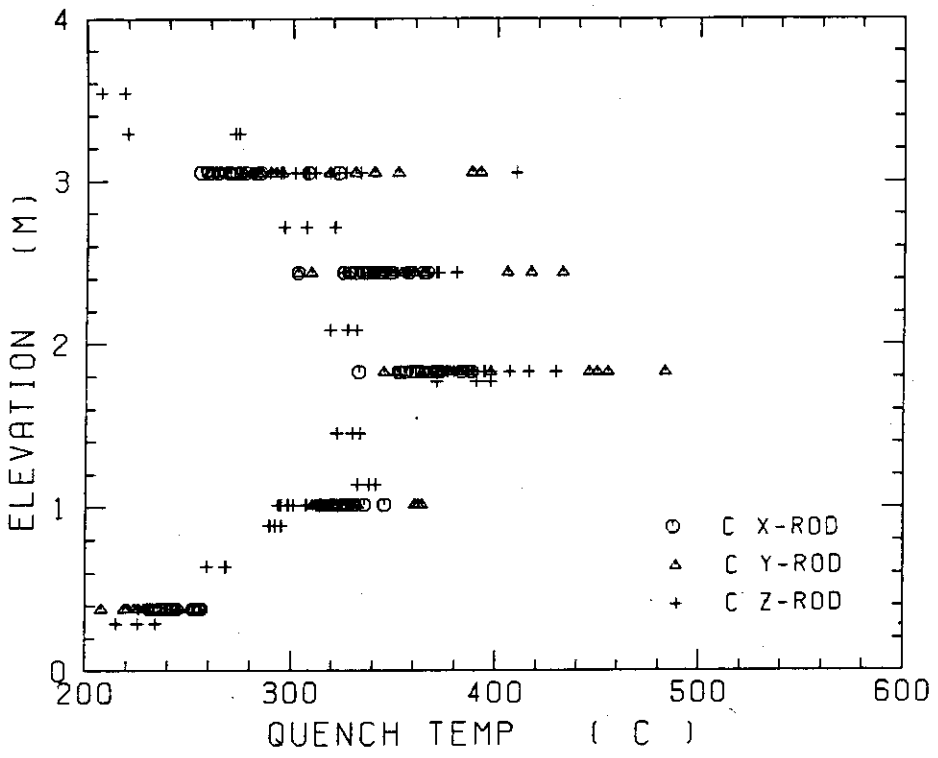

Fig. C-17 Quench temperature in low power region (C region)

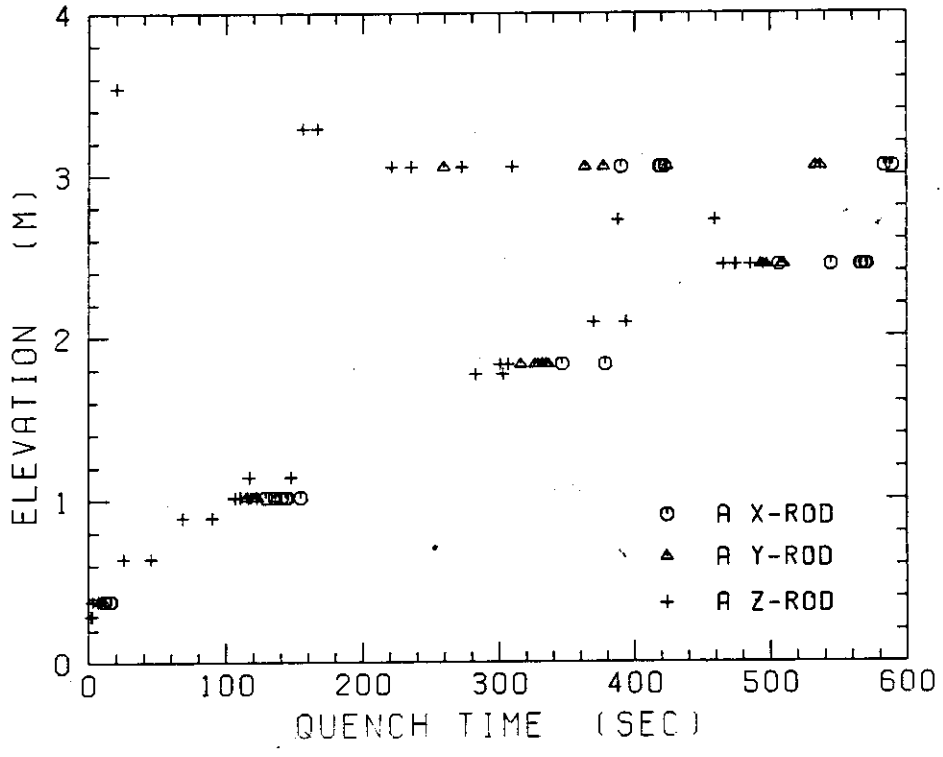

Fig. C-18 Quench time in high power region (A region)

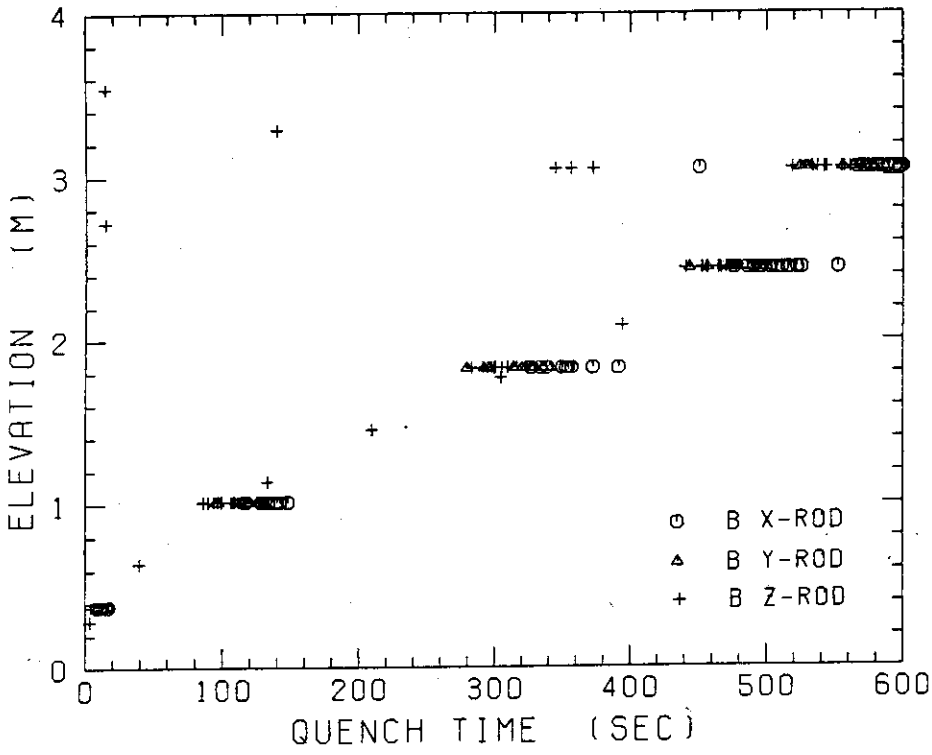

Fig. C-19 Quench time in medium power region (B region)

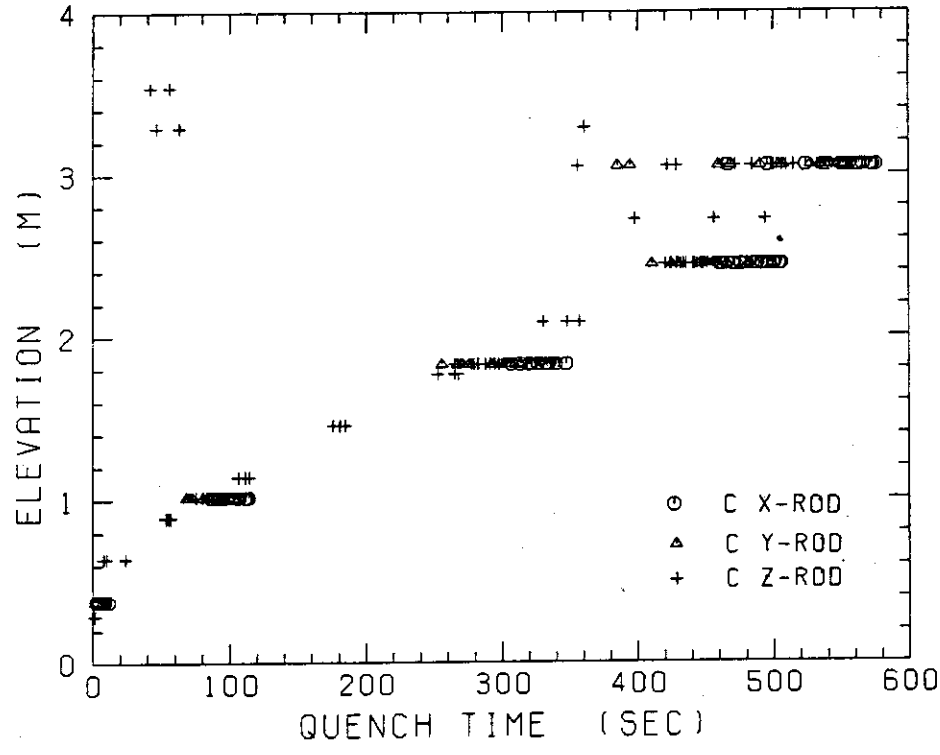

Fig. C-20 Quench time in low power region (C region)

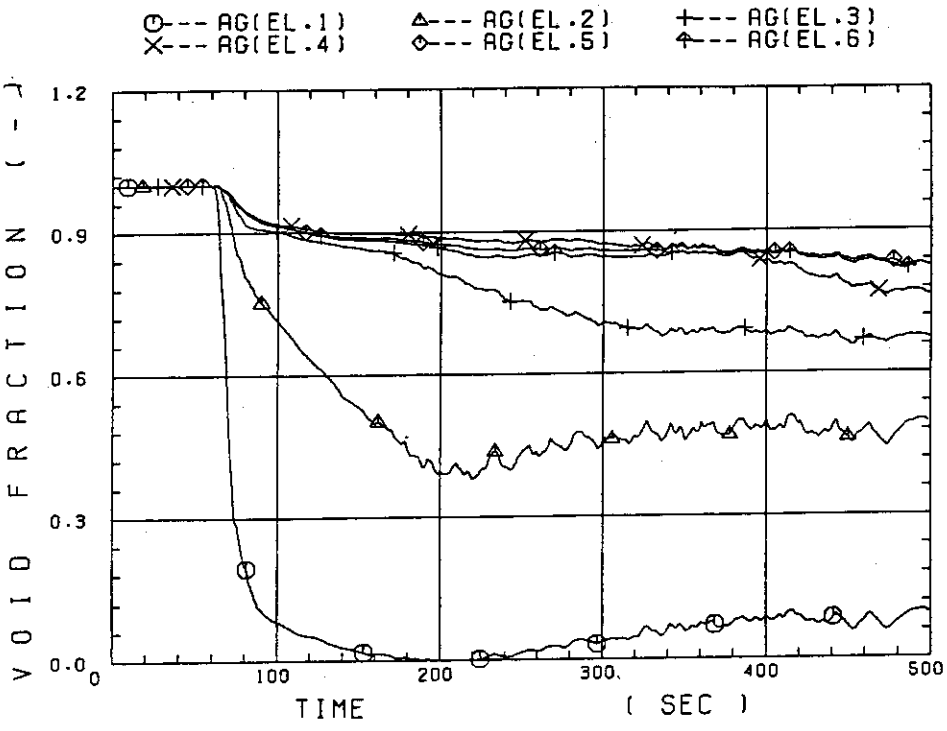

Fig. C-21 Void fraction in core

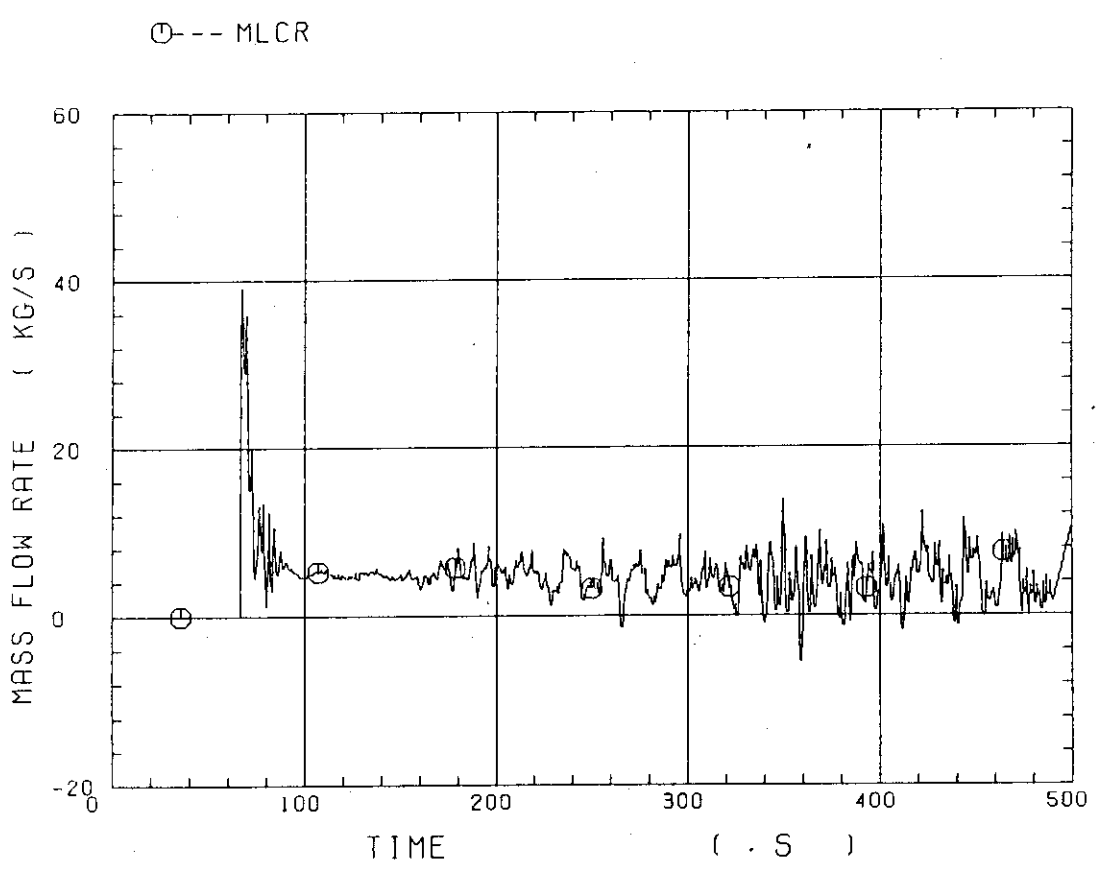

Fig. C-22 Core inlet mass flow rate

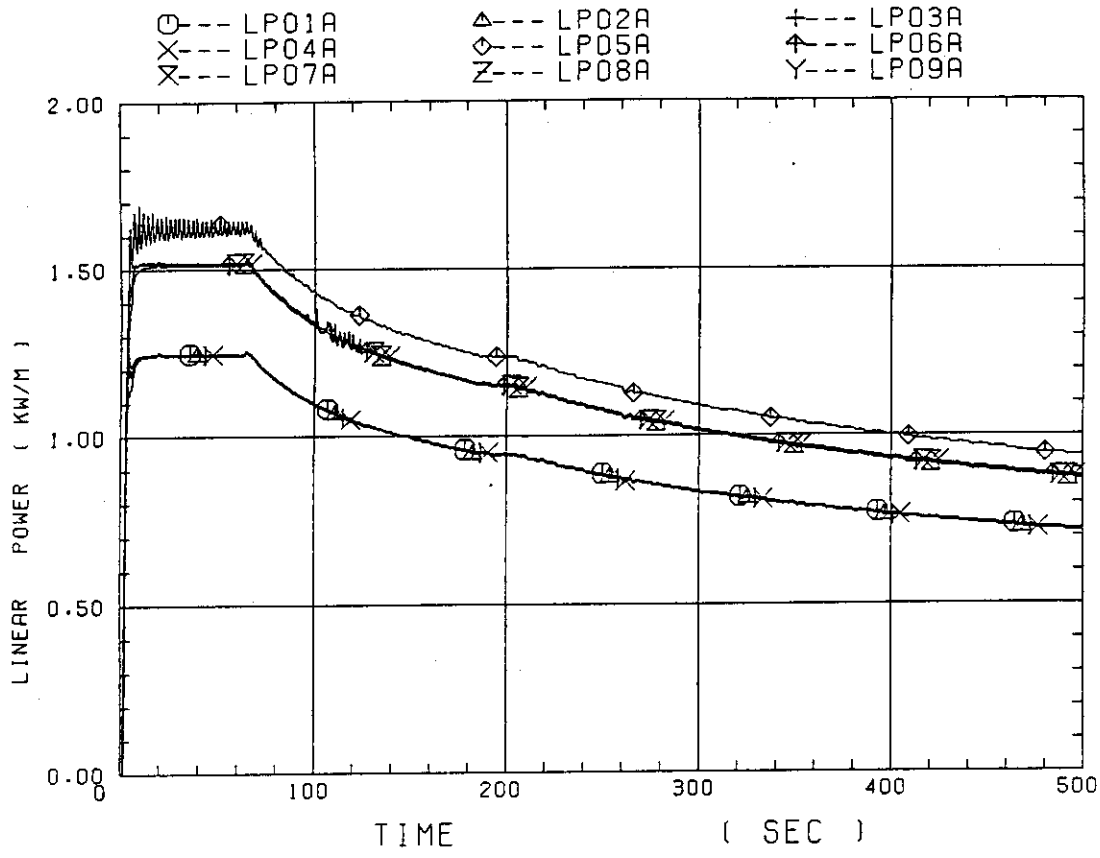

Fig. C-23 Average linear power of heater rod in each power unit zone

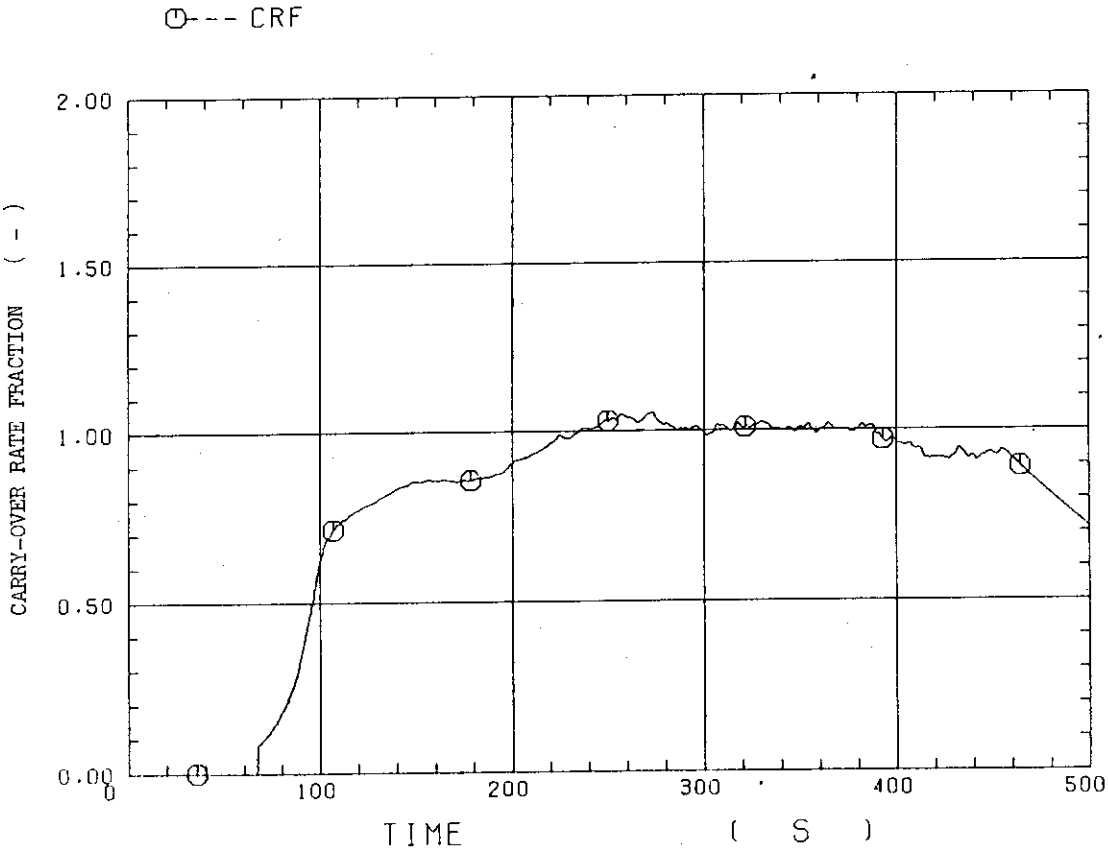

Fig. C-24 Carry-over rate fraction

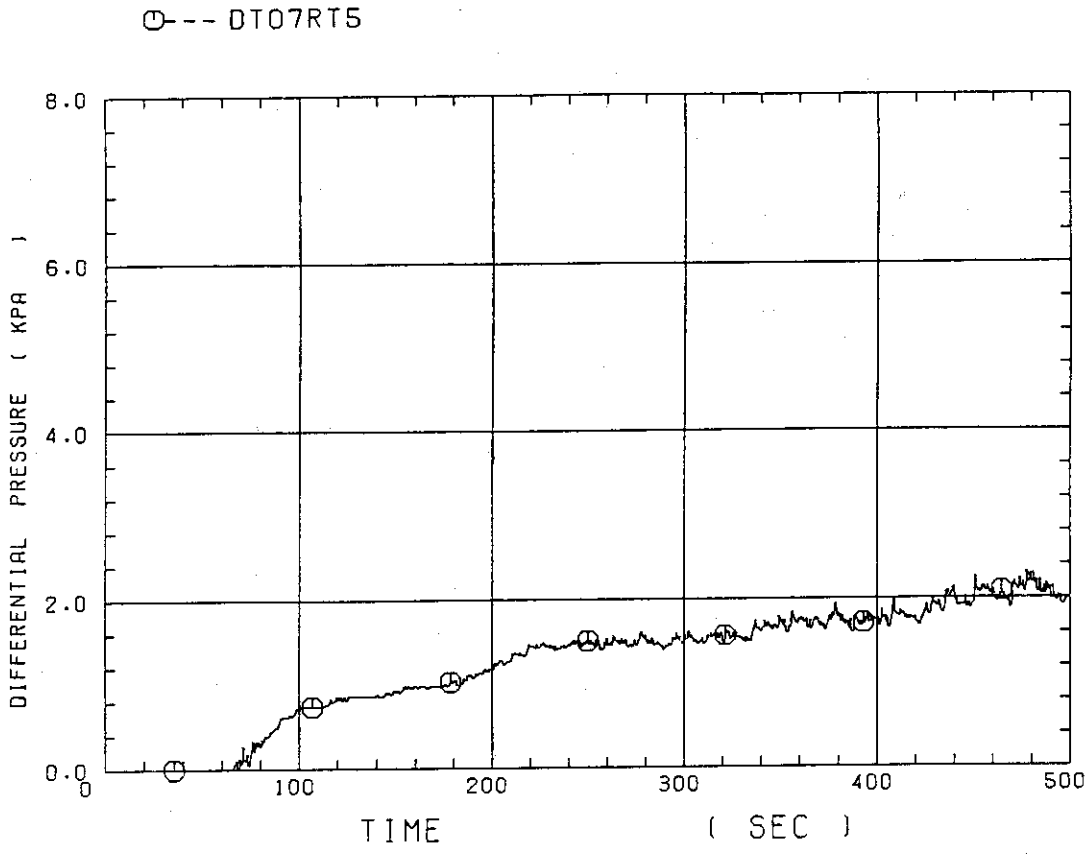

Fig. C-25 Differential pressure through upper plenum

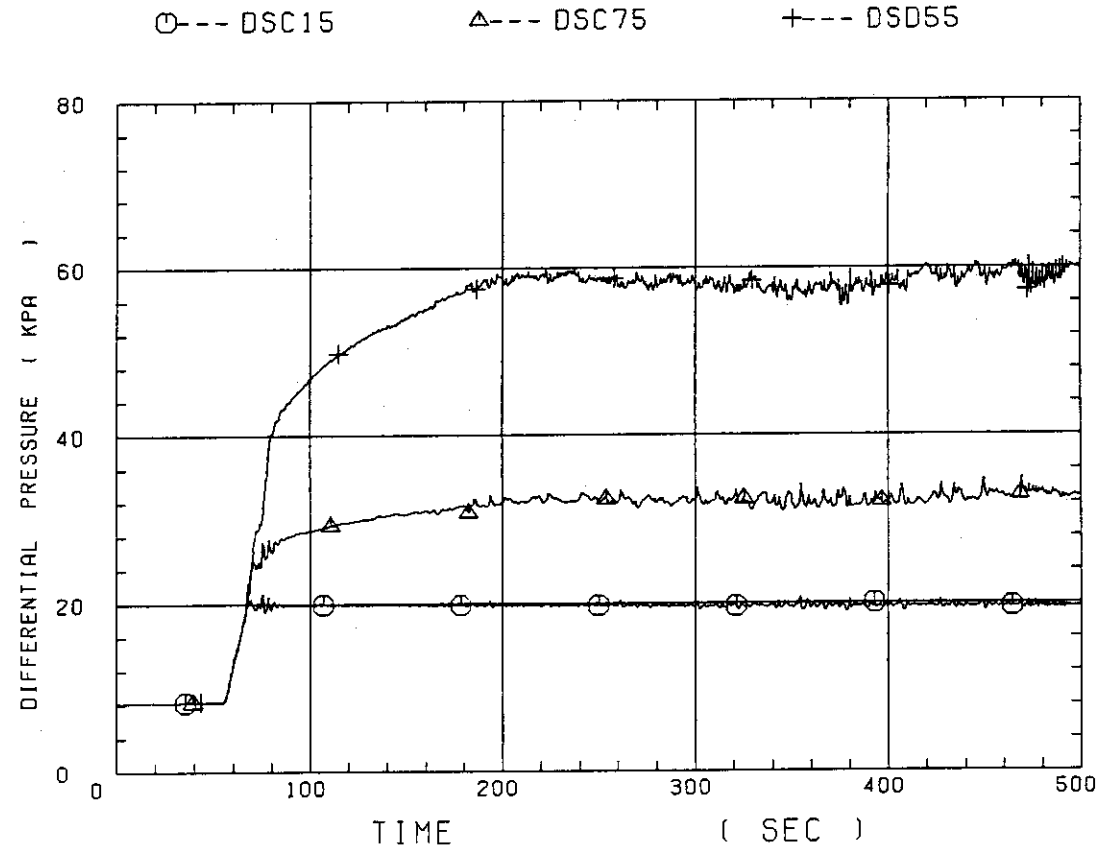

Fig. C-26 Differential pressure through downcomer, core, and lower plenum

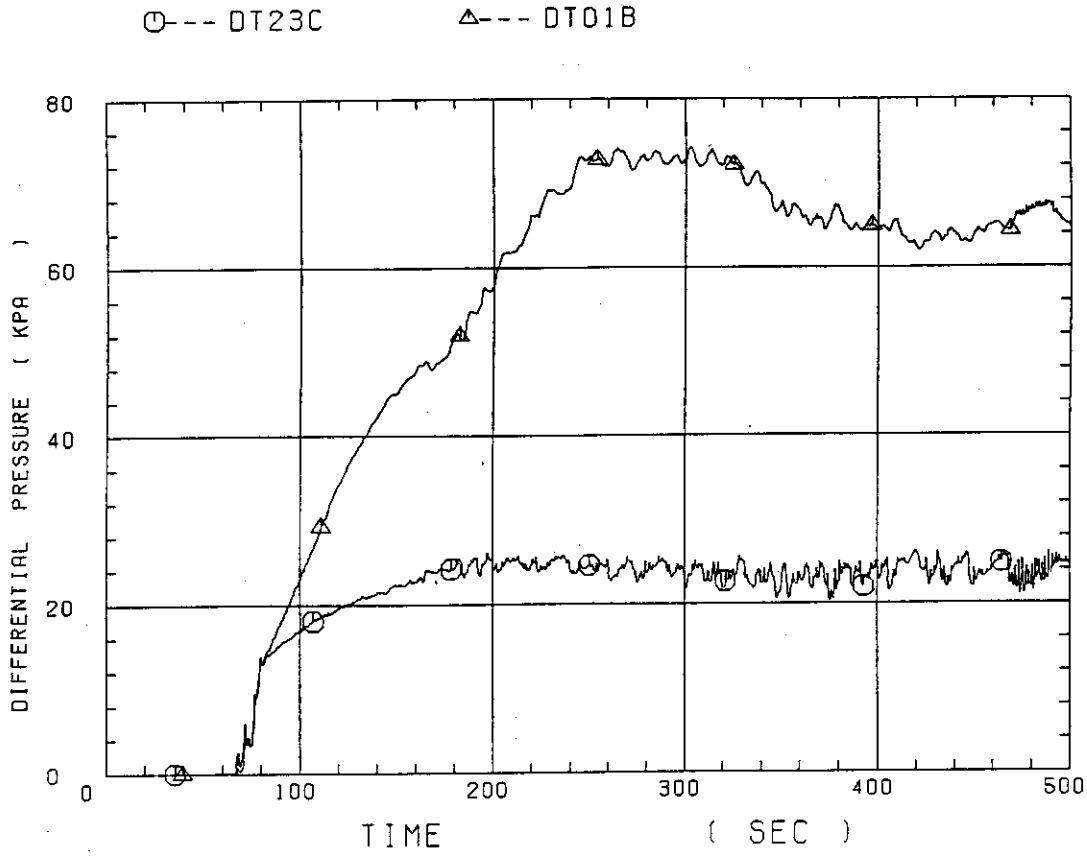

Fig. C-27 Differential pressure through intact and broken loops

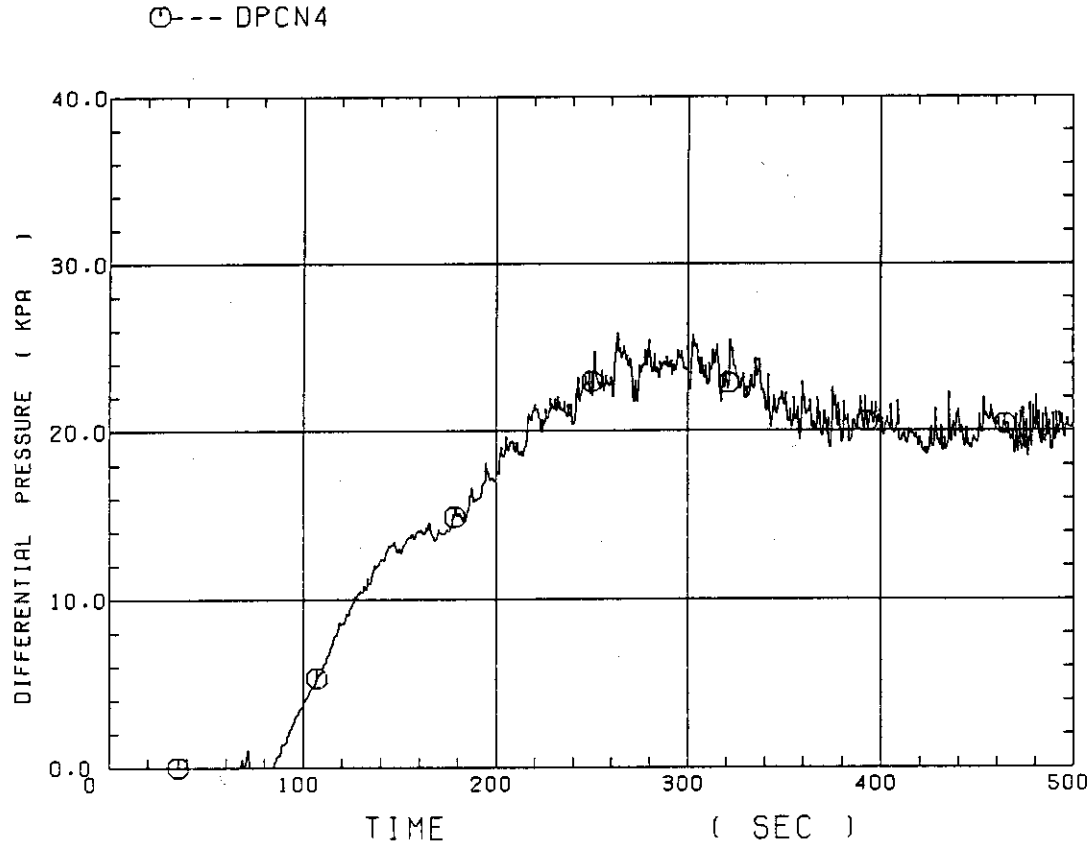

Fig. C-28 Differential pressure through broken cold leg nozzle

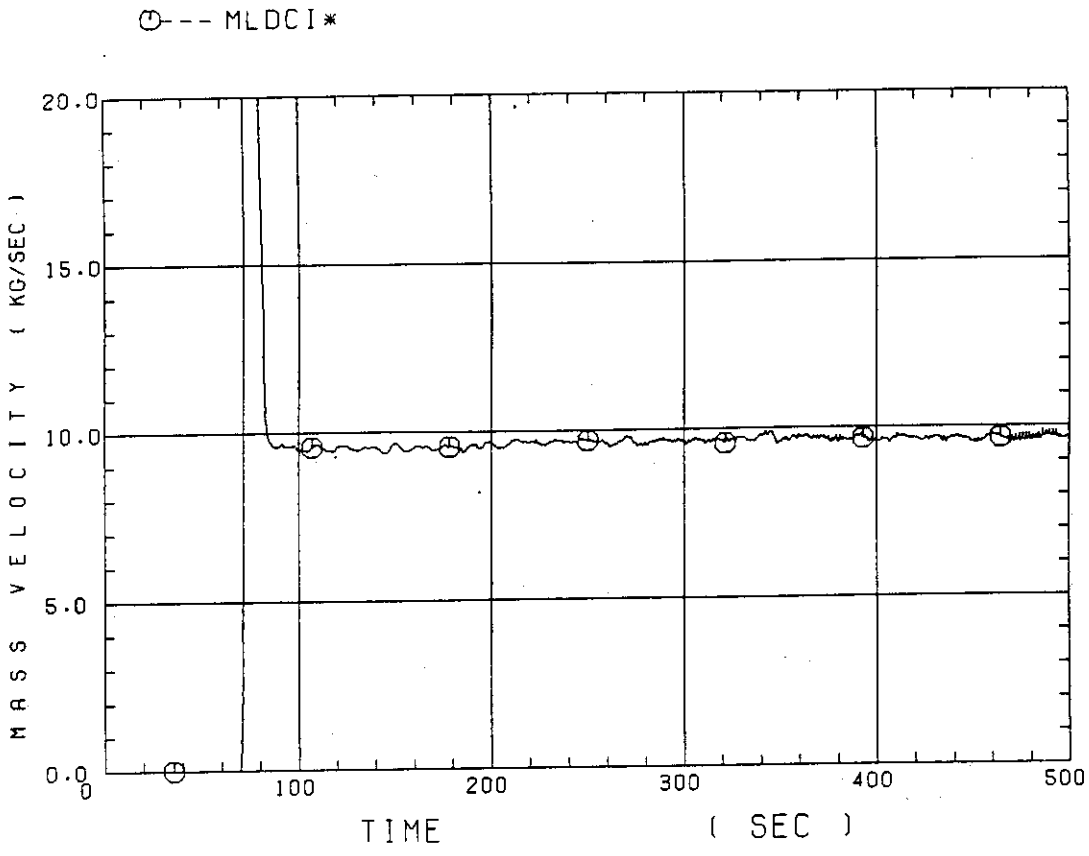

Fig. C-29 Total water mass flow rate from intact loops to downcomer

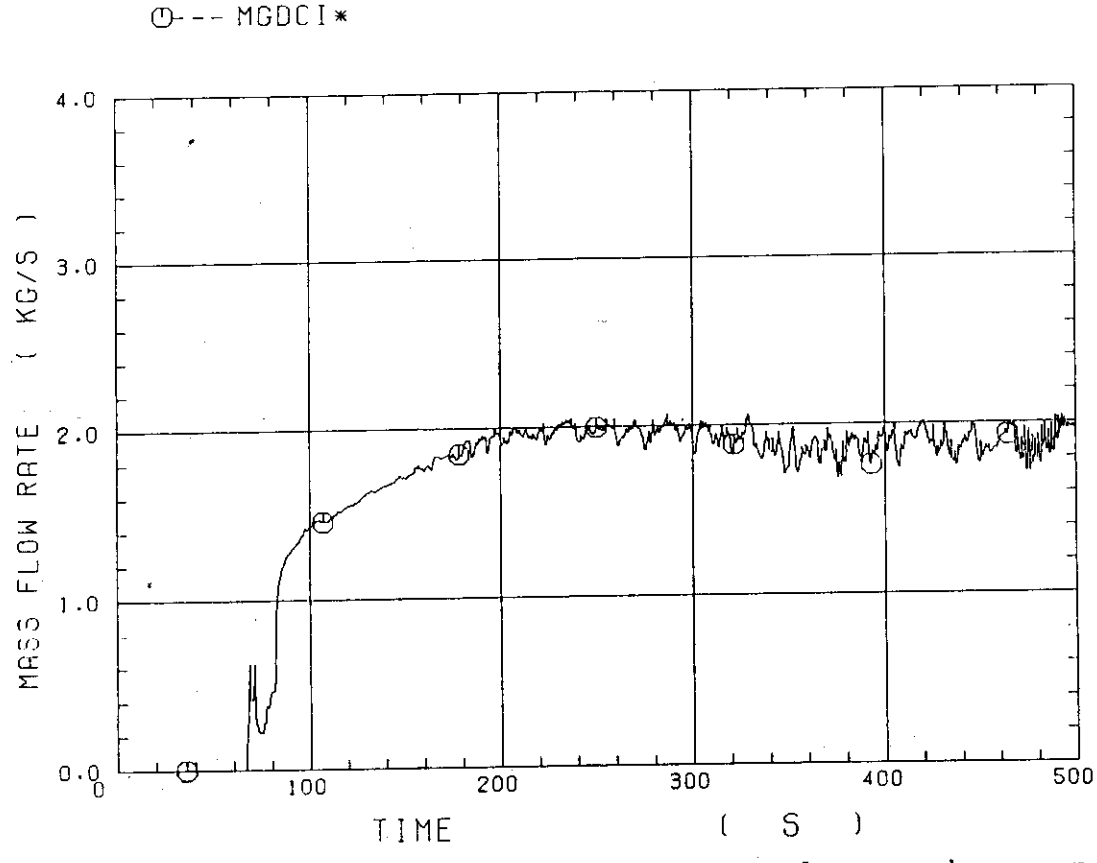

Fig. C-30 Total steam mass flow rate from intact loops to downcomer

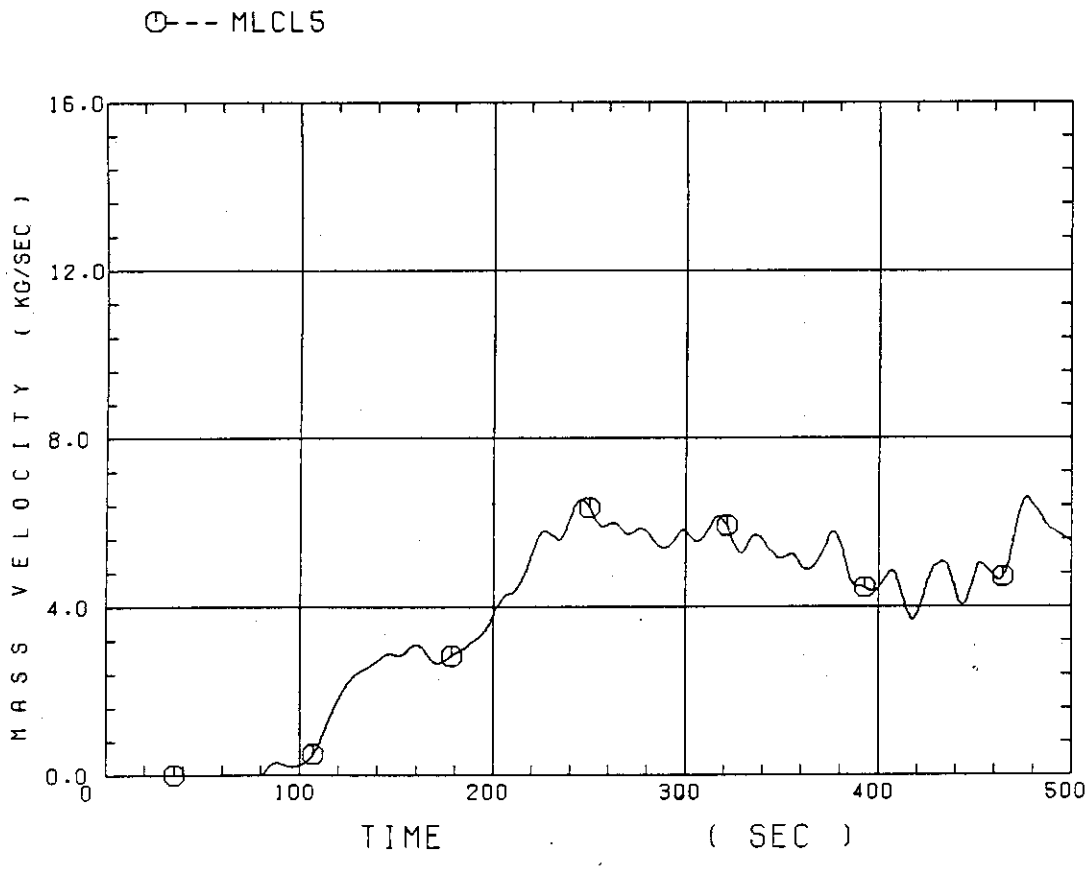

Fig. C-31 Water mass flow rate through broken cold leg nozzle

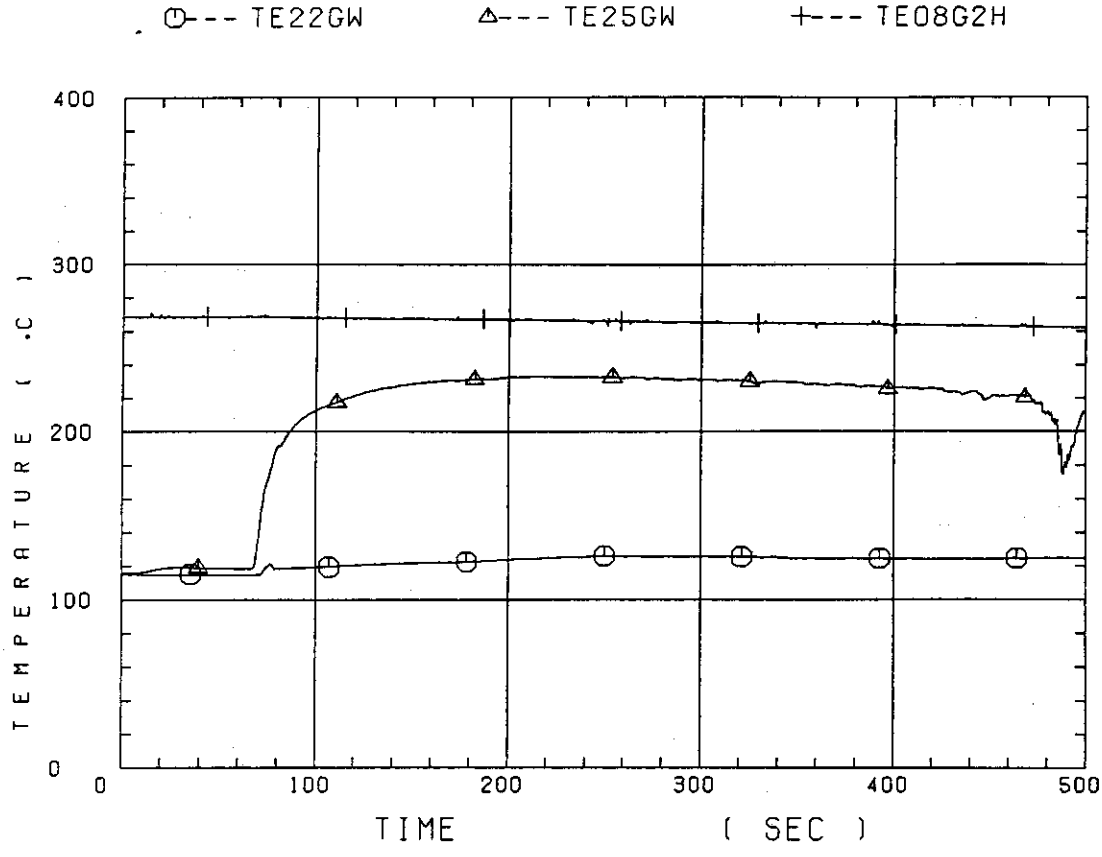

Fig. C-32 Fluid temperature in inlet plenum, outlet plenum, and secondary of steam generator 1

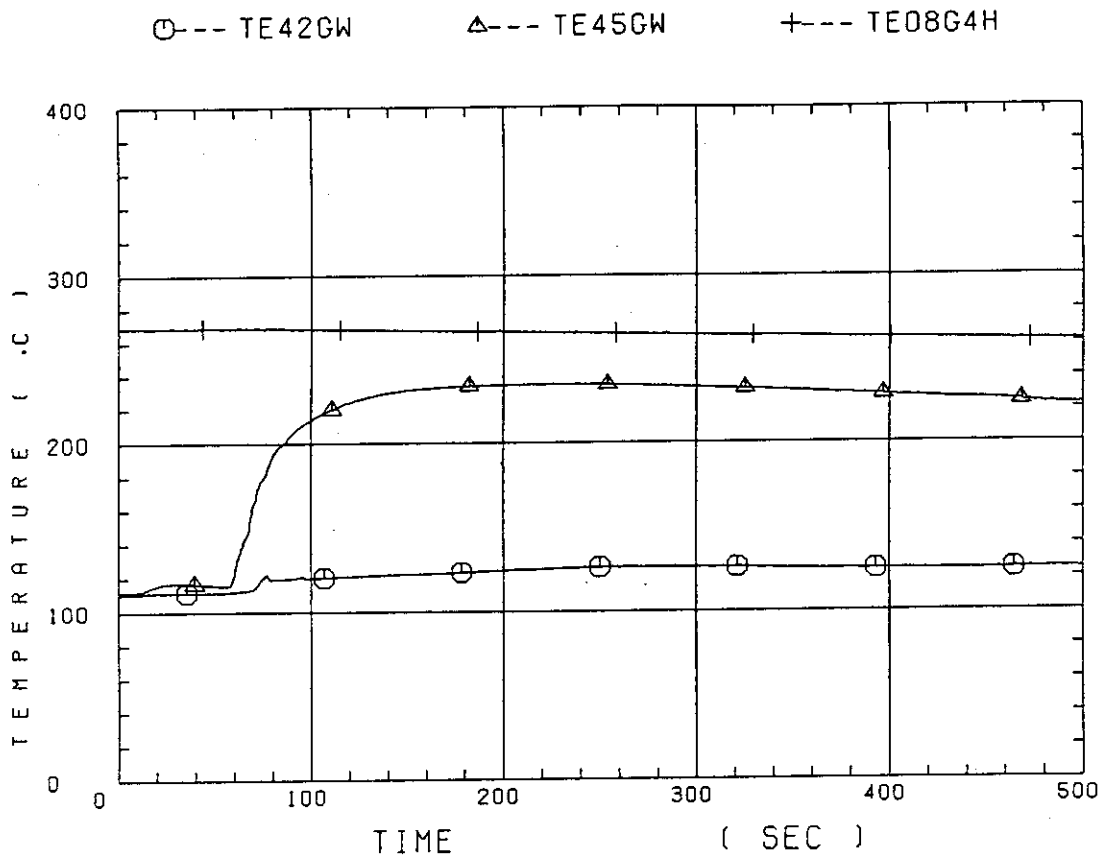

Fig. C-33 **Fluid temperature in inlet plenum, outlet plenum, and secondary of steam generator 2**

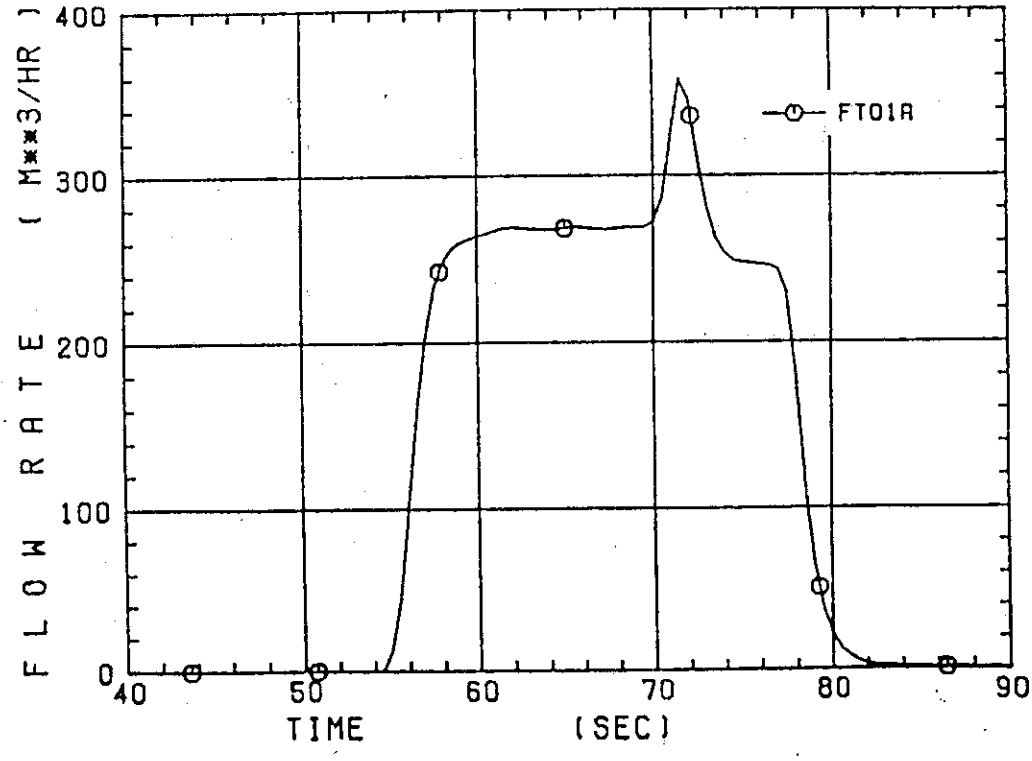

Fig. C-34 **Total accumulator injection rate**

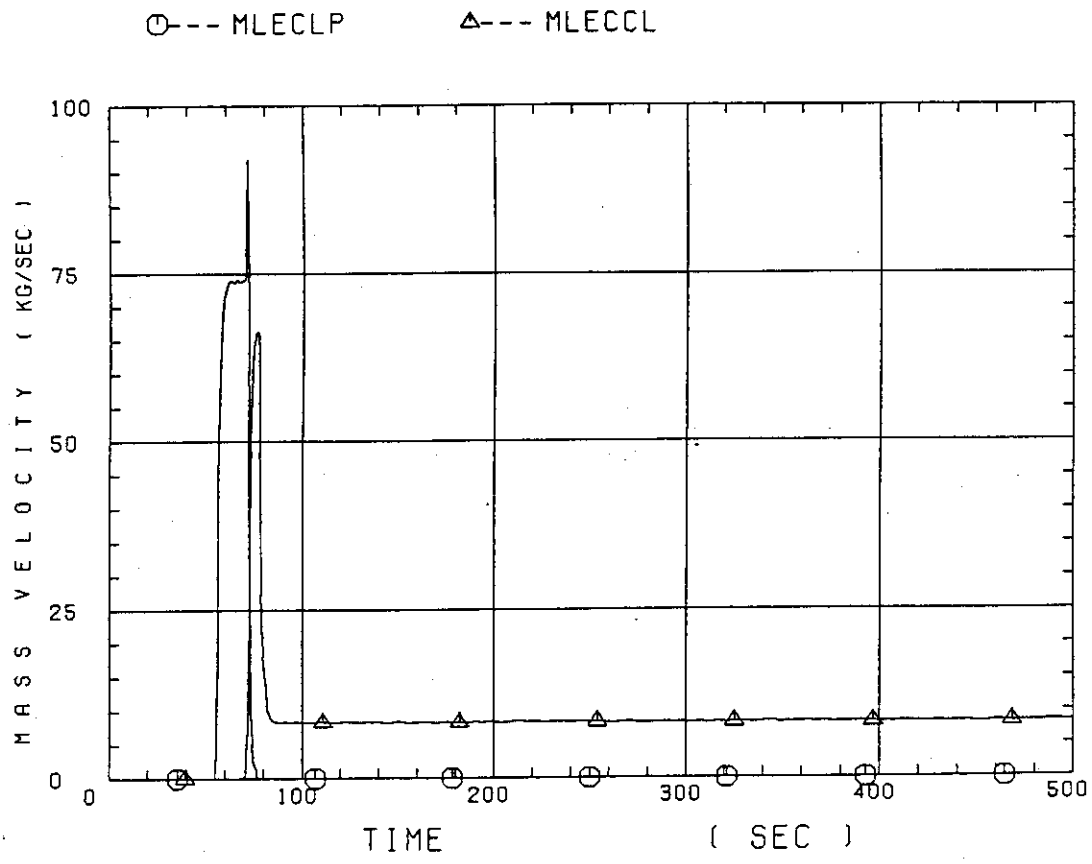

Fig. C-35 ECC water injection rates to lower plenum and to cold legs

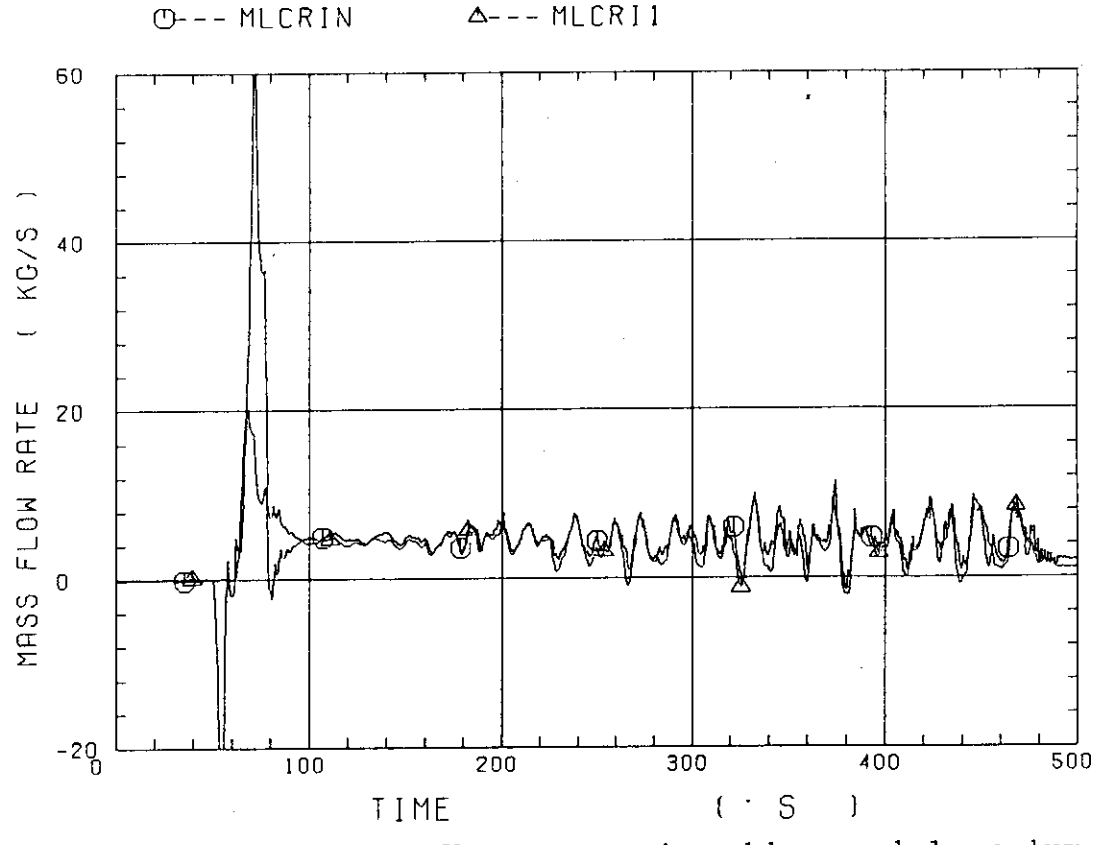

Fig. C-36 Core inlet mass flow rates estimated by mass balance downstream and upstream of core inlet

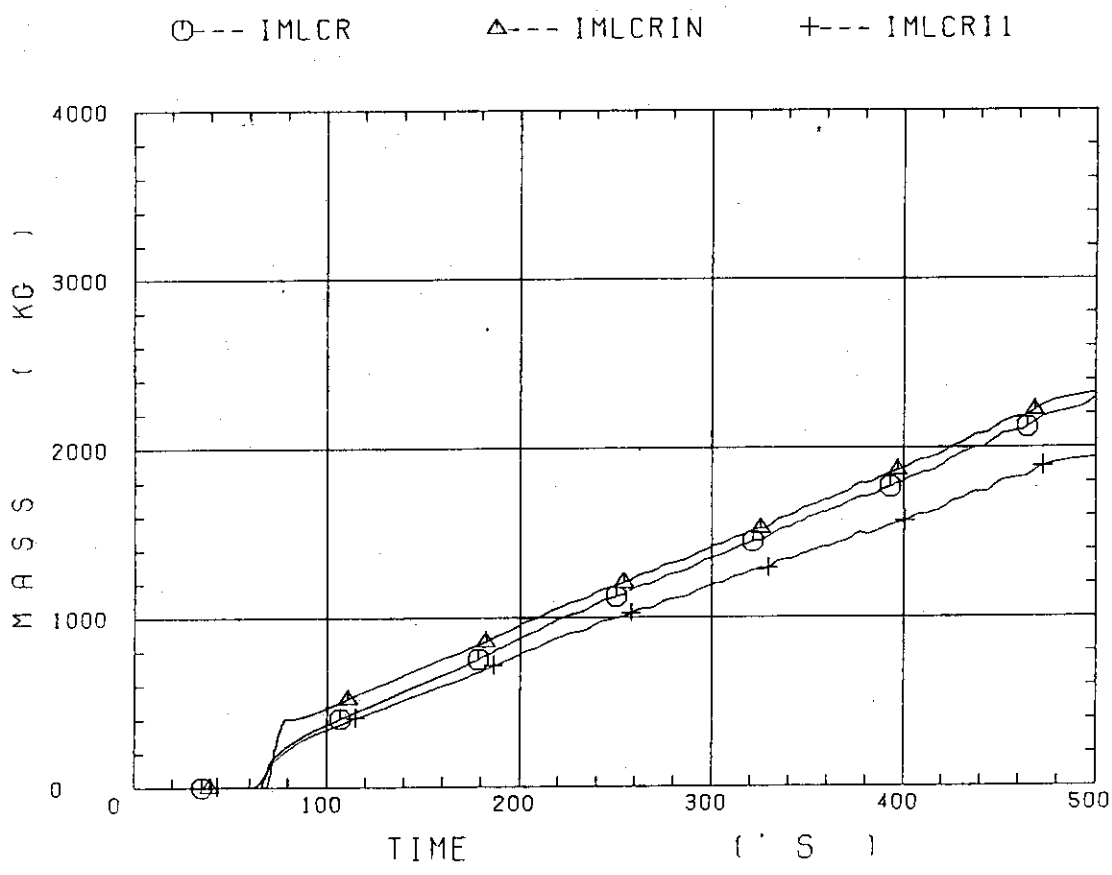

Fig. C-37 Comparison of injected mass into core among two estimation methods and evaluated mass

Appendix D

Main results of the test C1-12

Table and Figure List

Table D-1 Summary of test conditions

1. TEST TYPE : High System Pressure Test
2. TEST NUMBER : Run 021 3. DATE : Jan.24, 1980
4. POWER : A: TOTAL: 9.40 MW; B:LINEAR: 1.4 KW/M
5. RELATIVE RADIAL POWER SHAPE :

   A: ZONE: A B C

   B: RATIO: 1.07 : 1.0 : 0.82
6. AXIAL POWER SHAPE : CHOPPED COSINE
7. PRESSURE (KG/CM^2A) :

   A: SYSTEM: 3.05, B: CONTAINMENT 3.05,

   C: STEAM GENERATOR SECONDARY: 51
8. TEMPERATURE (DEG.C) :

   A: DOWNCOMER WALL 190, B: VESSEL INTERNALS 131,

   C: PRIMARY PIPING WALL 133, D: LOWER PELNUM LIQUID 126,

   E: ECC LIQUID 39.9, F: STEAM GENERATOR SECONDARY 265,

   G: CORE TEMPERATURE AT ECC INITIATION 524
9. ECC INJECTION TYPE: C

   A: COLD LEG, B: LOWER PLENUM, C: LOWER PLENUM + COLD LEG
10. PUMP K-FACTOR : ∿ 15
11. ECC FLOW RATES AND DURATION :

    A: ACCUMULATOR 289 M^3/HR FROM 0 TO 24.5 SECONDS

    B: LPCI 30.7 M^3/HR FROM 24.5 TO 7.56 SECONDS

    C: ECC INJECTION TO LOWER PLENUM : FROM 0 TO 17.5 SECONDS

    (VALVE OPENING AND CLOSING TIMES ARE INCLUDED IN THE INJECTION DURATION)
12. INITIAL WATER LEVEL IN LOWER PLENUM : 0.86 M.
13. POWER CONTROL : ANS x 1.2 + ACTINIDE (30 SEC AFTER SCRAM)
14. EXPECTED BOCREC TIME FROM ECC INITIATION 12 SEC
15. EXPECTED PEAK TEMPERATURE AT BOCREC 600 C

Table D-2 Chronology of events

EVENT	TIME (sec)
Test Initiated (Heater Rods Power on) (Data Recording Initiated)	0.0
Accumulator Injection Initiated	52
Power Decay Initiated (Bottom of Core Recovery)	63.5
Accumulator Injection Switched from Lower Plenum to Cold Leg	69.5
Accumulator Injection Ended and LPCI Injection Initiated	76.5
All Heater Rods Quenched	445
Power Off	528
LPCI Injection Ended	808
Test Ended (Data Recording Ended)	1071

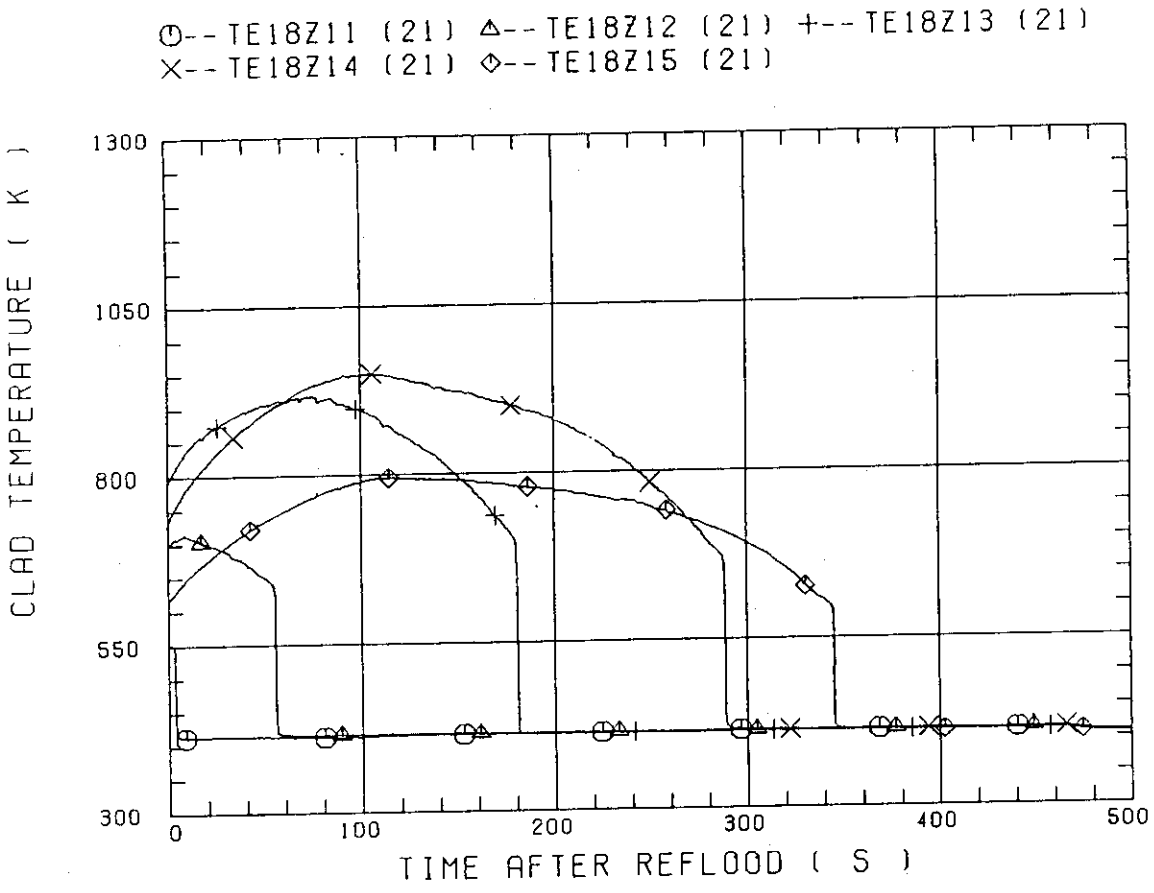

Fig. D-1 **Surface temperature on low power rod (Z-rod) in medium power region (B region) (average power rod)**

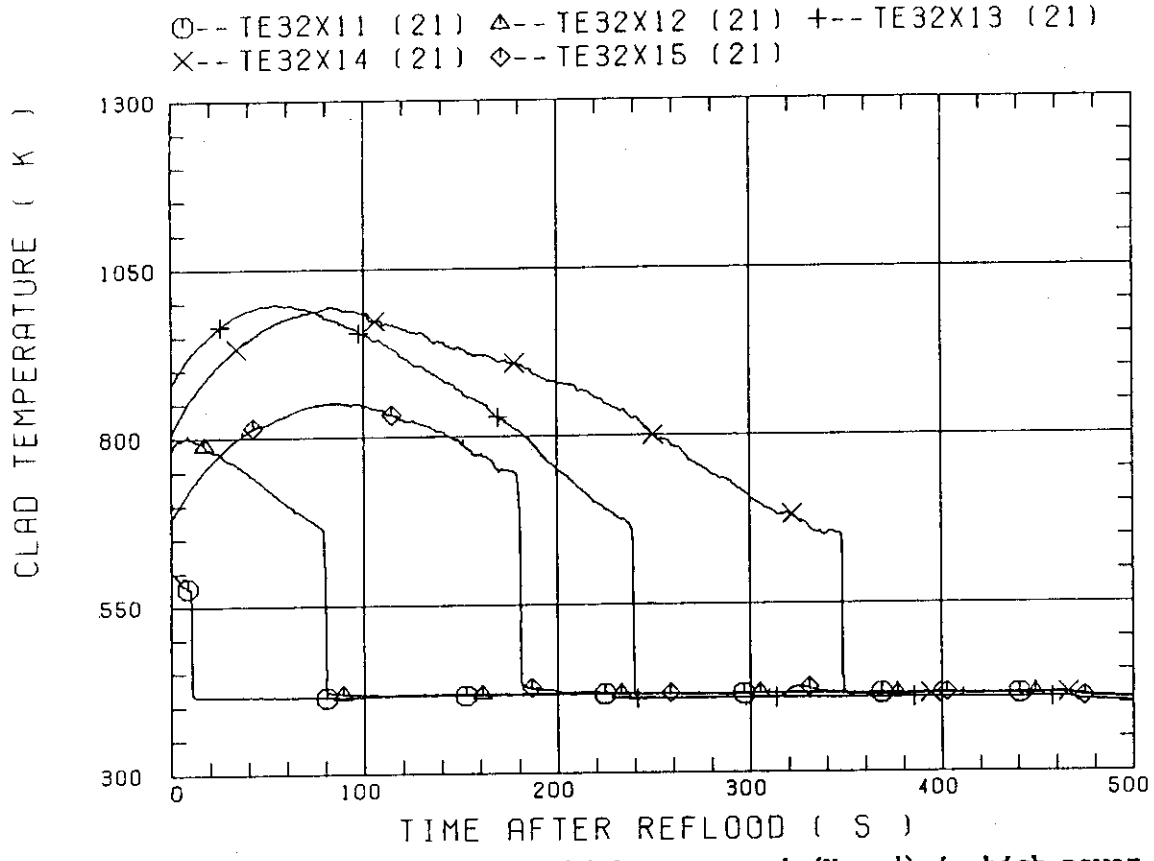

Fig. D-2 **Surface temperature on high power rod (X-rod) in high power region (A region) (peak power rod)**

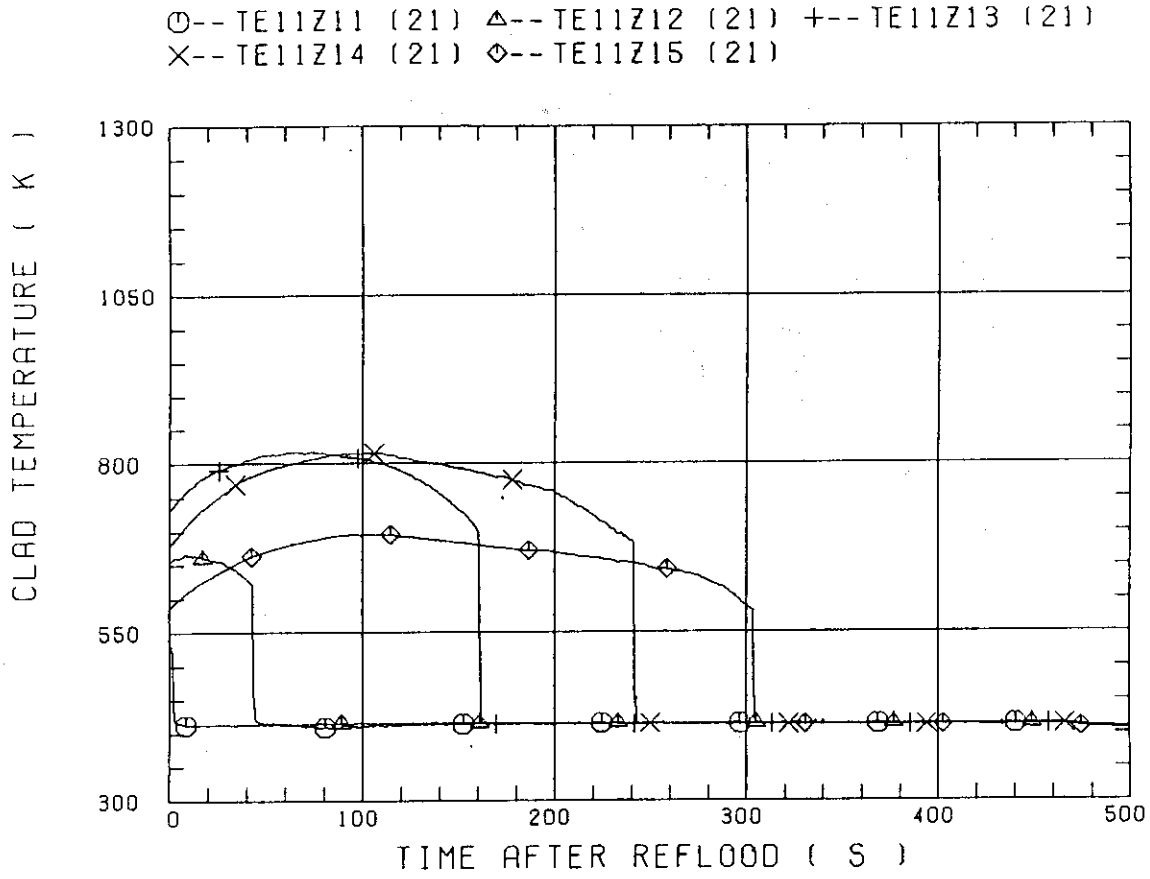

Fig. D-3 **Surface temperature on low power rod (Z-rod) in low power region (C region) (lowest power rod)**

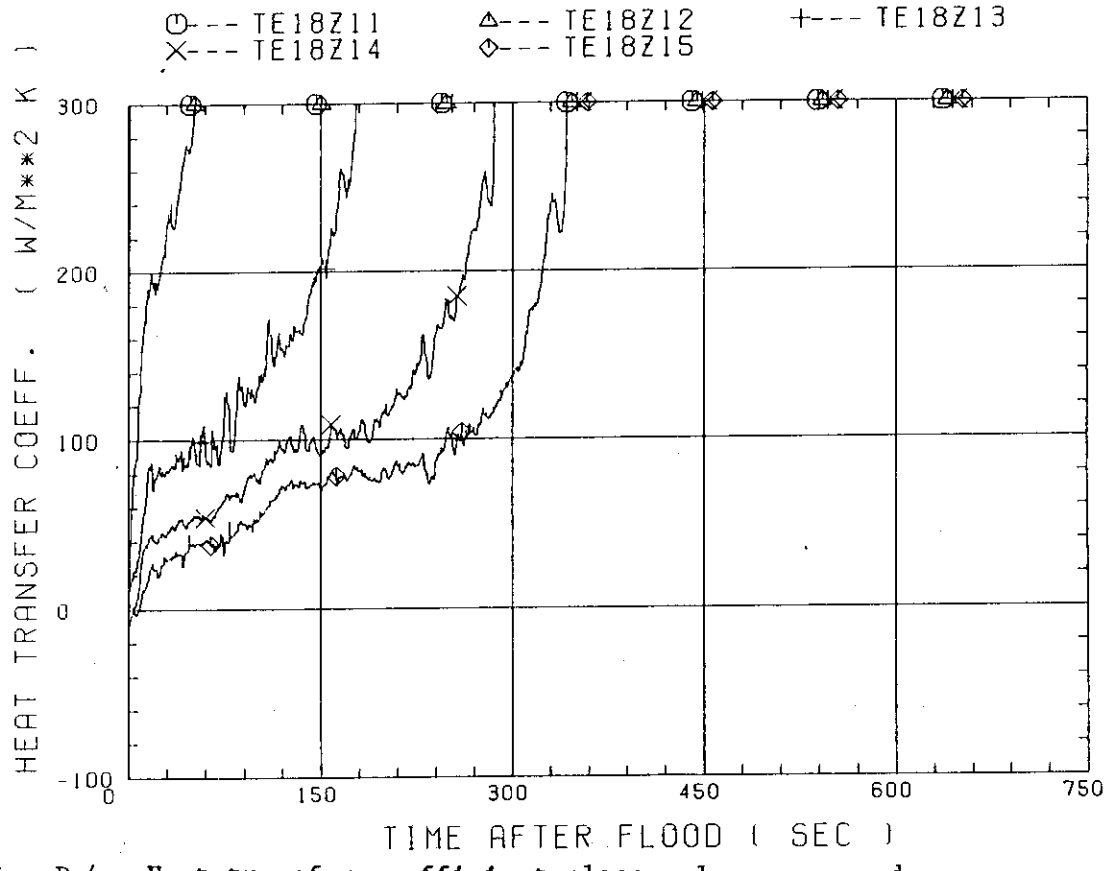

Fig. D-4 **Heat transfer coefficient along a low power rod (Z-rod) in medium power region (B region) (average power rod)**

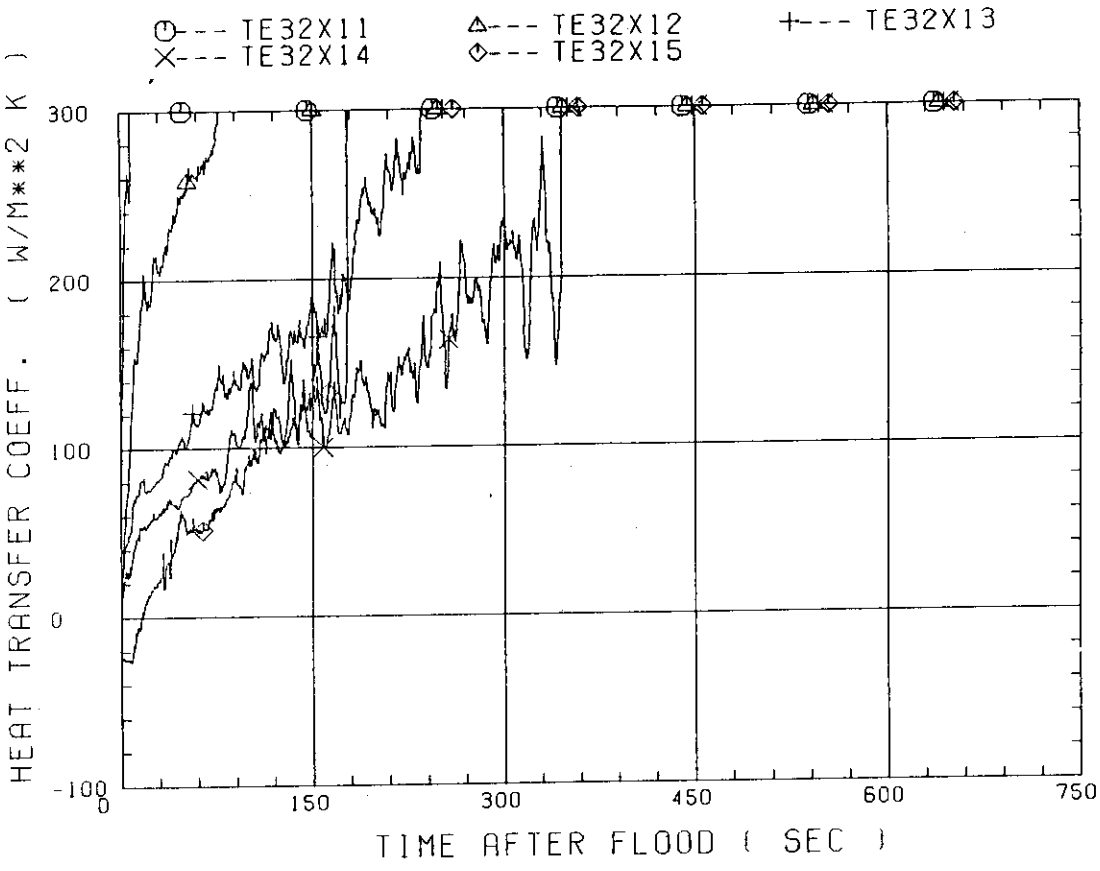

Fig. D-5 **Heat transfer coefficient along a high power rod (X-rod) in high power region (A region) (peak power rod)**

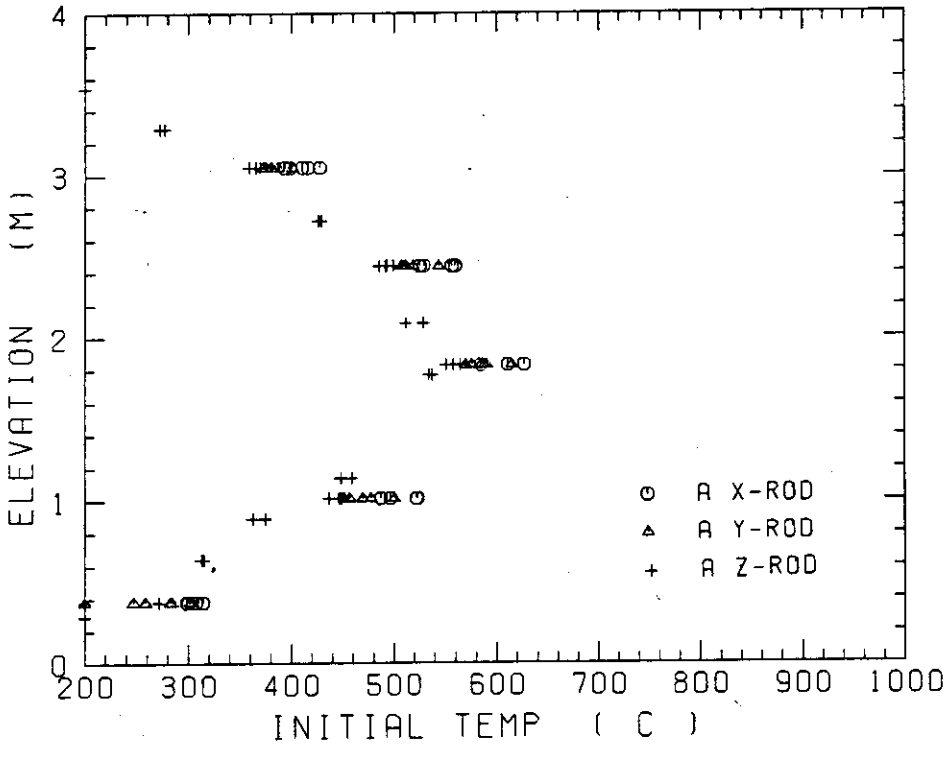

Fig. D-6 **Initial rod surface temperature in high power region (A region)**

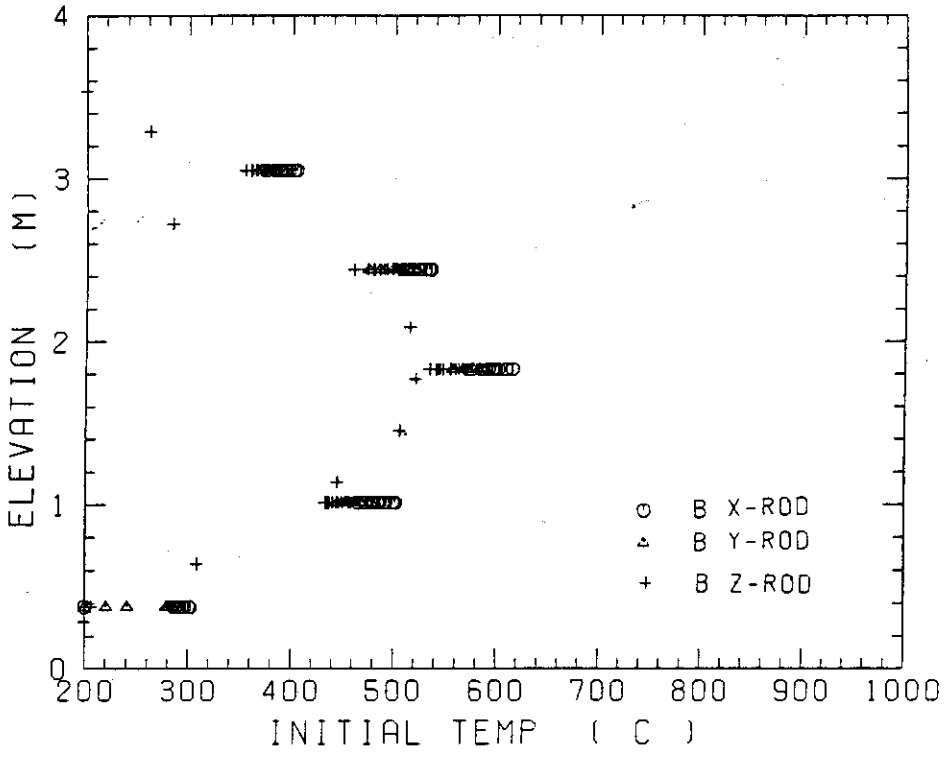

Fig. D-7 Initial rod surface temperature in medium power region (B region)

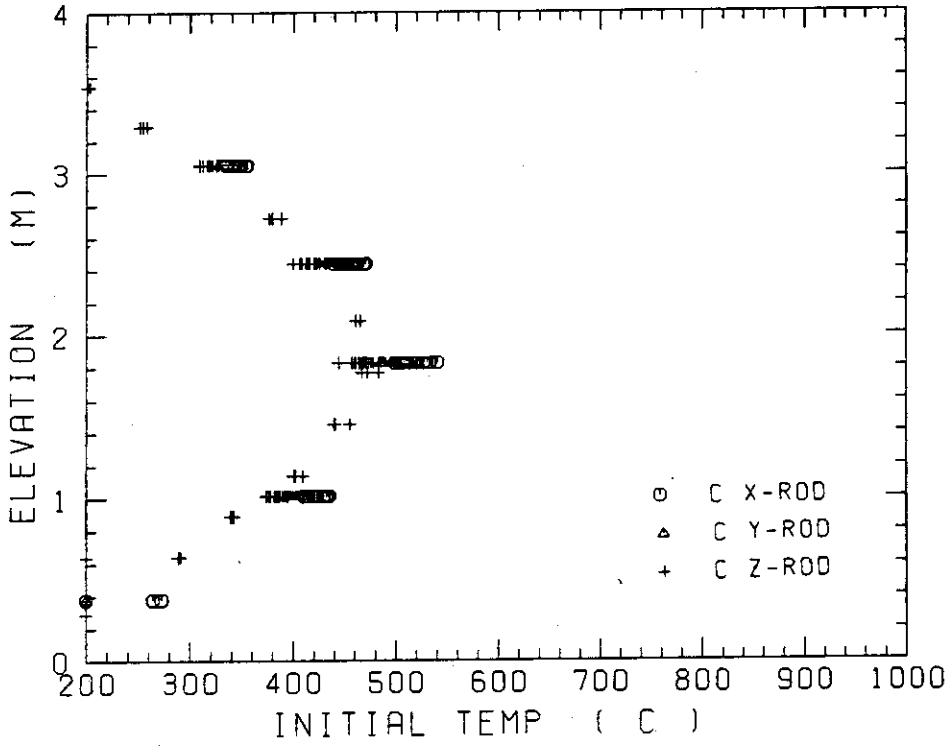

Fig. D-8 Inital rod surface temperature in low power region (C region)

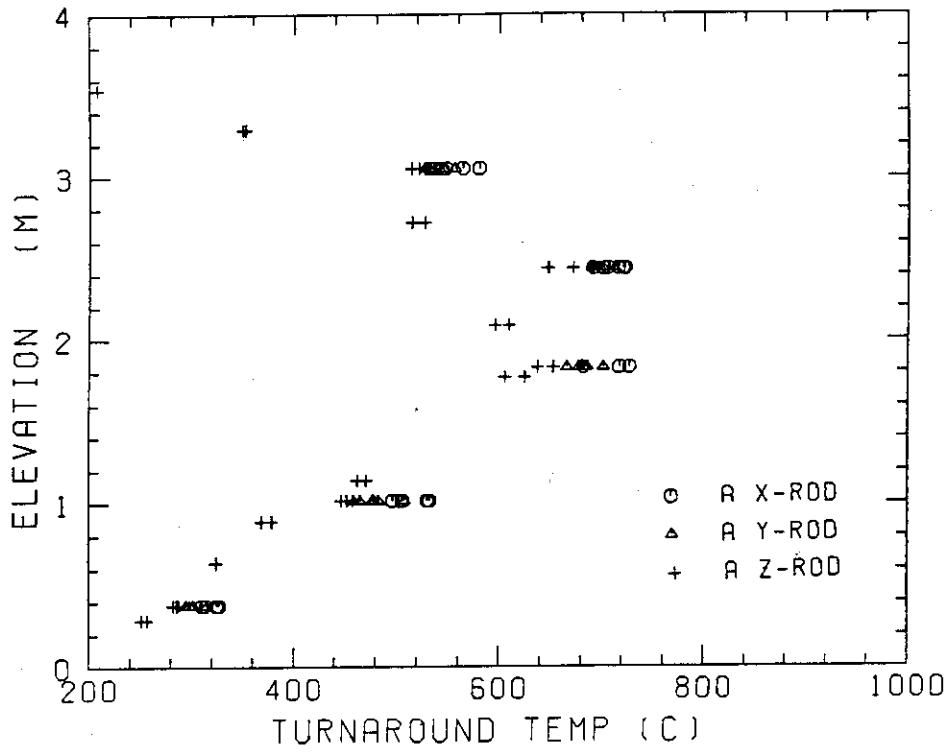

Fig. D-9 Turnaround temperature in high power region (A region)

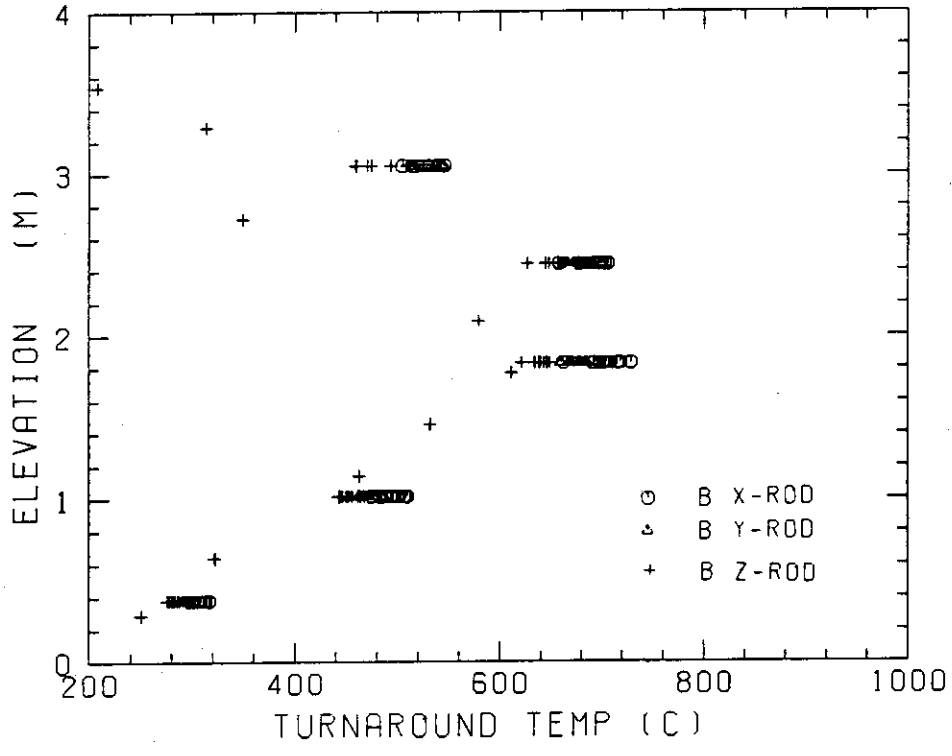

Fig. D-10 Turnaround temperature in medium power region (B region)

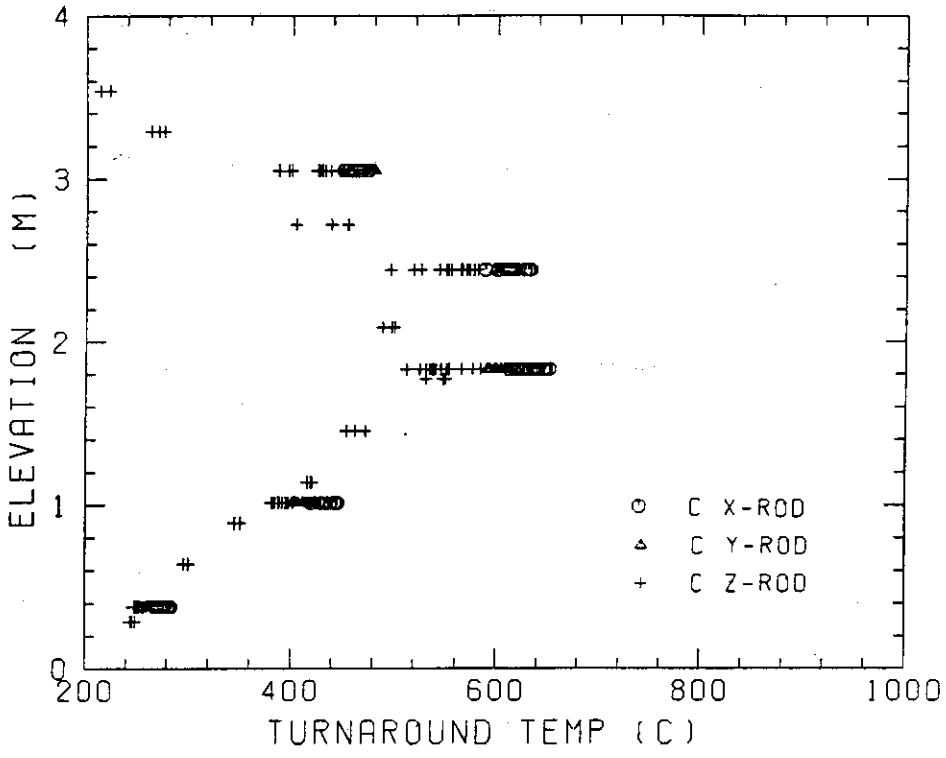

Fig. D-11 Turnaround temperature in low power region (C region)

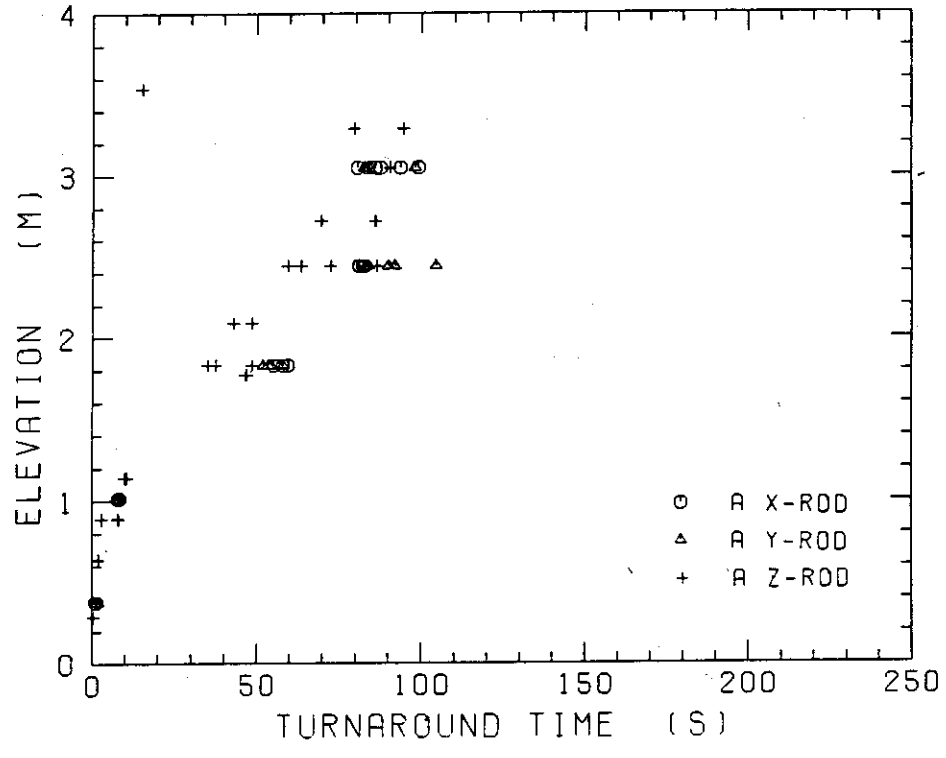

Fig. D-12 Turnaround time in high power region (A region)

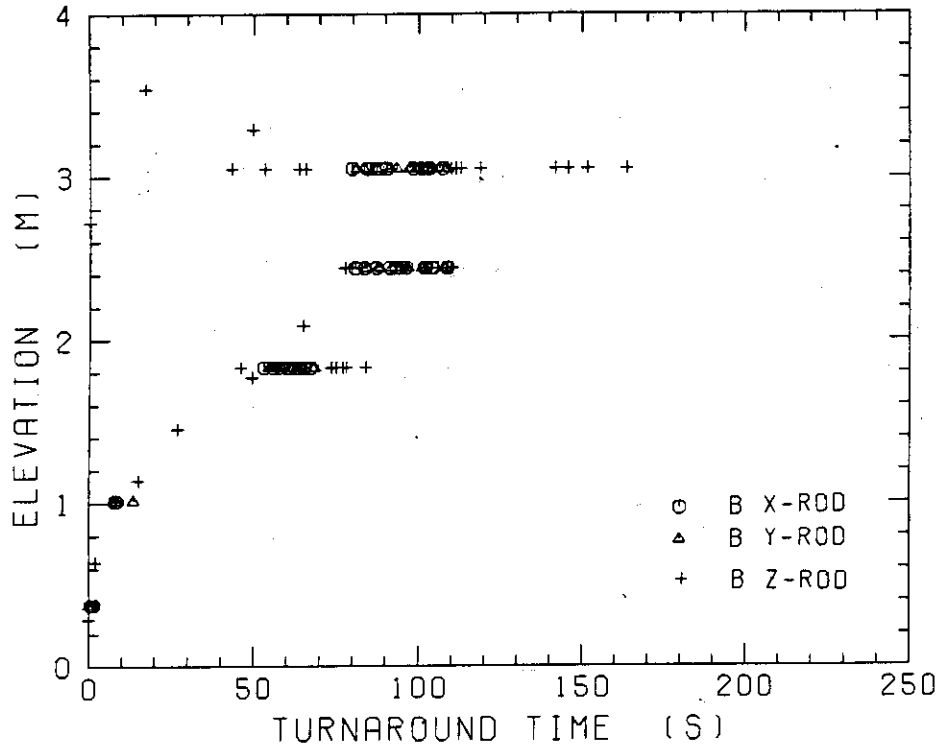

Fig. D-13 Turnaround time in medium power region (B region)

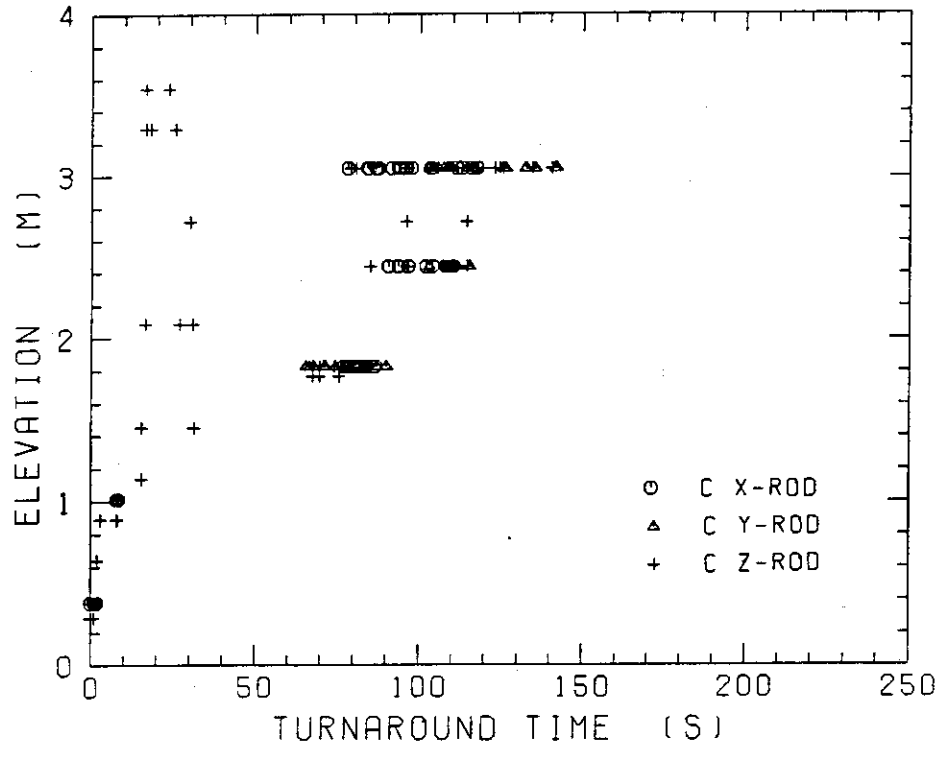

Fig. D-14 Turnaround time in low power region (C region)

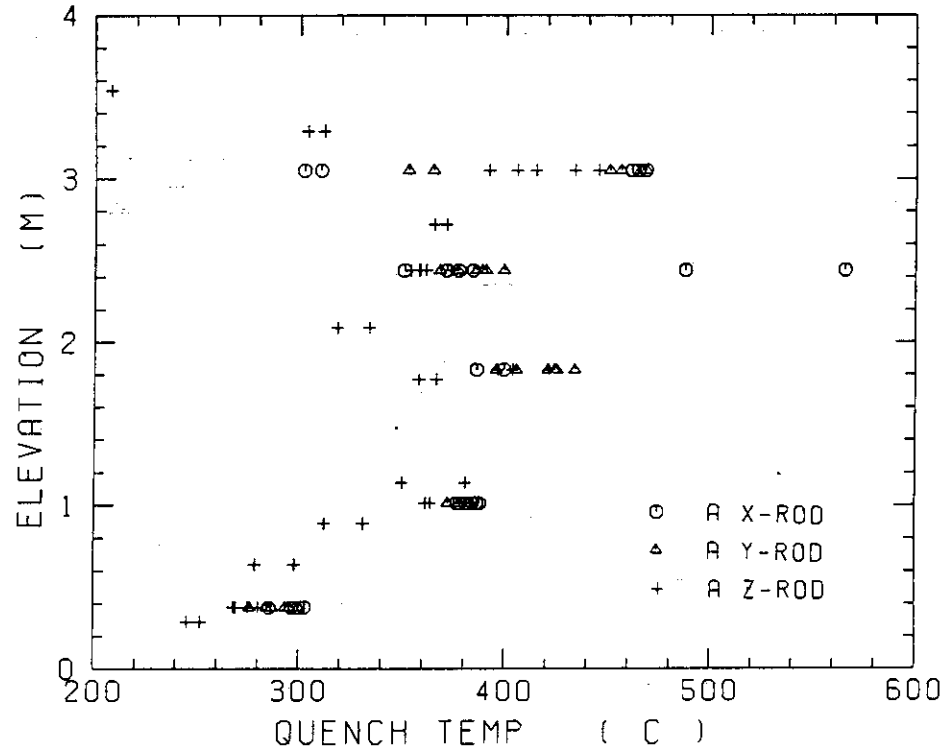

Fig. D-15 Quench temperature in high power region (A region)

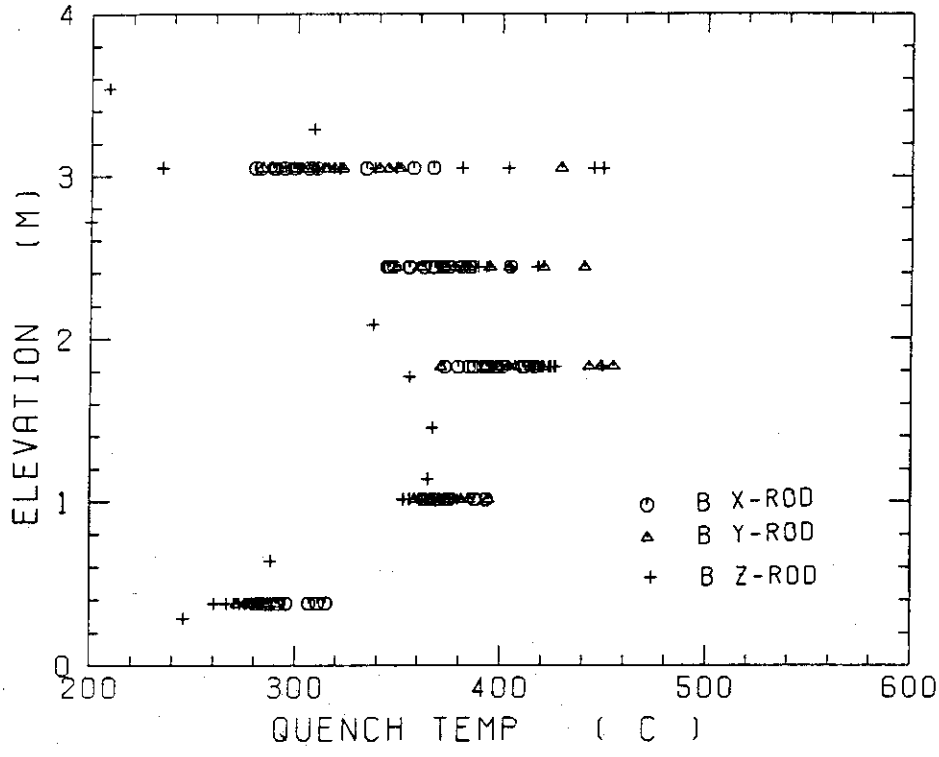

Fig. D-16 Quench temperature in medium power region (B region)

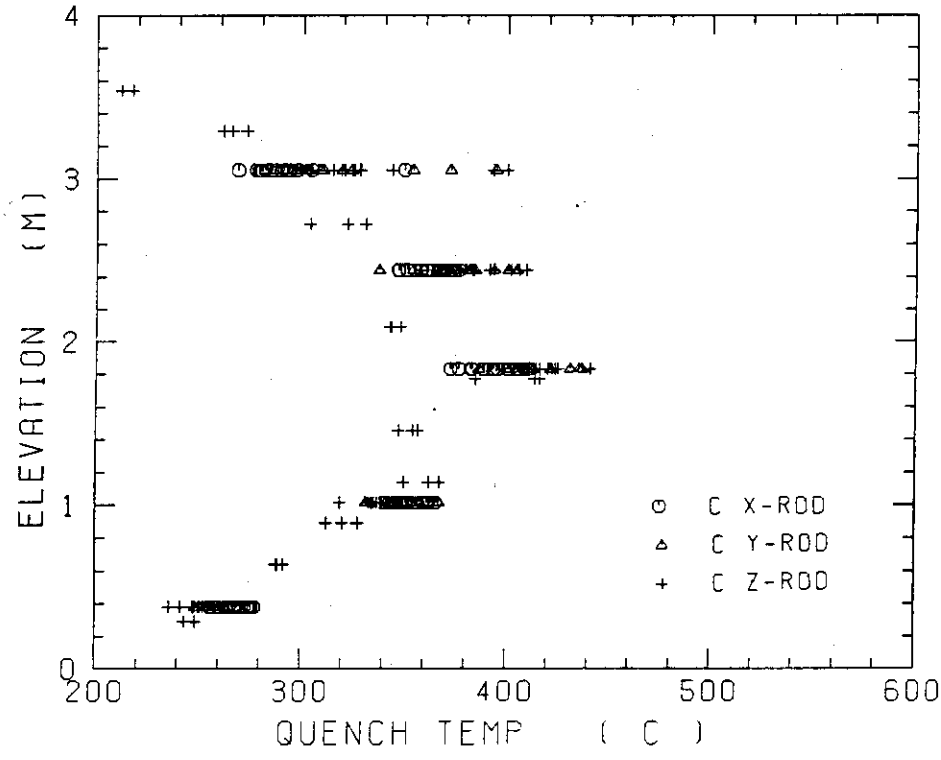

Fig. D-17 Quench temperature in low power region (C region)

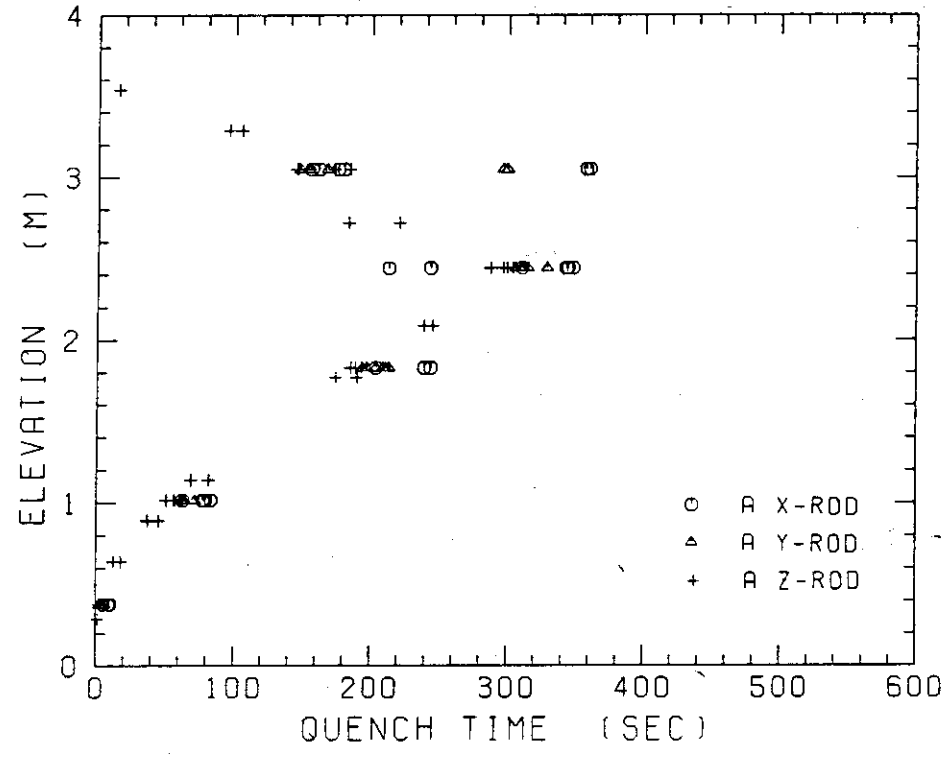

Fig. D-18 Quench time in high power region (A region)

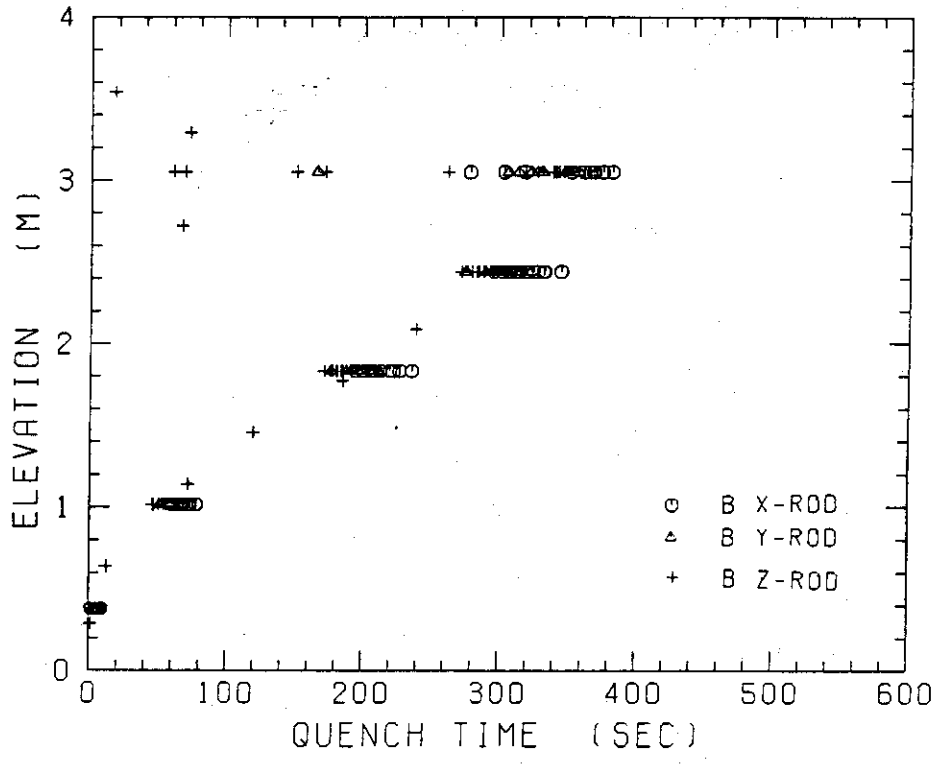

Fig. D-19 Quench time in medium power region (B region)

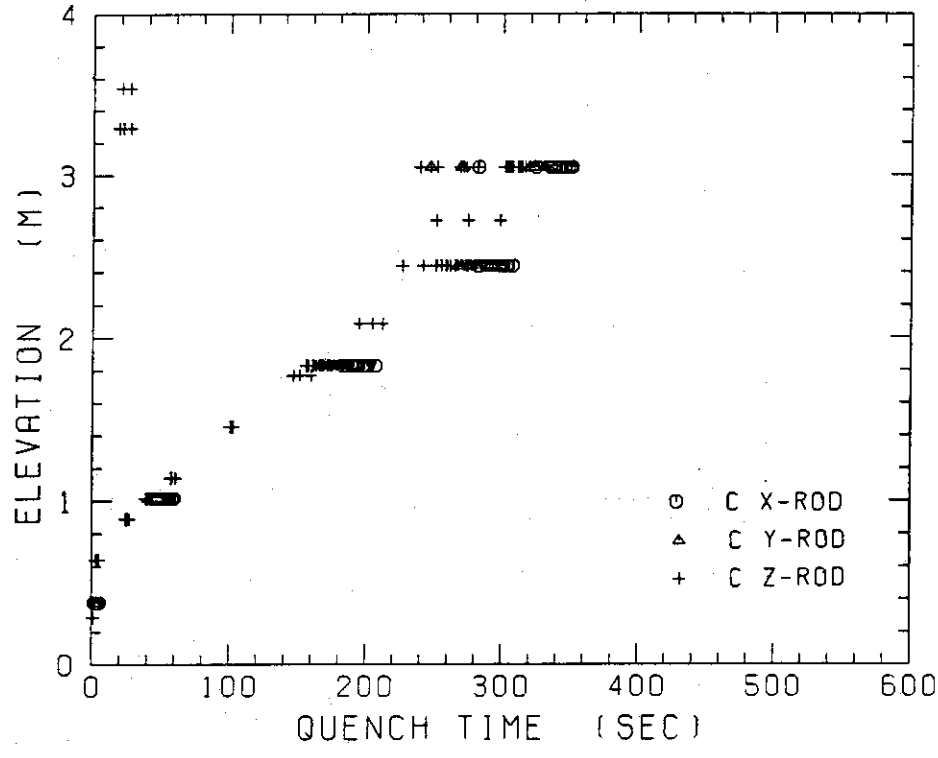

Fig. D-20 Quench time in low power region (C region)

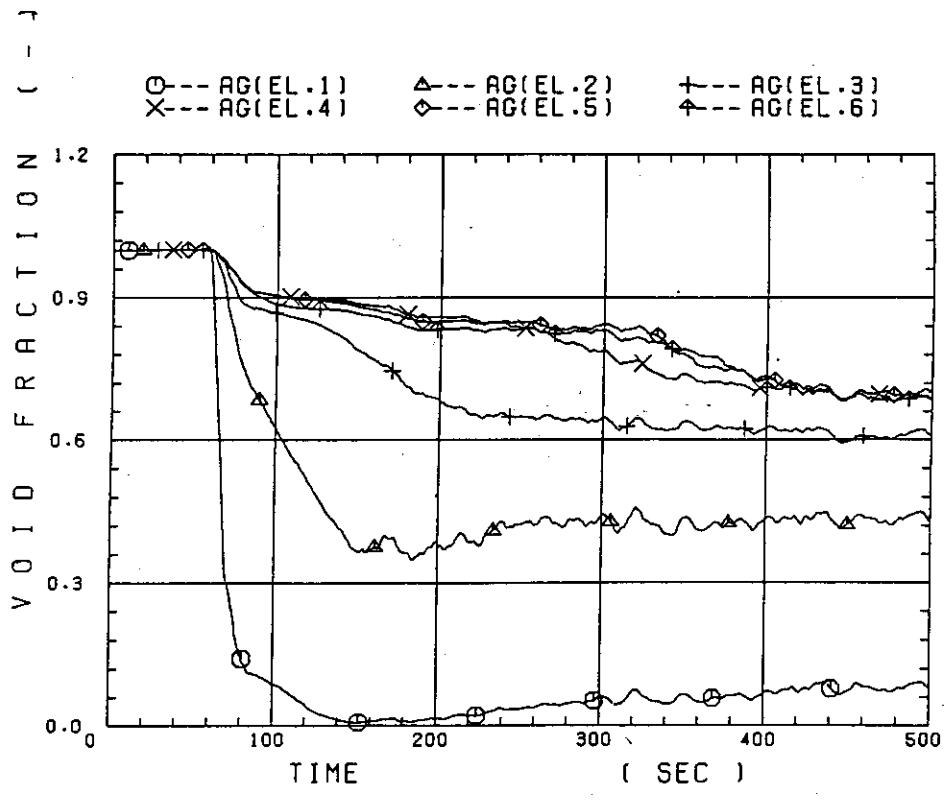

Fig. D-21 Void fraction in core

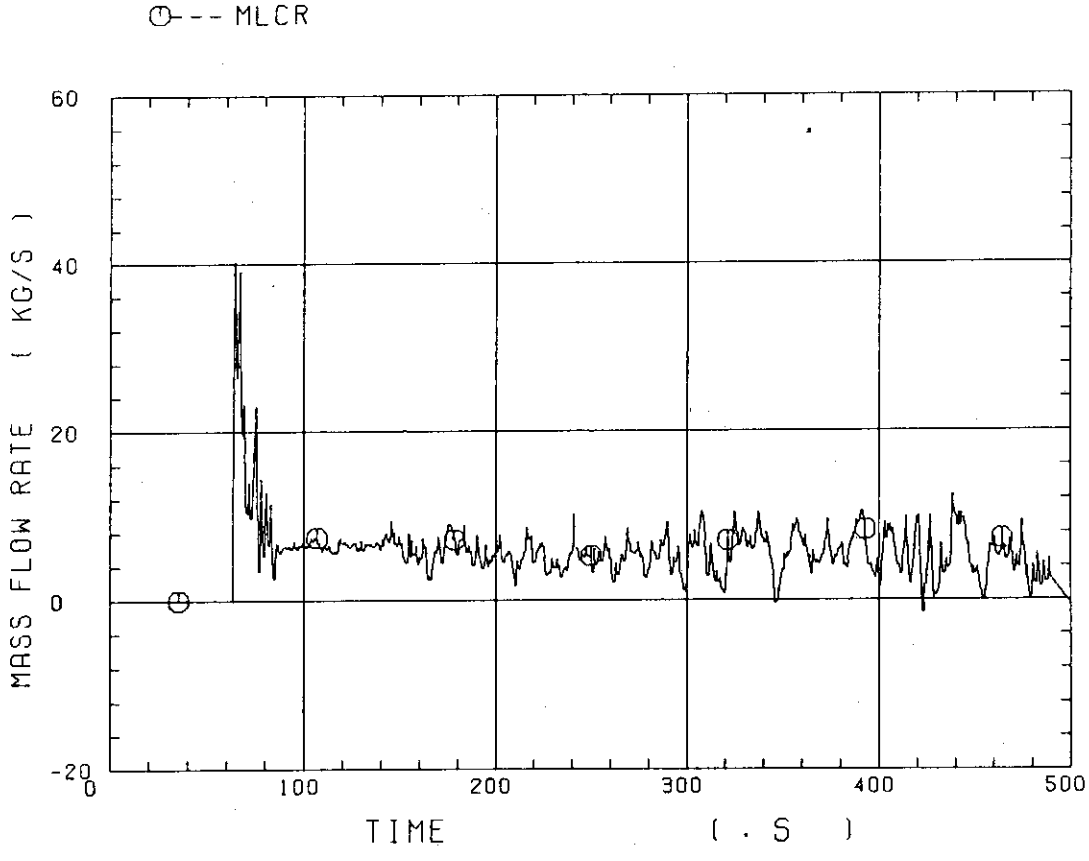

Fig. D-22 Core inlet mass flow rate

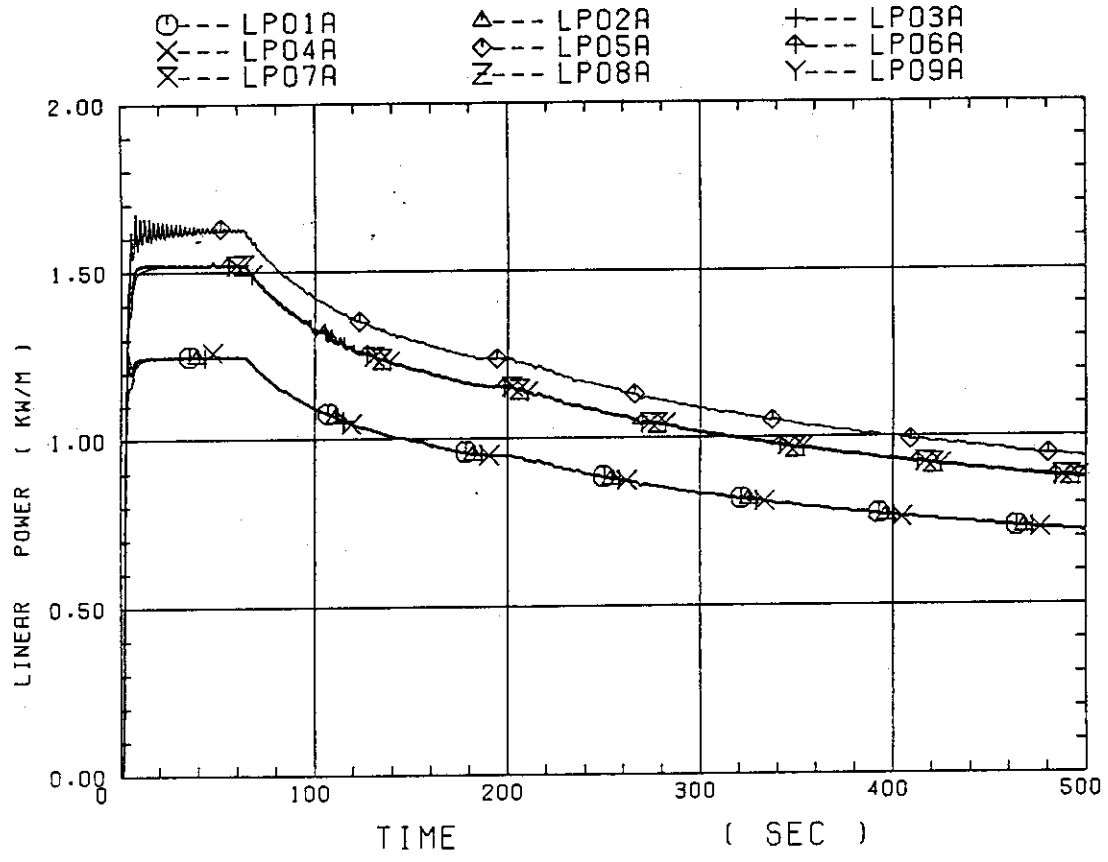

Fig. D-23 Average linear power of heater rod in each power unit zone

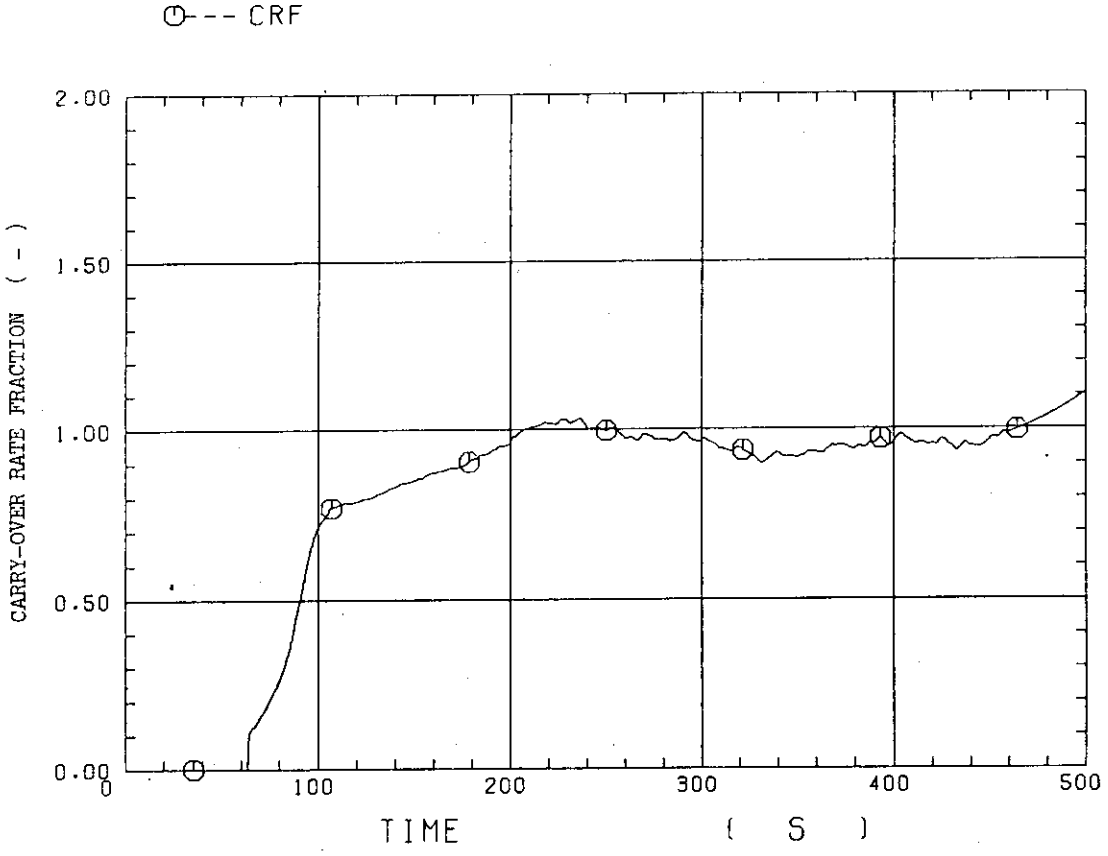

Fig. D-24 Carry-over rate fraction

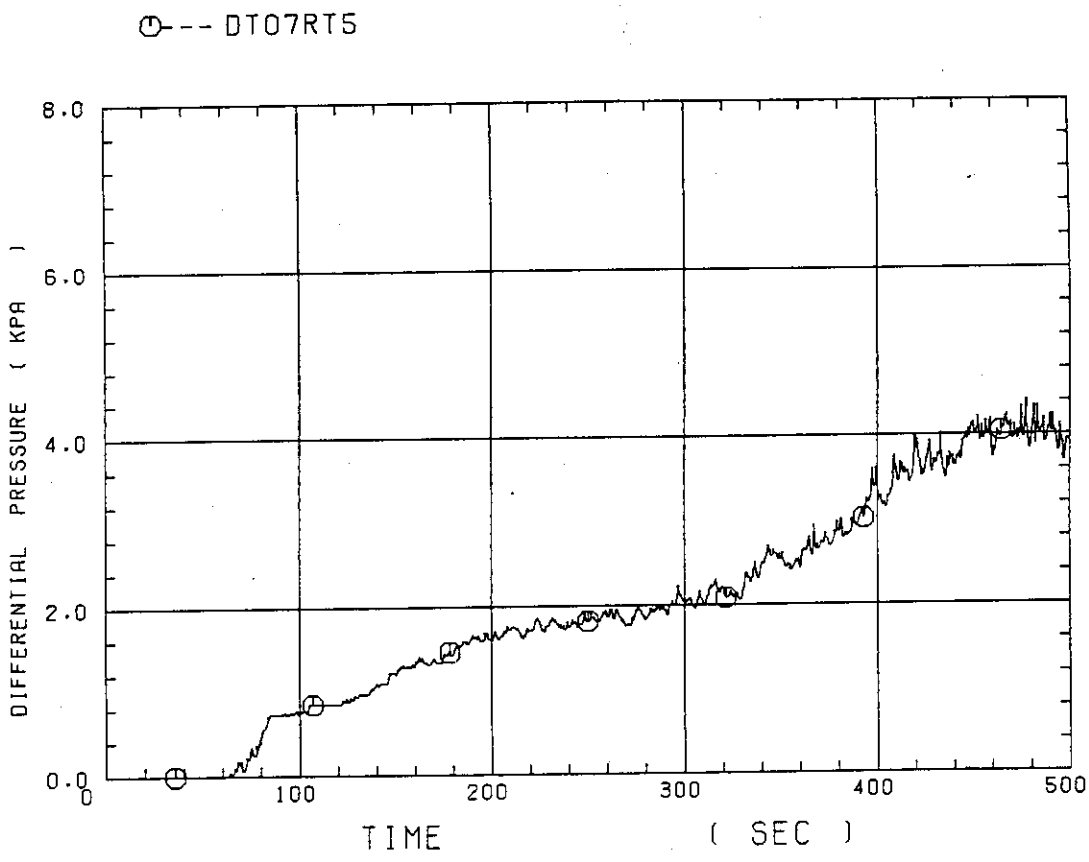

Fig. D-25 Differential pressure through upper plenum

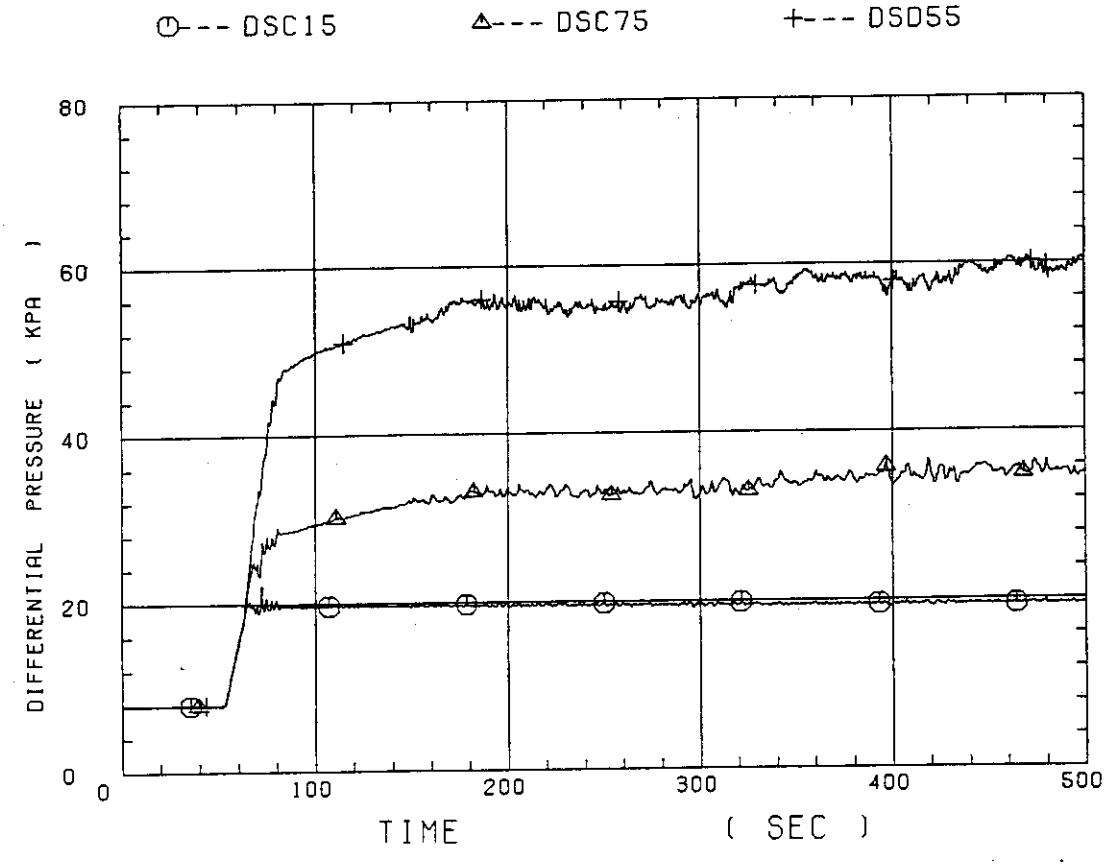

Fig. D-26 Differential pressure through downcomer, core, and lower plenum

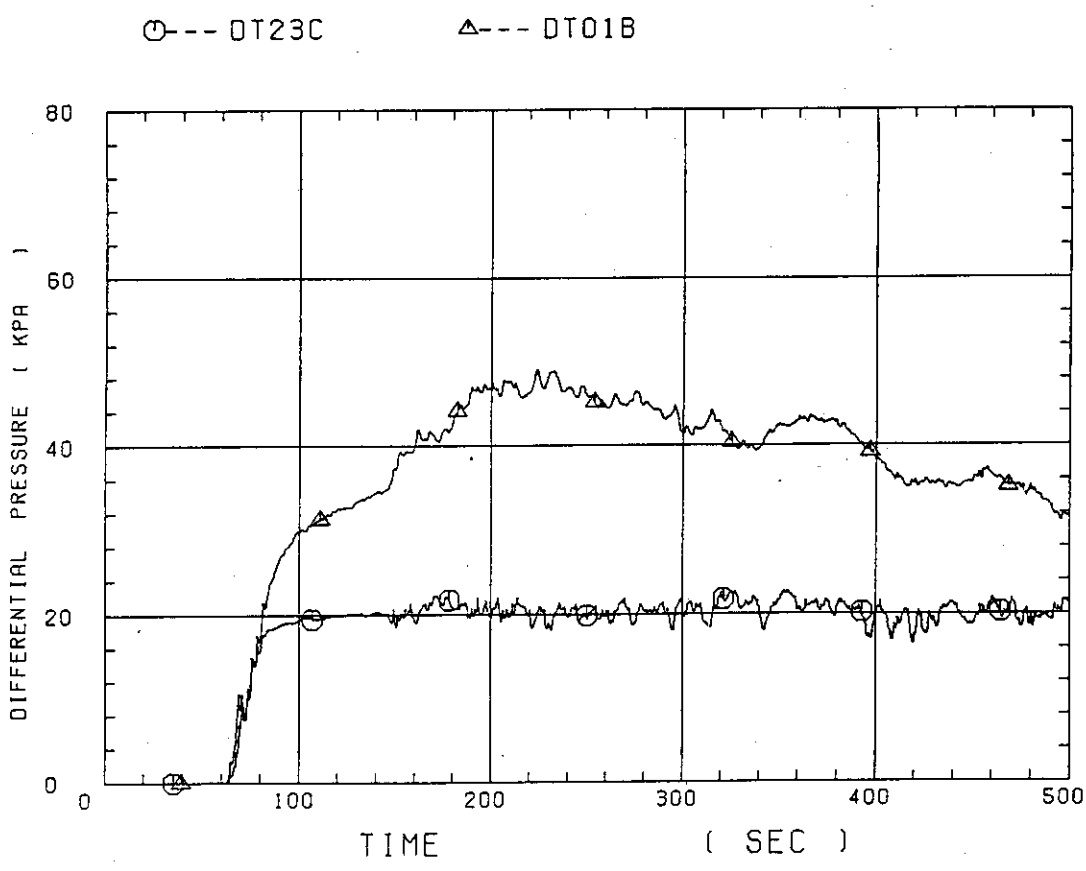

Fig. D-27 Differential pressure through intact and broken loops

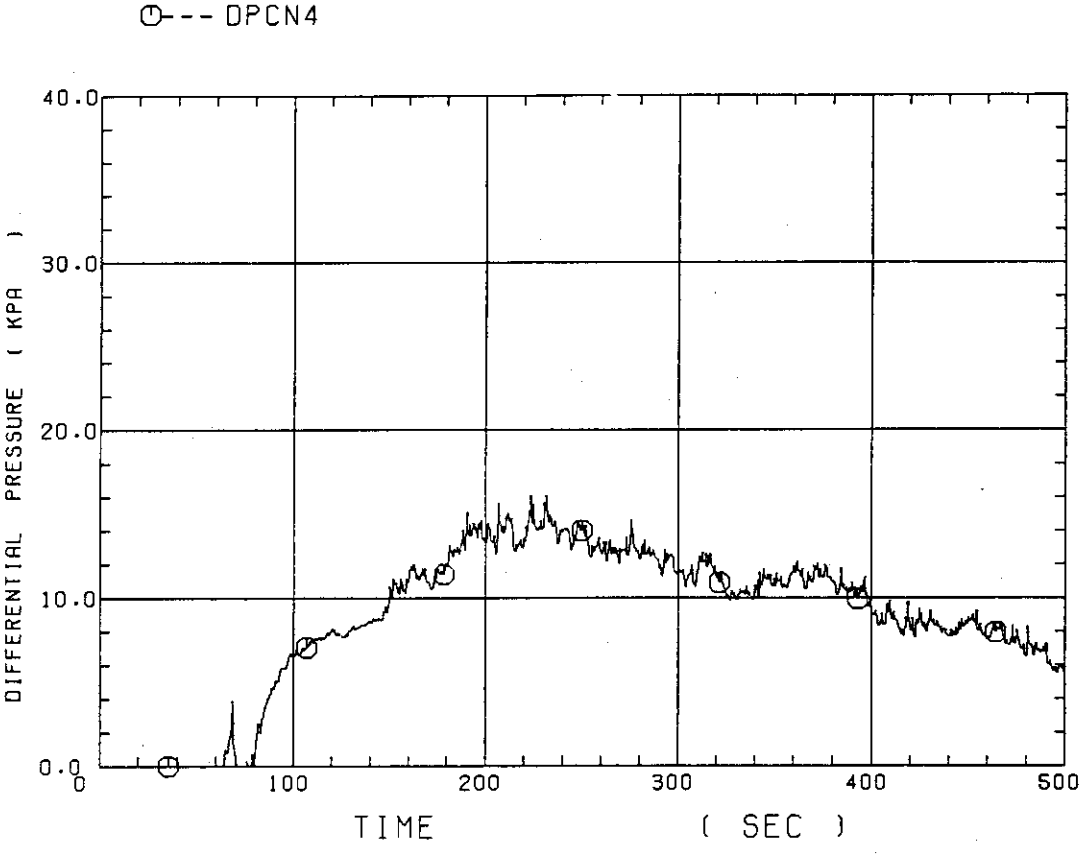

Fig. D-28 Differential pressure through broken cold leg nozzle

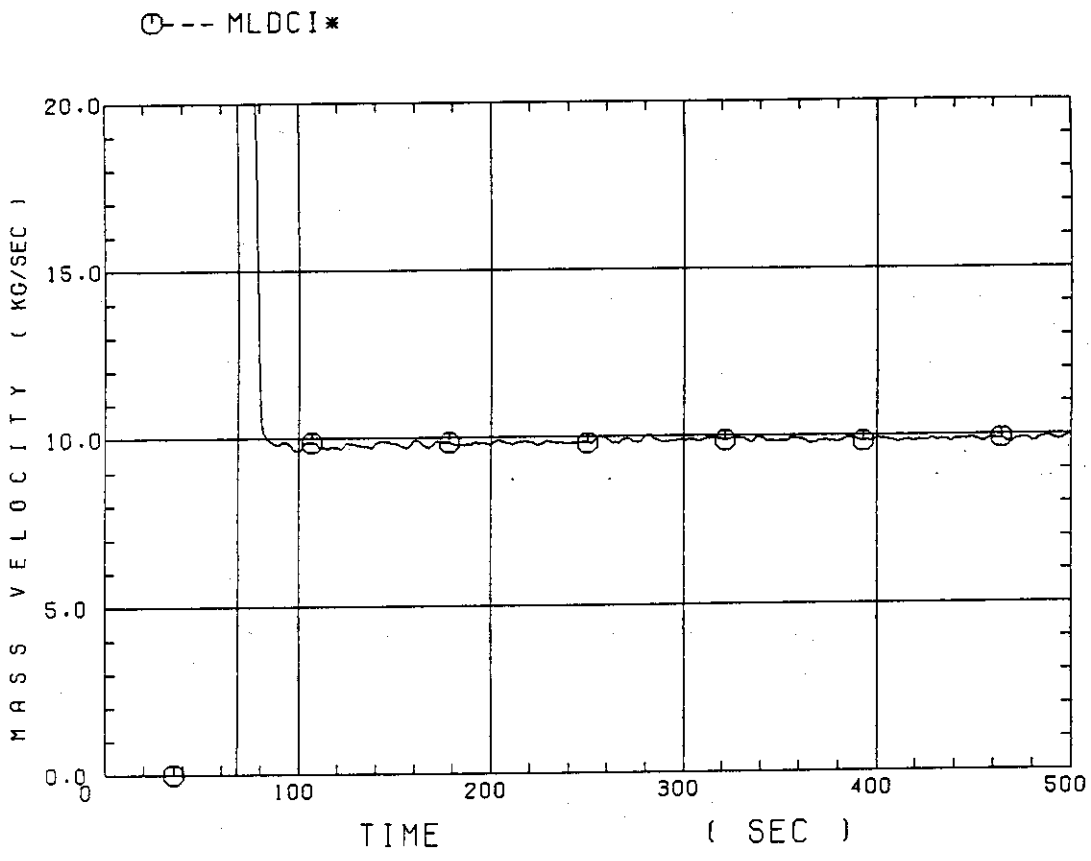

Fig. D-29 Total water mass flow rate from intact loops to downcomer

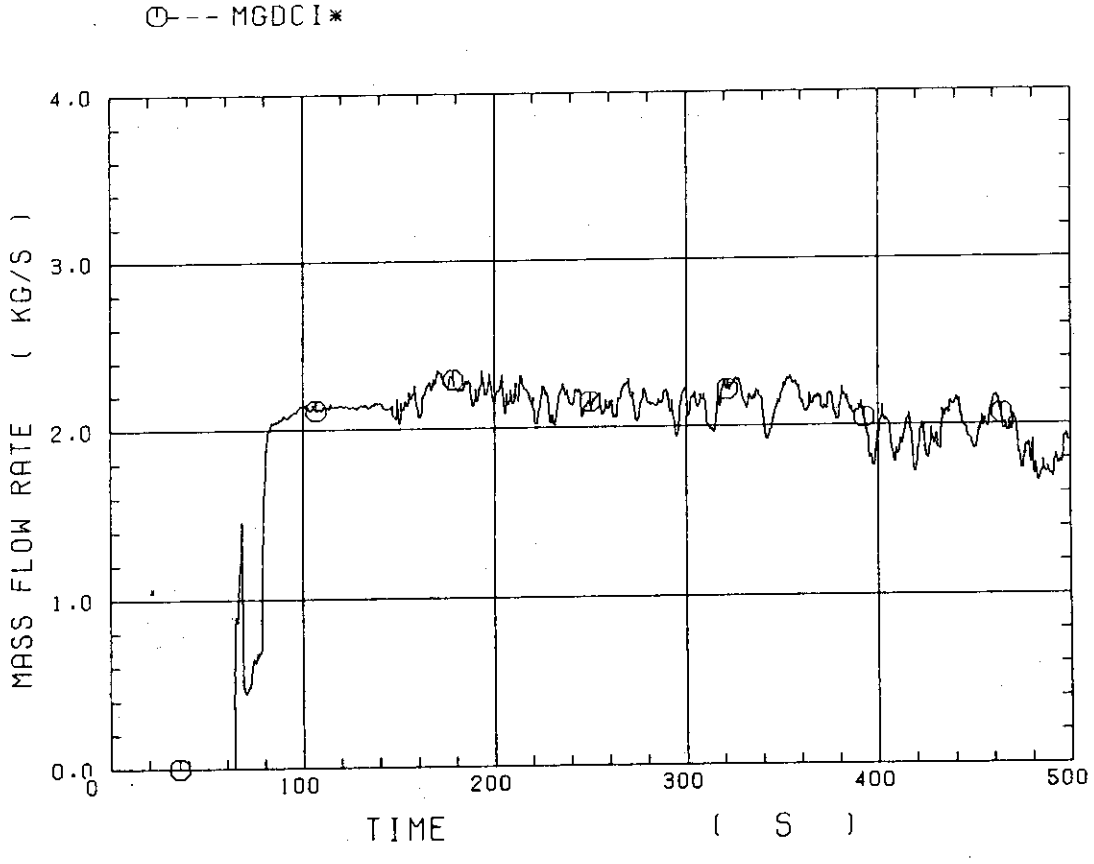

Fig. D-30 Total steam mass flow rate from intact loops to downcomer

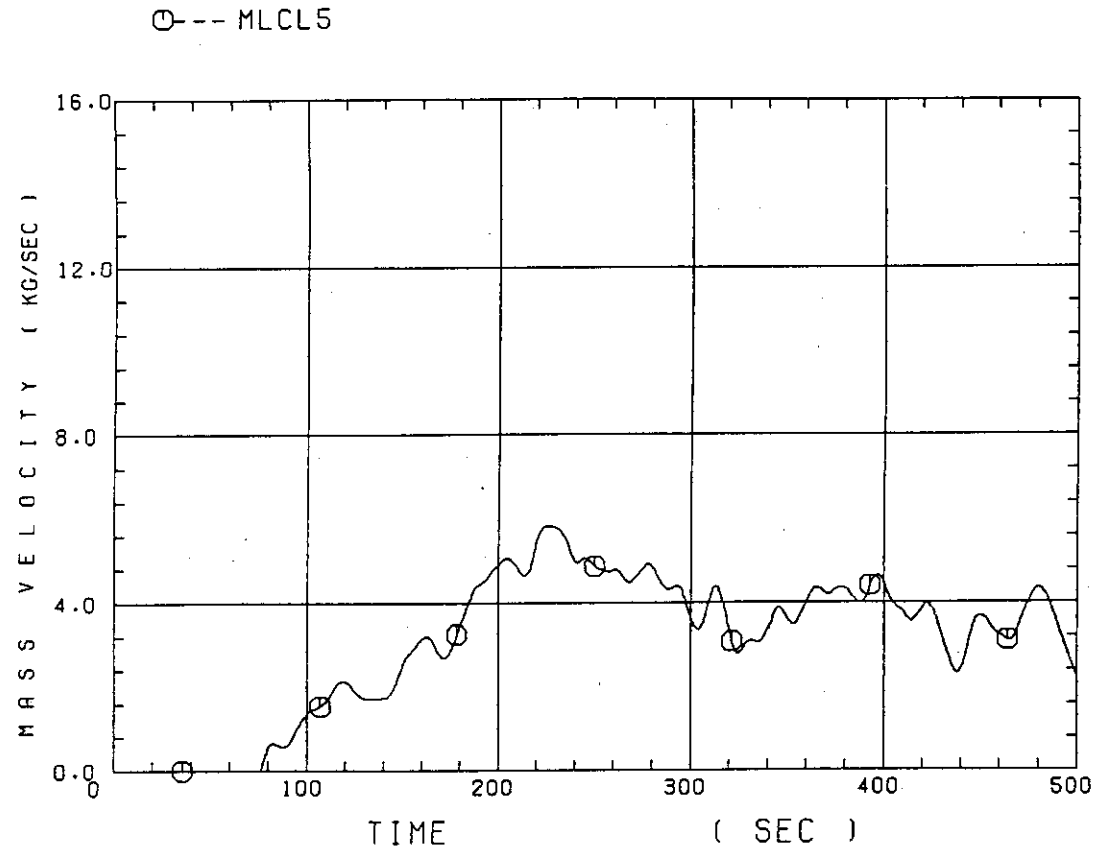

Fig. D-31 Water mass flow rate through broken cold leg nozzle

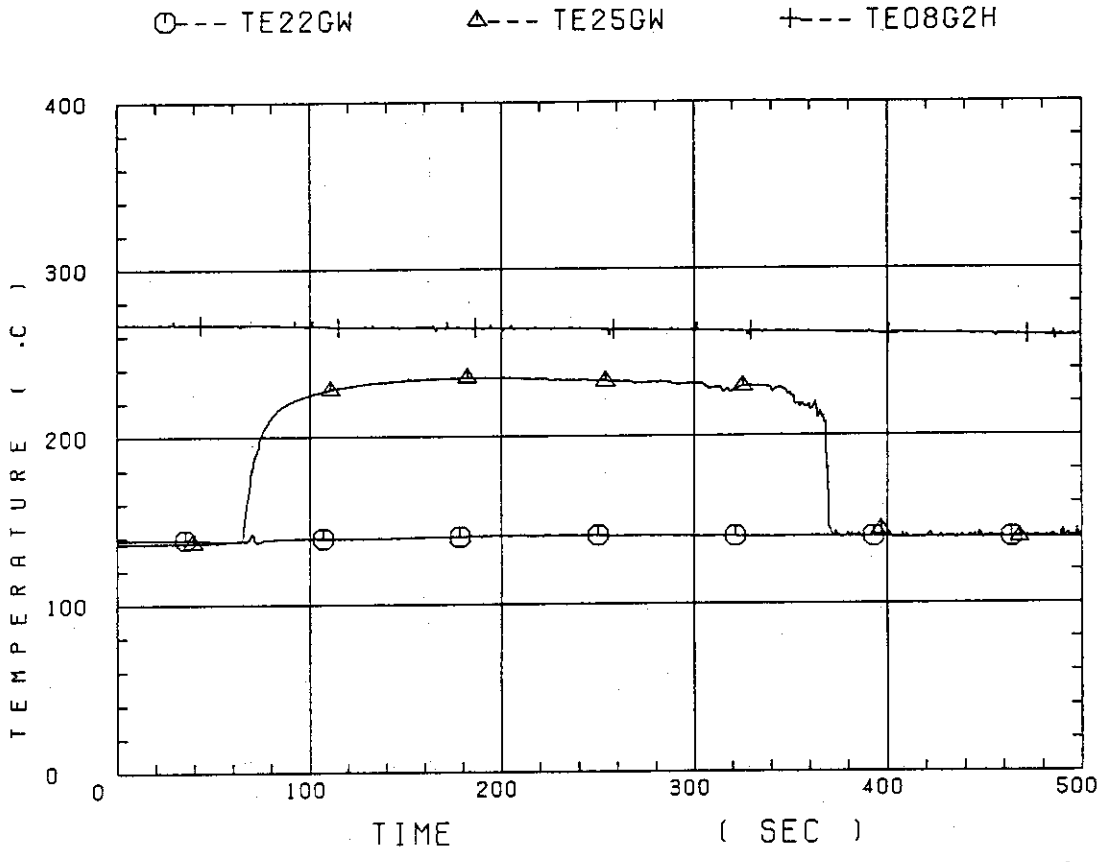

Fig. D-32 Fluid temperature in inlet plenum, outlet plenum, and secondary of steam generator 1

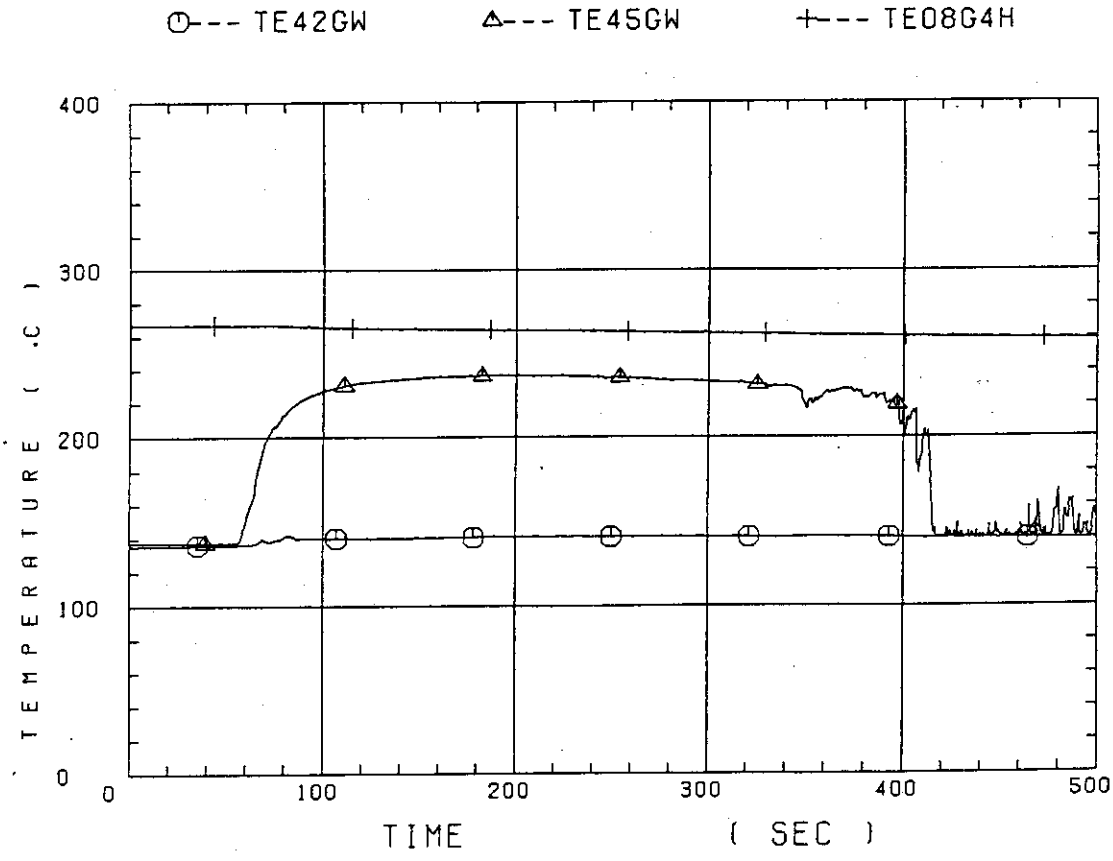

Fig. D-33 Fluid temperature in inlet plenum, outlet plenum, and secondary of steam generator 2

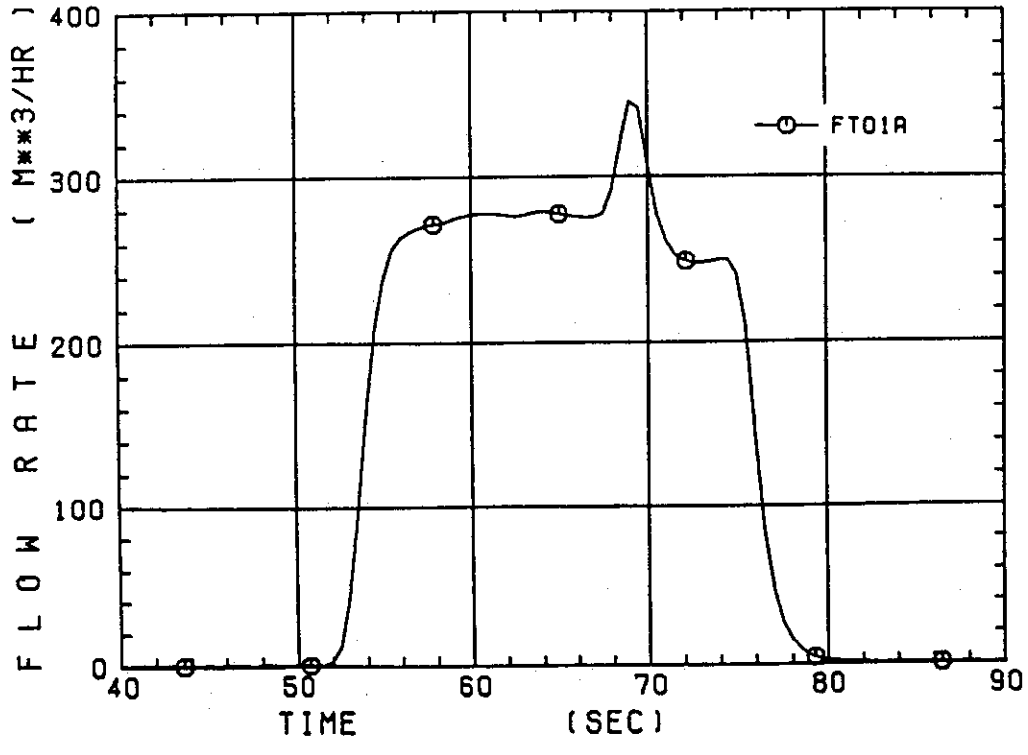

Fig. D-34 Total accumulator injection rate

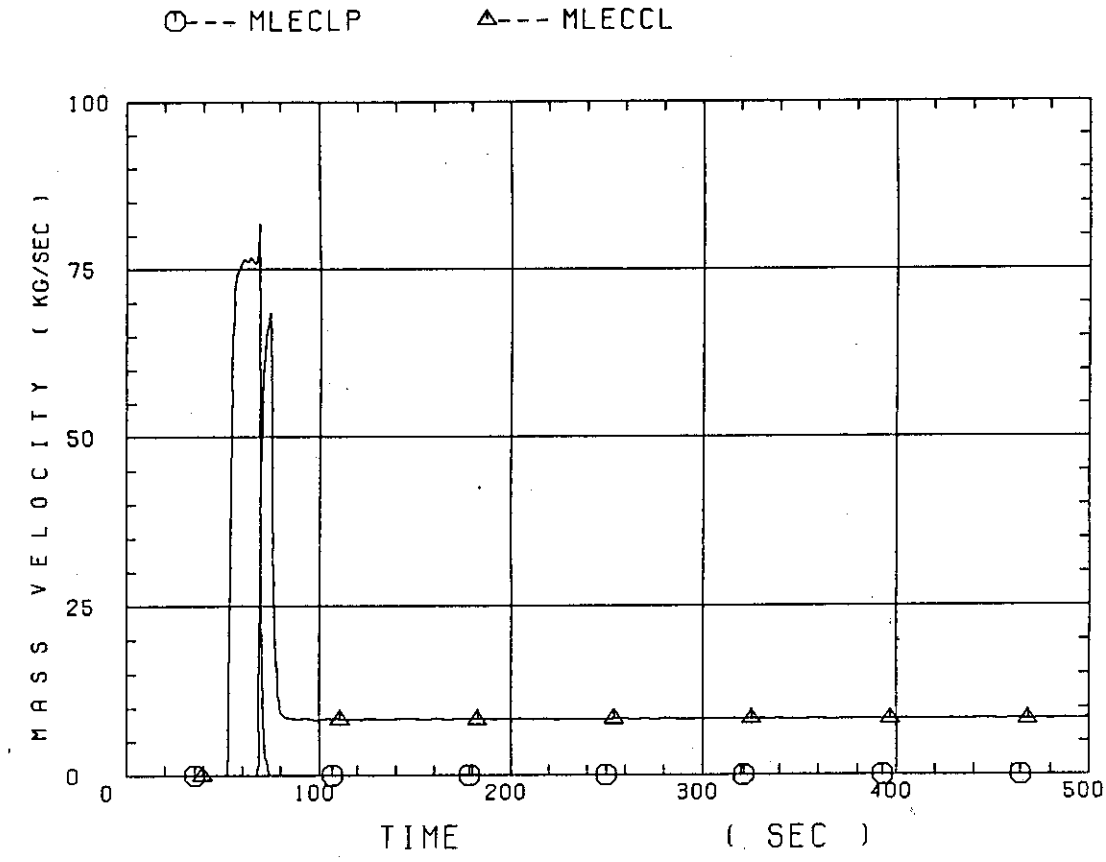

Fig. D-35 ECC water injection rates to lower plenum and to cold legs

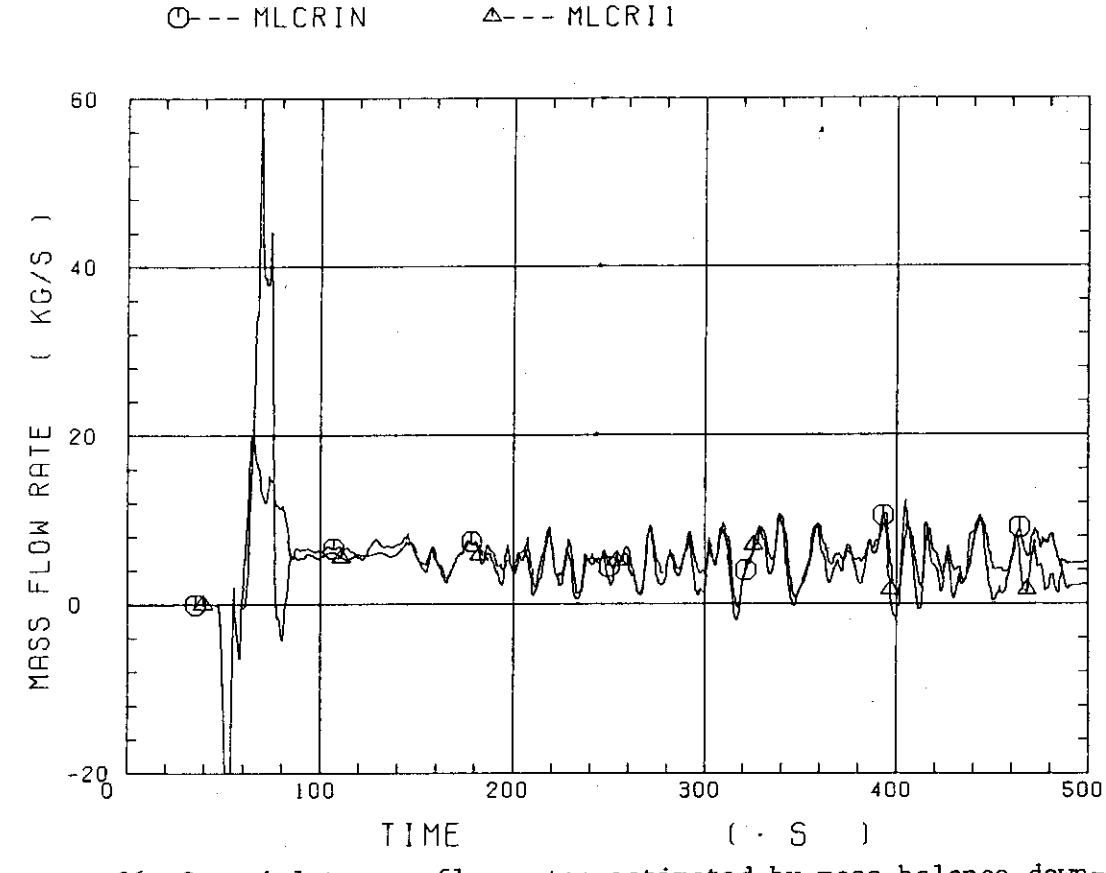

Fig. D-36 Core inlet mass flow rates estimated by mass balance downstream and upstream of core inlet

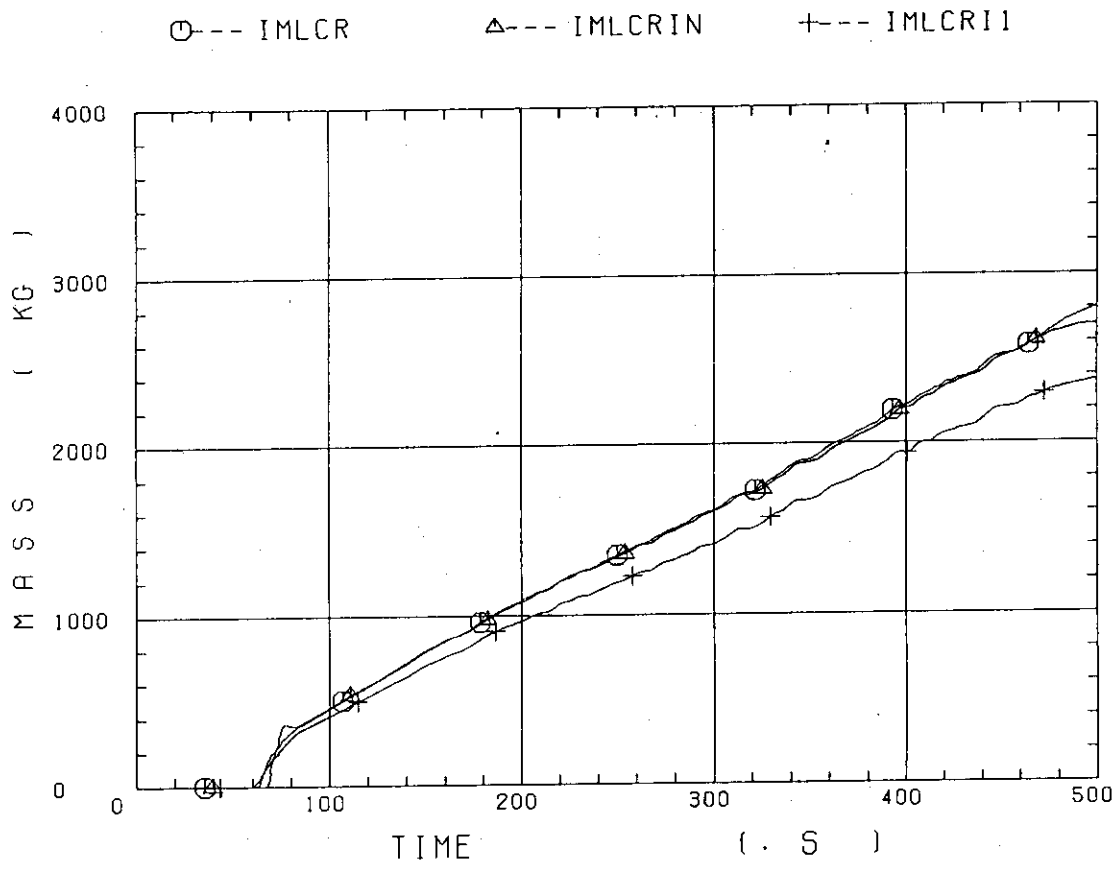

Fig. D-37 Comparison of injected mass into core among two estimation methods and evaluated mass